IN VIVO IMAGING OF CEREBRAL BLOOD FLOW AND NEURAL ACTIVITY CHANGES IN THE CONTEXTS OF ALHEIMER'S DISEASE AND PSYCHEDELICS

A Dissertation

Presented to the Faculty of the Graduate School

of Cornell University

In Partial Fulfillment of the Requirements for the Degree of

Doctor of Philosophy

by

Rick Thomas Zirkel

May 2025

IN VIVO IMAGING OF CEREBRAL BLOOD FLOW AND NEURAL ACTIVITY CHANGES IN THE CONTEXTS OF ALHEIMER'S DISEASE AND PSYCHEDELICS

Rick Thomas Zirkel, Ph.D.

Cornell University 2025

The brain is a highly dynamic organ in which neural activity, vascular regulation, and molecular signaling are intricately intertwined. Understanding these relationships is essential for uncovering the mechanisms that underlie both cognitive function and dysfunction. In vivo imaging enables the direct measurement of neural activity and cerebral blood flow in living animals with cellular resolution, providing a powerful window into brain function in both health and disease (chapter 1). This dissertation leverages a range of optical imaging tools to examine how cerebral blood flow and neural dynamics, and the relationship between them, are impacted in two distinct contexts: Alzheimer's disease (AD) (chapter 4) and psychedelic drug action (chapter 5).

Alzheimer's disease is characterized by disruptions in both neural activity and blood flow, yet the precise mechanisms through which these impairments arise—and whether they can be reversed—remain unclear. In the first focus of this thesis, I review our understanding of these impairments, as well as current research examining therapeutic targets to eliminate such dysfunction (chapter 2). Next, using in vivo two-photon microscopy, I demonstrate how a specific impaired activity pattern can be improved after the restoration of cerebral blood flow

(CBF) deficits. Increasing CBF in AD model mice leads to enhanced orientation tuning in visual cortex neurons, providing a potential therapeutic mechanism for restoring cortical function (chapter 4).

For the second focus of this thesis, I leverage in vivo imaging techniques to evaluate cerebral blood flow and neural activity changes in the context of psychedelics, specifically psilocybin. Psychedelics are known to profoundly alter consciousness and have promising therapeutic potential for treating mood disorders such as anxiety, depression, and addiction (chapter 3). However, their effects on the coordination between neural and vascular activity in the brain, a relationship known as neurovascular coupling (NVC), are less well understood. Clinical fMRI studies investigating psychedelic drug action rely on NVC to examine blood flow changes as a proxy for neural activity. Using micro- and mesoscale in vivo imaging techniques, I show that psilocybin alters stimulus-evoked neurovascular coupling in mouse visual cortex and discuss potential mechanisms underlying these changes, and how these alterations may influence the interpretation of fMRI imaging with psychedelics (chapter 5).

Together, these studies highlight the power of in vivo imaging to uncover complex, dynamic interactions between neural activity and cerebral blood flow across multiple spatial and temporal scales. This dissertation not only demonstrates the utility of these imaging techniques in identifying neural and vascular impairments in AD and psychedelic drug action but also provides a framework for how these tools can be used to guide future therapeutic strategies. By combining cellular-resolution imaging with systems-level analysis, this work contributes to a deeper understanding of brain function in both pathological and pharmacologically altered states (chapter 6).

BIOGRAPHICAL SKETCH

Rick Thomas Zirkel was born on Long Islang, NY and grew up in the small town of Blue Point, NY. He graduated *Summa Cum Laude* from University at Buffalo with a Bachelor of Science in Biomedical Engineering in 2019. At Buffalo, Rick began his studies as an Engineering Undecided major, where he was introduced to Biomedical Engineering in his sophomore year, and was drawn to the idea of combining biology and neuroscience with engineering practices. In the summer of his junior year, Rick participated in a research experience for undergrads (REU) program through NeuroNex at Cornell University, where he worked in the lab of Dr. Joe Fetcho. During this time, he was introduced to in vivo brain imaging by performing light-sheet microscopy in larval zebrafish. During the same program, Rick was able to attend a research talk about studying blood flow changes in Alzheimer's disease (AD) using two-photon microscopy in mice, given by none other than his eventual PhD advisor Dr. Chris Schaffer. In his senior year at Buffalo, Rick worked as an undergraduate researcher in the lab of Dr. Anirban Dutta, using VICON imaging to analyze gait patterns of healthy participants in preparation for using the same technology to correct for impaired gait in patients with Parkinson's disease. Outside of the lab, Rick was an avid intramural and club sports participant, including volleyball, soccer, and most notably was a member of an intramural flag football dynasty.

After becoming fascinated with neuroscience and in vivo imaging techniques to study the brain in living organisms, Rick joined the Biomedical Engineering Ph.D. program at Cornell University in the Fall of 2019. There, he joined the lab of Dr. Chris Schaffer and Dr. Nozomi Nishimura to research what changes in neural activity could contribute to an improvement in memory performance after rescuing cerebral blood flow deficits in an AD mouse model. A few

years into his Ph.D., Rick was asked by Dr. Schaffer if he would want to lead a collaborative study with the lab of Dr. Alex Kwan to understand the effects of psilocybin on neurovascular coupling. Knowing nothing about psychedelics, Rick agreed, a decision that would be a major influence on his future career trajectory. Rick has been a middle author on 2 manuscripts, one of which was the result of his time working in the lab of Dr. Michael Kaplitt at Weill Cornell Medicine in the summer of 2021, as part of the Clinical Immersion Program. Rick was awarded the NSF Graduate Research Fellowship, which fully funded his research for 3 years of his Ph.D. While at Cornell, Rick also served as Outreach Co-Chair of the Biomedical Engineering Society graduate student chapter at Cornell and was a four-time undefeated BMES Cornhole Tournament Champion, alongside his partner Dr. Ruben Trujillo.

Following graduation, Rick will be working as a post-doc with Dr. Robert Malenka and Dr. Boris Heifets at Stanford University, studying mechanisms of psychedelic drug action.

Dedicated to my family and friends, without whose support this would not have been possible.

ACKNOWLEDGMENTS

Thanking everyone who has supported me in some way throughout this Ph.D. would be longer than the dissertation itself. I have had an amazing experience here at Cornell and would like to acknowledge all you for helping me get to where I am today.

Firstly, I would like to thank my advisor Dr. Chris Schaffer for supporting me throughout these last 6 years. Your mentorship has helped me grow immensely as a researcher and an individual and has prepared me for taking on the next steps of my career. I'd also like to thank Dr. Nozomi Nishimura, my unofficial second advisor. It has been incredible to work in your lab and be able to be a part of such a great group. Thank you to the other members of my thesis committee: Dr. Ian Ellwood, Dr. Warren Zipfel, and Dr. Alex Kwan, for providing critical feedback and guidance to me on my research. And especially thank you to Alex for joining our department, as Chris would never have asked me to start a research project involving psychedelics.

There are so many people who have contributed to this work that I would like to thank. Most importantly, thank you to Dr. Matt Isaacson, my postdoc advisor in the lab. Joining the lab at the same time was incredibly fortunate for me. Absolutely none of this work would have been possible without your help, research, and mentorship. I have learned so much from you and appreciate all the time you have taken to mentor me, especially convincing me that it wasn't the end of the world when I hit some minor bumps in my Ph.D. Thank you to past and current members of the Schaffer-Nishimura Lab who helped and taught me so much, including but not limited to Mike Lamont, Chi-Yong Eom, Kawasi Lett, Laura Berkowitz, Daniel Rivera, Oliver Bracko, Nancy Ruiz, Lianne Trigiani, Becka Irwin, David Xiang, Nicole Chernavsky, Seth Lieberman, Silvia Zhang, and many more. Thank you to the undergrads in our lab I had the

pleasure of working with Katharine Yang, Matthew Yi, and Keri Yamaguchi. Thank you to collaborators from other labs including Clara Liao, Sam Woodburn, Neil Savalia, Yating Yang, Hongyu Chang, Xi Chen, Tianyu Wang, Aaron Mok. From Weill Cornell Dr. Michael Kaplitt and Dr. Santiago Unda.

Thank you to 515 N Aurora St. for housing me these last 6 years, as well as the 14 roommates that I have lived with in my time here. Thank you to Leo's Legion and Ithaca soccer for being able to continue to play a sport I love. Thank you, Matt, Justin, Julien, Martik, Peter, Nick, Patrick, for playing Mario Strikers and losing to me in smash. Thank you to my UB friends for getting together at Delhi every year and spreading democracy across the galaxy. An immense thank you to Becka (Dr. BOB), Ruben (Ruboo) and Sera (Cookies), my closest friends I have had during my time here, and who have helped me through so much, including Covid-19. Thank you for all the laughs and late nights of Avatar Pong, charades, Taco Tuesdays, cornhole championships, and hundreds of hours of smash bros. You have made this such an incredible experience and I am so thankful that I've been able to share this time with you. Thank you to my godson Cosmo and anxious Higgins for being such handsome and amazing dogs, keep up the great work. Thank you to my own family's dogs, Coby and Jackie. Thank you, Coby, for being my best friend for 15 years. Jackie, you're okay too. Finally, thank you to my family, grandparents, cousins, aunts, and uncles. My mom Ellen, my dad Paul, my brothers Cory and Keith, and their partners Brandi and Chris. Thank you for supporting me throughout this entire Ph.D. I am so lucky to have such an amazing family.

TABLE OF CONTENTS

LIST OF FIGURES

LIST OF TABLES

CHAPTER 1: OPTICAL TOOLS FOR MEASURING NEURAL ACTIVITY AND BLOOD FLOW IN VIVO

1.1 Introduction: The Need for In Vivo Imaging

Understanding complex physiological systems in healthy and diseased states requires techniques that allow direct measurement of real-time dynamics in living organisms, for which the focus and purpose of this thesis will be on blood flow and neural activity in the brain. In vivo imaging provides spatially and temporally precise insights into physiological processes, enabling researchers to study how brain function changes in neurodegenerative disorders and in response to therapeutic interventions. Measuring brain tissue perfusion and neural activity in vivo provides critical insights into both healthy and pathological brain function. Perfusion imaging allows us to assess how blood flow supplies oxygen and nutrients to neurons, which is essential for maintaining normal brain function and supporting metabolic demands [1,2]. Neural activity measurements, on the other hand, reveal how neurons communicate, encode information, and drive behavior. When studied together, these measurements offer a deeper understanding of neurovascular coupling — how changes in neural activity influence blood flow regulation. This is particularly important for investigating conditions such as Alzheimer's disease, stroke, and psychiatric disorders, where disruptions in neurovascular function contribute to cognitive and functional impairments [3,4,5,6]. Even in healthy brains, simultaneous imaging of neural activity and perfusion can help us understand fundamental principles of brain function, plasticity, and homeostasis. By studying these dynamics in vivo, researchers can also assess how therapeutic interventions, such as pharmacological treatments or neuromodulation techniques, impact both

neural function and blood supply, providing a more comprehensive picture of brain health and disease. This chapter provides an overview of key optical imaging techniques used to measure neural activity and brain blood flow, covering methods for fluorescent labeling, high-resolution microscopy, widefield imaging, and data analysis approaches.

1.2 Fluorescent Labeling Strategies for Optical Imaging

Since most brain structures and physiological processes are not inherently fluorescent, specialized labeling techniques are required to visualize them. Of particular interest are detecting activity and structural changes of various cell types, including neurons, astrocytes, glial cells, and more, as well as of dynamic systems such as perfusion of brain tissue.

1.2.1 Genetically Encoded Indicators

Genetically encoded indicators are fluorescent proteins engineered to respond to specific physiological changes, allowing real-time imaging of cellular activity. These indicators are typically introduced into cells via viral vectors such as adeno-associated virus (AAV), enabling targeted expression in specific neuronal populations [7,8,9].One of the most widely used examples is genetically encoded calcium indicators (GECIs), such as GCaMP, which increase fluorescent capability in response to conformational changes induced by intracellular calcium fluctuations. Since calcium influx closely follows neuronal activation, GCaMP provides an indirect but highly reliable measure of neural activity, making it an invaluable tool for in vivo imaging [10,11,12,13,14].

A major advantage of calcium imaging over direct electrophysiological recordings is its compatibility with modern optical imaging techniques, allowing for high spatial resolution and long-term recordings in awake, behaving animals [15]. While calcium indicators provide robust

signals on a timescale well suited for monitoring neural dynamics, they have limitations in capturing the millisecond-scale speed of action potentials. In contrast, genetically encoded voltage indicators (GEVIs) offer direct fluorescence-based measurements of membrane potential changes, enabling real-time tracking of action potentials and subthreshold events [16,17,18]. However, GEVIs present technical challenges, including lower signal-to-noise ratios, greater photobleaching, and the need for high-speed imaging systems, which currently limit their widespread adoption compared to calcium indicators.

In addition to viral delivery, recent advances in genetic engineering have facilitated the development of transgenic mouse lines that stably express these genetically encoded indicators without the need for viral injections [19,20]. These approaches enable precise, long-term expression in specific cell types and brain regions, reducing the invasiveness of traditional viral delivery methods, however issues such as aberrant cortical activity in GcaMP6-expressing transgenic mouse lines are necessary to consider [21]. By using Cre-lox systems, researchers can achieve conditional expression in genetically defined populations, such as excitatory or inhibitory neurons [22,23]. Crossbreeding various transgenic lines allows for cell-type and region-specific expression, providing a powerful tool for studying neuronal circuits under both normal and pathological conditions.

These advances in genetically encoded indicators, combined with improvements in imaging technology, continue to refine our ability to measure neural activity with high specificity, spatial resolution, and chronic stability in vivo.

1.2.2 Vascular Labeling

Fluorescent vascular labeling enables high-resolution imaging of cerebral blood flow by visualizing blood vessels and tracking individual blood cells in vivo. One widely used approach involves injecting fluorescently conjugated dextrans, with labels such as Texas Red or fluorescein (FITC), which bind to the blood plasma and provide contrast for imaging vascular structures. These dextrans, when injected retro-orbitally or intravenously into a live mouse, rapidly distribute throughout the circulatory system, making the plasma fluoresce while leaving blood cells unlabeled. This results in a negative contrast effect, where individual red blood cells appear as dark voids moving against a bright fluorescent background, facilitating precise tracking of blood flow dynamics [24].

High-resolution two-photon microscopy or laser-scanning imaging can then be used to measure red blood cell (RBC) velocity within individual vessels [24,25,26]. By tracking the movement of these unlabeled cells over time, researchers can quantify cerebral blood flow (CBF) at both macroscopic and microscopic levels, providing critical insights into neurovascular coupling and cerebrovascular health. This approach is particularly valuable in studies of stroke, Alzheimer's disease, and other conditions where blood flow regulation is disrupted.

These labeling strategies form the foundation for high-resolution in vivo imaging using both two-photon microscopy and widefield multimodal imaging.

1.3 Two-Photon Microscopy: High-Resolution Imaging of Physiological Phenomenon

Two-photon excitation fluorescence microscopy (2PE, 2PEF or 2PFM) is a high-resolution imaging technique developed here at Cornell University in the lab of Watt Webb in 1990 [27]. This

technique requires the nonlinear absorption of two photons, near simultaneously, by a fluorophore to reach an excited state and emit a photon as it decays back to the ground state (Fig. 1.1 A) [28,29]. A pulsed laser is focused to concentrate the photons (increase their spatial density) to thereby increase probability of simultaneous absorption for 2P excitation. The probability of this occurrence is very low throughout most parts of the tissue, however, it increases exponentially at the focal point. A pulsed laser is used as the excitation source, providing high peak power per laser pulse. This enables a high influx of low energy and longer wavelength photons temporally concentrated in the range of femtoseconds, while providing lower average laser power to prevent live tissue damage. The resultant emitted fluorescent signal from a single absorption event is then comprised of a single photon of half the wavelength and double the energy of the excitation photons. This results in a much more localized point of excitation and fluorescent emission, leading to an ability to get very high signal-to-noise signal (Fig. 1.1 B). Compared to one-photon (1P) imaging techniques, 2PFM utilizes longer wavelength laser photons, which therefore have lower energy than shorter wavelength laser photons used in 1P. The use of 2PFM results in several advantages over 1P, including reduced photodamage and photobleaching of the focus and

surrounding volume, reduced background fluorescence, and submicrometer resolution at volumes several hundred micrometers thick [30].

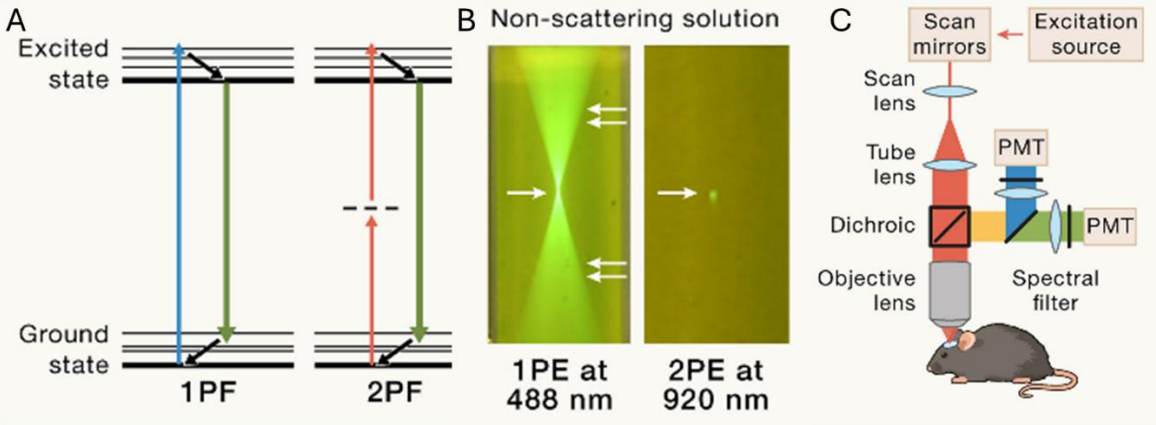

Figure 1.1 Principle and implementation of multiphoton laser scanning fluorescence microscopy (MPFM).1 **A:** Simplified demonstration of 1P vs 2P transition states. The simultaneous absorption of two photons, each at half the energy of a corresponding 1P imaging photon, excites a fluorophore, which then emits a fluorescent photon as it return to its ground state. **B:** 2P fluorescence generation confined to a focal volume compared to 1P where fluorescence is generated both in and out of the focal plane. **C:** A typical implementation of a multiphoton laser scanning microscope with epi-fluorescence collection using two photomultiplier tubes (PMTs).[28] (Adapted from Xu 2024)

A 2PFM microscope consists of several key components that work together to enable deep tissue imaging with high resolution and minimal photodamage (Fig. 1.1 C). At the core of the system is the femtosecond-pulsed laser, typically a Ti:Sapphire laser, which generates ultrafast pulses of near-infrared (NIR) light. Such lasers have an output power of ~2 W, either at a fixed or tunable wavelength, the latter of which being between ~ 670-1070 nm. As longer-wavelength light is scattered less than shorter, this NIR light penetrates deeper into biological tissues than visible wavelengths and is essential for the nonlinear absorption process in two-photon excitation. The laser beam is directed through a beam expander and pulse compressor, which optimizes the beam profile and corrects for dispersion, respectively. Laser power is precisely controlled using a combination of Pockels cells (electro-optic modulators, EOMs), acousto-optic

modulators (AOMs), or wave plates (e.g., half-wave plates, HWPs) and polarized beam splitters/cubes (PBS). Pockels cells rapidly modulate laser intensity by altering the polarization of the beam in response to an applied voltage, often used for fast, real-time power adjustments. AOMs apply sound waves to a crystal to produce a variable amplitude diffraction grating to diffract a portion of laser light, allowing fine-tuned control of power via amplitude modulation and frequency shifts to alter the diffraction efficiency. HWPs, when paired with polarizing beam splitters (PBSs), provide a slower but more stable and precise way to adjust intensity by rotating the polarization of the laser before it enters the imaging path. These components work together to ensure optimal excitation efficiency while preventing photodamage and maintaining stable imaging conditions.

Next, the beam is steered by a pair of galvanometric or resonant scanning mirrors, which rapidly deflect the laser to scan across the sample. The scanned beam passes through a tube lens and scan lens, which together form a 4f optical system that prevents vignetting and ensures uniform illumination across the field of view. The beam then encounters a short-pass dichroic mirror, which reflects the excitation light toward the objective lens while allowing emitted fluorescence to pass through, or vice versa using a long-pass dichroic. The objective lens, typically a high numerical aperture (NA) water-immersion lens, focuses the laser into the sample, where two-photon absorption occurs at the focal point, generating fluorescence confined to a small volume.

The emitted fluorescence is collected by the same objective and passes back through the dichroic mirror, where it is separated from the excitation path. A series of bandpass filters and other dichroics help eliminate unwanted wavelengths, isolating the emitted signal from background light, and guiding desired wavelengths to different recording channels. Finally, the

fluorescence signal is detected by photomultiplier tubes (PMTs), which are highly sensitive to low-light signals. These detectors convert photons into electrical signals, which are processed to construct an image.

Different scanning modes can be used to optimize imaging for specific applications, and for the purposes of this thesis we will focus on methods used for recording neural activity or blood flow.

1.3.1 Neuronal activity

Two-photon fluorescence microscopy is a widely used technique that can be used for measuring neuronal calcium activity, providing high spatial resolution and depth penetration while minimizing phototoxicity [31,32,28]. The most common imaging modality for capturing neuronal activity is galvanometric mirror frame scanning, which sequentially moves a laser beam line by line, acquiring an entire field of view pixel by pixel. This approach offers excellent spatial resolution but is limited by slower scanning speeds, typically used in the range of several hertz (Hz), restricting its ability to capture fast neuronal dynamics. Sacrificing certain imaging parameters can allow for much higher frame rates on the scale of hundreds of Hz. However, it is particularly useful for imaging cellular-resolution calcium activity, where neurons expressing genetically encoded calcium indicators (GECIs) such as GCaMP emit fluorescence in response to intracellular calcium influx following neuronal activation. While the rise and decay times of calcium indicators vary depending on the variant used, they remain within the constraints of galvanometric scanning, making this method well-suited for capturing population-level neuronal activity over extended time periods.

For applications requiring higher temporal resolution, resonant scanning is the preferred 2PFM modality.[33] Unlike galvanometric scanning, resonant scanning uses a rapidly oscillating mirror that continuously moves at a fixed high frequency (typically 8–12 kHz per line), allowing for dramatically faster frame rates, typically used around 30-100 Hz (at 512-128 lines/frame). This speed advantage enables near real-time imaging of rapid calcium transients, facilitating the study of fast synaptic and network-level activity. Although resonant scanning generally produces a slightly lower signal-to-noise ratio (SNR) due to the continuous oscillatory motion of the mirror, the increase in temporal resolution makes it ideal for capturing fast neuronal dynamics, such as spontaneous and evoked calcium transients in large neuronal populations. Consequently, resonant scanning is optimal for fast functional imaging, whereas galvanometric scanning is better suited for high-resolution static imaging or slow activity patterns.

Once imaging data is collected, advanced computational tools are necessary to extract meaningful physiological information. Suite2p, for instance, provides automated neuron detection and activity extraction from 2P datasets, enabling large-scale analysis of neuronal dynamics (Fig 1.2 C) [34]. Other algorithms, such as CaImAn[35] and CNMF-E[36], incorporate machine learning approaches to improve segmentation and denoise signals, ensuring accurate extraction of calcium transients from background fluorescence. These computational methods are essential for transforming raw imaging data into interpretable neuronal activity maps, facilitating quantitative studies of network dynamics and neurophysiological processes.

1.3.2 Blood Flow

Unlike neuronal calcium activity, which occurs on a slower timescale, cerebral blood flow is a highly dynamic process that requires high-frame-rate imaging to accurately capture rapid changes in flow velocity. One of the most effective methods for measuring blood flow at the

microscopic level is 2PEF linescan imaging, which provides high temporal resolution for tracking the movement of RBCs within cerebral vessels [24,25,26].

To achieve contrast between the plasma and RBCs, high-molecular-weight fluorescently tagged dextrans (e.g., Texas Red, fluorescein (FITC)) are injected intravenously, saturating the blood plasma with fluorescence while RBCs remain non-fluorescent. This negative contrast allows RBCs to be visualized as dark shadows traveling through the vasculature, enabling precise tracking of their movement.

A standard approach involves scanning a laser along the centerline of a blood vessel, continuously acquiring fluorescence intensity changes over time. The resulting image appears as a spatiotemporal plot where the x-axis represents distance along the vessel and the y-axis represents time. The displacement of RBCs in this plot forms streaks, and the slope of these streaks corresponds to instantaneous RBC velocity (Fig. 1.2B). This method allows for highly precise blood flow measurements in capillaries, arterioles, and venules, though it is limited in its ability to measure larger vessels, where flow velocities exceed the temporal resolution of the imaging system.

To extend this method beyond individual vessel imaging, arbitrary linescanning enables high-speed measurements of multiple vessels simultaneously. This technique involves dividing the scan path into segments connected by splines, allowing for customized scanning trajectories across several regions of interest. This approach is particularly advantageous for capturing both flow velocity and vessel diameter. Blood flow velocity is determined from the displacement of RBCs over time, as described above. Vessel diameter is measured by extracting the fluorescence intensity profile perpendicular to the vessel axis and calculating the full-width at half-maximum (FWHM) of the intensity profile [24] (Fig. 1.2).

A significant advantage of 2PEF linescanning is its ability to be integrated with neuronal calcium imaging, enabling the simultaneous measurement of cerebral blood flow and neural activity dynamics. By incorporating regions of interest (ROIs) corresponding to neurons within the same arbitrary linescan path, calcium transients from individual neurons can be recorded alongside blood flow measurements (Fig. 1.2A). This combined approach is essential for understanding neurovascular coupling, the relationship between neuronal activation and vascular responses.

Overall, 2PEF linescan imaging provides a powerful tool for investigating microvascular dynamics, allowing for precise measurements of RBC velocity, vessel diameter, and neuronal activity within the same imaging field. These insights are crucial for studying cerebral blood flow regulation, neurovascular coupling, and pathological alterations in vascular function, such as those observed in Alzheimer's disease and stroke.

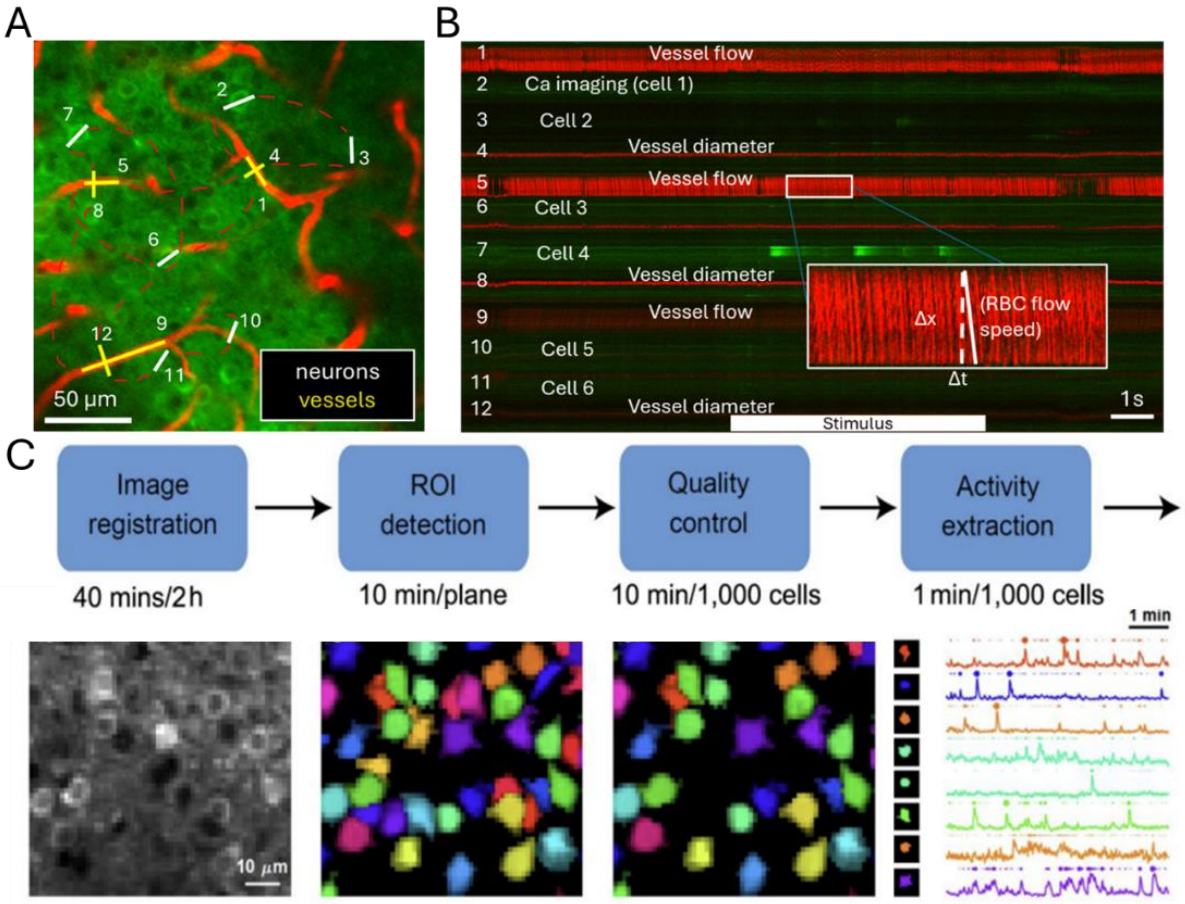

Figure 1.2 Multiphoton imaging of neural activity and blood flow in vivo at the microscale. A: Frame scan of calcium fluorescence in neurons (green) and vasculature (red), and overlayed arbitrary linescan imaging path. Dotted lines indicate non-recorded path, yellow and white lines indicate recorded ROI signal. **B:** Linearized linescan imaging corresponding to path drawn in A, numbers indicate individual ROIs. White box shows example calculation of RBC flow speed by calculating slope of line. **C:** Suite2P image processing pipeline [34]. (Adapted from Pachitariu 2016)

1.4 Widefield Multimodal Imaging: Large-Scale Measurement of Brain Activity and Perfusion

While 2PM provides microscale insights, widefield imaging techniques allow measurement of broader cortical dynamics and blood flow regulation. Simultaneous multimodal recording of blood flow and calcium activity enables researchers to measure the direct relationships between neuronal activation and vascular responses, particularly how increases in brain activity result in a

localized increase in perfusion, a process known as neurovascular coupling. Various techniques can be used to record blood flow dynamics, particularly laser speckle contrast imaging (LSCI) and optical intrinsic imaging (OII). A combined approach using 1-photon laser excitation and LEDs at various wavelengths enables acquisition of these measurements in rapid succession, making the data collection effectively simultaneous. [37,38].

1.4.1 Laser-Speckle Contrast Imaging

Laser speckle contrast imaging (LSCI) is a high-speed, label-free optical technique used to measure cerebral blood flow by analyzing the speckle pattern produced when coherent laser light scatters off moving red blood cells in the microvasculature [39,40,41,42]. A laser illuminates the cortical surface, and the scattered light undergoes constructive and destructive interference, forming a random grainy speckle pattern at the detector, typically a high-speed camera.

Regions with static structures, such as brain parenchyma where microvascular flow is slow or absent, produce a relatively stable speckle pattern over time. In contrast, areas with dynamic movement, such as blood vessels where red blood cells are constantly in motion, cause the speckle pattern to fluctuate at a rate proportional to blood flow speed. By analyzing these temporal fluctuations, LSCI generates real-time, high-resolution maps of relative blood flow across the cortical surface.

This appears in the image as variations in pixel intensity. By integrating the fluctuating speckle pattern over a few milliseconds, slower-moving regions, such as the parenchyma, exhibit a wider range of gray values, while faster-moving regions, like blood vessels, display a narrower range. This reduced variation in intensity results in a blurred appearance, with greater blurring

corresponding to higher blood flow speeds. This blurring, or speckle contrast (K), is quantified as the ratio of intensity variation to the mean intensity within a small moving window of pixels:

$$K = \sigma / \langle I \rangle \qquad \textit{Eq. 1.1}$$

where σ is the standard deviation of pixel intensities within the window, and $\langle I \rangle$ is the mean intensity. The degree of speckle blurring is inversely related to blood flow velocity, following the approximation:

$$v \propto 1/K^2 \qquad \textit{Eq. 1.2}$$

where higher blood flow speeds result in reduced speckle contrast. By integrating speckle fluctuations over a few milliseconds, LSCI allows researchers to visualize dynamic changes in cerebral perfusion.

LSCI is widely used in functional brain imaging, neurovascular coupling studies, and cerebrovascular disease models, such as stroke and Alzheimer's disease. Its ability to provide rapid, wide-field assessment of blood flow dynamics makes it a powerful tool for studying vascular function in both health and disease.

1.4.2 Optical Intrinsic Imaging (OII)

Optical intrinsic imaging (OII) is a label-free technique that measures changes in light reflectance from the cortical surface to infer hemodynamic activity [43,44,45,46]. Since oxyhemoglobin (HbO) and deoxyhemoglobin (HbR) have distinct absorption spectra, OII can track fluctuations in tissue oxygenation and total hemoglobin concentration, serving as indirect measures of neuronal activity and vascular responses. By imaging at multiple wavelengths, researchers can separate changes in blood oxygenation from total hemoglobin levels, offering insights into neurovascular coupling (NVC) and metabolic demand across large cortical areas.

OII is widely used for functional brain mapping and has applications in both healthy and disease models.

The technique operates by detecting variations in light reflectance caused by differences in light absorption as it passes through tissue. Fluctuations in HbO and HbR alter absorption properties, leading to corresponding changes in reflectance intensity. This relationship follows the Beer-Lambert law:

$$I = I_0 e^{-\mu_a x} \qquad \textit{Eq. 1.3}$$

where is the initial light intensity, I is the transmitted light intensity after traveling a distance x through the tissue, and is the absorption coefficient, which depends on the concentration of chromophores such as HbO and HbR. The total absorption coefficient of all chromophores in the tissue is given by:

$$\mu_a(\lambda) = \sum \varepsilon_n(\lambda) c_n \qquad \textit{Eq. 1.4}$$

where $\epsilon_n(\lambda)$ is the molar absorption coefficient for each chromophore at wavelength λ and c_n is the molar concentration of each chromophore.

By recording these reflectance changes in vivo during neural stimulation, OII allows for the extraction of total hemoglobin concentration as well as the relative contributions of HbO and HbR. Imaging at two or more wavelengths enables researchers to solve a system of linear equations to quantify changes in oxygenated, deoxygenated, and total hemoglobin.

These real-time measurements provide valuable information on cerebral blood oxygenation, a critical component of functional neuroimaging. Notably, blood oxygenation level-dependent (BOLD) functional magnetic resonance imaging (fMRI) relies on similar principles, where

changes in HbO and HbR modulate local magnetic field properties. Since increased neuronal activity leads to a localized increase in oxygenated blood supply to meet metabolic demands, this relationship — known as neurovascular coupling — enables fMRI to infer neural activity noninvasively in humans. In vivo OII offers a comparable approach in animal models, providing high-resolution measurements of blood oxygenation dynamics that can be directly related to human fMRI studies.

1.4.3 Widefield Fluorescence Imaging

Widefield fluorescence imaging provides a complementary approach to measuring neural activity, using genetically encoded calcium indicators (e.g., GCaMP) or voltage-sensitive dyes to capture large-scale cortical activity [37,47]. Unlike OII and LSCI, which measure blood flow and hemodynamics, fluorescence imaging directly reports neuronal activation through intracellular calcium transients or membrane potential changes. Exciting fluorophores with LEDs or lasers and capturing the emitted light with sensitive cameras enables high-speed, population-level recordings of neuronal dynamics across broad cortical areas. Widefield calcium imaging is particularly useful for examining network-wide activity patterns, state-dependent neural processing, and how neural circuits respond to disease and pharmacological interventions.

Optical intrinsic imaging can be used to reliably detect changes in hemodynamic responses, and with appropriate corrections, it enables more accurate functional mapping of neural activity. In addition to measuring blood oxygenation and total hemoglobin concentration, OII plays a crucial role in correcting for absorption-related artifacts in widefield calcium imaging. Calcium indicators such as GCaMP, commonly used to examine neural activity, have a peak excitation at 496 nm and emission at 513 nm [48]. However, these wavelengths are differentially affected by changes in oxygenated and total hemoglobin concentrations due to neurovascular coupling,

leading to confounded fluorescence signals (Fig 1.3) [37].

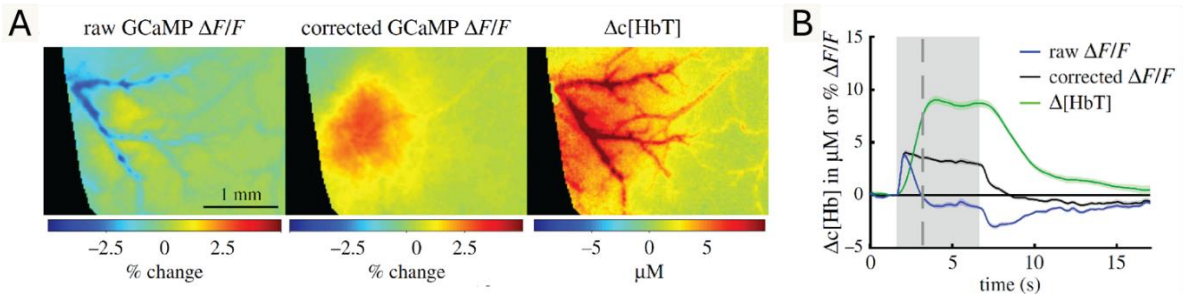

Figure 1.3 Correcting for hemoglobin absorption confounds of GCaMP fluorescence signal. A: 2 Raw and hemoglobin absorption corrected calcium fluorescence, as well as total hemoglobin (HbT) signal. **B:** Signal traces corresponding to example frames in A, demonstrating significant confound of raw fluorescence signal, and correction restoring accurate signal. [37] (Adapted from Ma 2016)

Fluctuations in hemoglobin concentration, particularly during functional hyperemia, introduce an optical artifact due to the strong absorption properties of oxy- and deoxyhemoglobin. As hemoglobin absorbs both excitation and emitted fluorescence light, local changes in blood volume and oxygenation can alter the detected fluorescence intensity independent of actual neural activity. Several methods have been developed to correct for these absorption-related distortions. One approach involves using diffuse green reflectance at an isosbestic wavelength, where oxygenated and deoxygenated hemoglobin have equal absorption, to minimize hemodynamic contamination. Another method, the excitation-emission attenuation (Ex-Em) approach, estimates how hemoglobin absorption alters both excitation and emission light and applies a correction factor, though it requires an additional measurement at a non-excitation wavelength. Blind-source separation techniques, such as principal component analysis (PCA), can also be employed to isolate neural activity from hemodynamic signals. Of these methods, the Ex-Em approach is preferred due to its specificity in accounting for both excitation and emission absorption effects. By integrating OII-based corrections, fluorescence imaging can

more accurately reflect neuronal activity rather than systemic vascular changes, improving the reliability of neurophysiological interpretations (Fig 1.3).

1.4.4 Integration of Multimodal Widefield Imaging

When combined in a multimodal imaging system, these techniques provide a comprehensive view of brain function (Fig 1.4 A). By rapidly cycling through different imaging modalities, researchers can simultaneously record neuronal activity (fluorescence imaging. Fig 1.4 B and E), hemodynamic responses (OII, Fig 1.4 C and F), and cerebral blood flow (LSCI, Fig 1.4 D and G). This approach allows for precise investigations into how neurovascular coupling is altered in different states, including during cognitive tasks, pharmacological manipulations, and disease progression [37,38,47,49,50]. The ability to capture multiple physiological signals with high temporal and spatial resolution makes widefield multimodal imaging a powerful tool for studying brain function at a systems level.

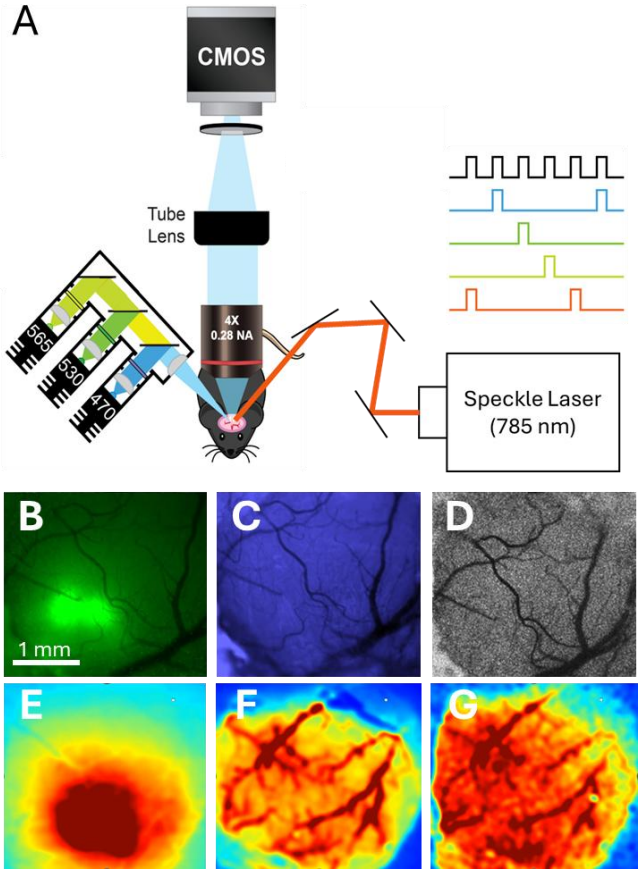

Figure 1.4 Widefield multimodal imaging. A: Simultaneous multimodal imaging in rapid succession of speckle laser (785 nm) and 470, 530 and 565 nm LED excitation. **B,C,D:** Example GCaMP6f calcium fluorescence, reflectance (HbT) and speckle contrast imaging frames. **E,F,G:** Example heat maps of single frames from each imaging mode. (A adapted from Rivera 2023 [54])

1.5 Awake vs Anesthetized Imaging

In vivo imaging has become an essential tool for investigating neural activity, cerebral blood flow, and neurovascular coupling. While anesthesia has long been used to facilitate imaging experiments by providing a controlled and stable environment, it introduces several physiological confounds that can significantly impact experimental outcomes. This has led to an increasing emphasis on awake imaging, which, despite its challenges, allows for the study of biological processes under more natural conditions. [51, 52]

The use of anesthetics has been particularly advantageous for techniques such as two-photon microscopy, where motion artifacts caused by breathing and voluntary movement can severely degrade image quality over time. By immobilizing the subject, anesthesia enables high spatial resolution imaging and reduces variability across experimental sessions. However, recent research has demonstrated that anesthesia alters multiple physiological processes, including cerebral blood flow, neural activity, and inflammation. Most anesthetics, such as isoflurane and ketamine/xylazine, induce vasodilation and lower blood pressure, leading to changes in cerebral perfusion. At the neuronal level, anesthesia suppresses activity by enhancing inhibitory GABAergic signaling, thereby distorting network dynamics and reducing spontaneous and stimulus-evoked activity. Additionally, some anesthetic agents have been linked to neuroinflammatory responses, which can further complicate the interpretation of experimental results. These effects are highly dependent on the depth and duration of anesthesia, requiring careful monitoring of heart rate and breathing rate to maintain physiological stability. Another significant consideration is thermoregulation, as anesthetized mice are unable to maintain body temperature, necessitating external heating to prevent hypothermia. (Fig 1.5 A and B)

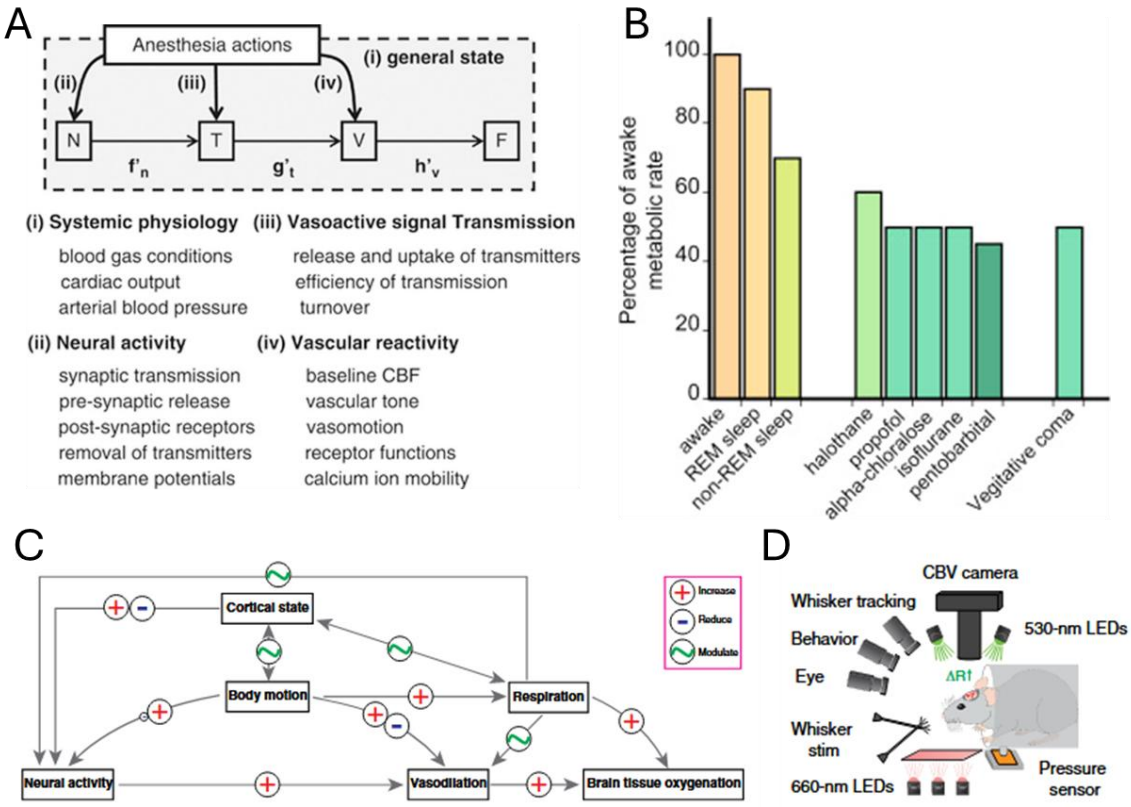

Figure 1.5 Effects of anesthesia and awake imaging on neural activity and blood flow. A: 3 Summary of the effects of anesthesia on neurovascular coupling.[52] **B:** Summary plot of measured brain metabolic rates under different anesthetics and conditions.[51] **C:** Schematic showing how the movement-related signals modulate the relationship between neural activity and brain hemodynamics. **D:** Awake imaging and behavioral monitoring of a restrained mouse in a plastic tube.[53] (Adapted from Zhang 2022)

Due to these limitations, many researchers have shifted toward awake imaging, which allows for more physiologically relevant measurements [53]. Awake imaging provides the opportunity to study spontaneous and evoked neuronal activity without the suppressive effects of anesthetics and to examine neurovascular coupling under natural conditions. It also enables the integration of behavioral paradigms, such as sensory processing and decision-making, with real-time imaging of neural and vascular responses. However, this approach presents several technical and biological challenges. Head fixation, necessary for most high-resolution imaging modalities, can induce stress in mice, leading to changes in neural activity and behavioral states that could

confound experimental results (Fig 1.5 C) [53,54]. To mitigate this, animals must undergo habituation protocols, which vary widely between laboratories and can be highly time-consuming. The effectiveness of habituation depends on factors such as the specific training regimen, the duration of the acclimation period, and even the experimenter's handling techniques, making standardization difficult.

Even with habituation, some level of stress may persist, necessitating behavioral monitoring to assess whether changes in imaging data correlate with animal discomfort or agitation. Parameters such as pupil size, whisking behavior, and body movement are often tracked alongside imaging data to ensure that physiological measurements are not confounded by stress-related artifacts (Fig 1.5 D). Despite these difficulties, awake imaging remains the preferred method for capturing dynamic, biologically relevant processes. Nevertheless, anesthetized imaging continues to be valuable for high-resolution anatomical imaging and experiments that require long acquisition times without motion interference.

Ultimately, the choice between anesthetized and awake imaging depends on the specific research question being addressed. While anesthesia facilitates stable and reproducible imaging, it introduces pharmacological confounds that may obscure the natural physiological state of the brain. Awake imaging, though technically more challenging, allows for the study of neural and vascular dynamics under more realistic conditions. Many studies incorporate a combination of both approaches, using anesthesia for structural imaging and awake imaging for functional studies, to obtain a comprehensive understanding of the system under investigation.

1.6 Conclusion

Optical imaging techniques provide an unparalleled window into brain function, allowing researchers to study how neuronal and vascular activity interact in both healthy and diseased states. By combining precise fluorescent labeling, high-resolution microscopy, and population-scale imaging, in vivo optical methods enable detailed investigations into neurovascular coupling, disease pathology, and therapeutic interventions.

References

1. Blake E. McGehee *et al.* Brain perfusion imaging: How does it work and what should I use? *J. Magn. Reson. Imaging* **36**, 1257–1272 (2012).
2. Max Wintermark *et al.* Comparative overview of brain perfusion imaging techniques. *J. Neuroradiol.* **32**, 294–314 (2005).
3. Amy R. Nelson *et al.* Neurovascular dysfunction and neurodegeneration in dementia and Alzheimer's disease. *Biochim. Biophys. Acta* **1862**, 887–900 (2016).
4. E. S. Sanches, Daniela Simões, F. Baptista, & Ana Paula Silva. Neurovascular dysfunction in psychiatric disorders: Underlying mechanisms and therapeutic approaches. *Eur. J. Clin. Invest.* (2024) doi:10.1111/eci.14319.
5. Wei Cai *et al.* Dysfunction of the neurovascular unit in ischemic stroke and neurodegenerative diseases: An aging effect. *Ageing Res. Rev.* **34**, 77–87 (2017).
6. Xiaoming Hu *et al.* Cerebral Vascular Disease and Neurovascular Injury in Ischemic Stroke. *Circ. Res.* **120**, 449–471 (2017).

7. Michael F. Naso *et al.* Adeno-Associated Virus (AAV) as a Vector for Gene Therapy. *BioDrugs* **31**, 317–334 (2017).

8. Susanne K. Golm, Wolfgang Hübner, & Kristian M. Müller. Fluorescence Microscopy in Adeno-Associated Virus Research. *Viruses* **15**, 1174–1174 (2023).

9. Leila Haery *et al.* Adeno-Associated Virus Technologies and Methods for Targeted Neuronal Manipulation. *bioRxiv* 759936 (2019) doi:10.1101/759936.

10. Loren L. Looger *et al.* Fast and sensitive GCaMP calcium indicators for imaging neural populations. *bioRxiv* (2021) doi:10.21203/rs.3.rs-1061816/v1.

11. Lin Tian *et al.* Imaging neural activity in worms, flies and mice with improved GCaMP calcium indicators. *Nat. Methods* **6**, 875–881 (2009).

12. Yan Zhang & Loren L. Looger. Fast and sensitive GCaMP calcium indicators for neuronal imaging. *J. Physiol.* (2023) doi:10.1113/jp283832.

13. Tsai Wen Chen *et al.* Ultrasensitive fluorescent proteins for imaging neuronal activity. *Nature* **499**, 295–300 (2013).

14. Atsushi Miyawaki *et al.* Fluorescent indicators for Ca2+based on green fluorescent proteins and calmodulin. *Nature* **388**, 882–887 (1997).

15. Joshua H. Siegle *et al.* Reconciling functional differences in populations of neurons recorded with two-photon imaging and electrophysiology. *bioRxiv* (2020) doi:10.1101/2020.08.10.244723.

16. Yang Hh *et al.* Subcellular Imaging of Voltage and Calcium Signals Reveals Neural Processing In Vivo. *Cell* **166**, 245–257 (2016).

17. Simon Chamberland *et al.* Fast two-photon imaging of subcellular voltage dynamics in neuronal tissue with genetically encoded indicators. *eLife* **6**, (2017).

18. Ahmed S. Abdelfattah *et al.* Bright and photostable chemigenetic indicators for extended in vivo voltage imaging. *Science* **365**, 699–704 (2019).

19. L.A. Kasatkina, Ludmila A. Kasatkina, Vladislav V. Verkhusha & Verkhusha, V. V. Transgenic mice encoding modern imaging probes: Properties and applications. *Cell Rep.* **39**, 110845–110845 (2022).

20. Waleid Mohamed El-Sayed Shakweer, Alexander Krivoruchko, Sh M Dessouki, & A. A. Khattab. A review of transgenic animal techniques and their applications. *J. Genet. Eng. Biotechnol.* **21**, (2023).

21. Nicholas A. Steinmetz *et al.* Aberrant Cortical Activity In Multiple GCaMP6-Expressing Transgenic Mouse Lines. *bioRxiv* 138511 (2017) doi:10.1101/138511.

22. András Nagy & Nagy, A. Cre recombinase: the universal reagent for genome tailoring. *Genesis* **26**, 99–109 (2000).

23. Micheal A. McLellan *et al.* Cre-loxP-Mediated Recombination: General Principles and Experimental Considerations. *Curr. Protoc. Mouse Biol.* **7**, 1–12 (2017).

24. Andy Y. Shih *et al.* Two-Photon Microscopy as a Tool to Study Blood Flow and Neurovascular Coupling in the Rodent Brain. *J. Cereb. Blood Flow Metab.* **32**, 1277–1309 (2012).

25. Emmanuelle Chaigneau, Emmanuelle Chaigneau, Serge Charpak, & Serge Charpak. Measurement of Blood Velocity With Laser Scanning Microscopy: Modeling and Comparison of Line-Scan Image-Processing Algorithms. *Front. Physiol.* **13**, (2022).

26. David Kleinfeld *et al.* Fluctuations and stimulus−induced changes in blood flow observed in individual capillaries in layers 2 through 4 of rat neocortex. *Proc. Natl. Acad. Sci. U. S. A.* **95**, 15741–15746 (1998).

27. Winifried Denk *et al.* Two-Photon Laser Scanning Fluorescence Microscopy. *Science* **248**, 73–76 (1990).

28. Chris Xu, M. Nedergaard, Deborah J. Fowell, Peter Friedl, & Na Ji. Multiphoton fluorescence microscopy for in vivo imaging. *Cell* (2024) doi:10.1016/j.cell.2024.07.036.

29. Warren R. Zipfel *et al.* Nonlinear magic: multiphoton microscopy in the biosciences. *Nat. Biotechnol.* **21**, 1369–1377 (2003).

30. Ulrike Tauer & Tauer, U. Advantages and Risks of Multiphoton Microscopy in Physiology. *Exp. Physiol.* **87**, 709–714 (2002).

31. Christine Grienberger *et al.* Two-photon calcium imaging of neuronal activity. *Nat. Rev. Methods Primer* **2**, (2022).

32. Jérôme Lecoq *et al.* Wide. Fast. Deep: Recent Advances in Multiphoton Microscopy of In Vivo Neuronal Activity. *J. Neurosci.* **39**, 9042–9052 (2019).

33. Annie Zhou *et al.* An evaluation of resonant scanning as a high-speed imaging technique for two-photon imaging of cortical vasculature. *bioRxiv* (2021) doi:10.1101/2021.11.11.468253.

34. Marius Pachitariu *et al.* Suite2p: beyond 10,000 neurons with standard two-photon microscopy. *bioRxiv* 061507 (2016) doi:10.1101/061507.

35. Andrea Giovannucci *et al.* CaImAn an open source tool for scalable calcium imaging data analysis. *eLife* **8**, (2019).

36. Pengcheng Zhou *et al.* Efficient and accurate extraction of in vivo calcium signals from microendoscopic video data. *eLife* **7**, 1–37 (2018).

37. Ying Ma *et al.* Wide-field optical mapping of neural activity and brain haemodynamics: considerations and novel approaches. *Philos. Trans. R. Soc. B* **371**, 20150360 (2016).

38. Patrick Doran *et al.* Widefield in vivo imaging system with two fluorescence and two reflectance channels, a single sCMOS detector, and shielded illumination. (2023) doi:10.1101/2023.11.07.566086.

39. Mitchell A. Davis *et al.* Imaging depth and multiple scattering in laser speckle contrast imaging. *J. Biomed. Opt.* **19**, 086001–086001 (2014).

40. J. C. Ramírez-San-Juan *et al.* Effects of speckle/pixel size ratio on temporal and spatial speckle-contrast analysis of dynamic scattering systems: Implications for measurements of blood-flow dynamics. *Biomed. Opt. Express* **4**, 1883–1889 (2013).

41. Cenk Ayata *et al.* Laser Speckle Flowmetry for the Study of Cerebrovascular Physiology in Normal and Ischemic Mouse Cortex. *J. Cereb. Blood Flow Metab.* **24**, 744–755 (2004).

42. Turgut Durdurán *et al.* Spatiotemporal Quantification of Cerebral Blood Flow During Functional Activation in Rat Somatosensory Cortex Using Laser-Speckle Flowmetry. *J. Cereb. Blood Flow Metab.* **24**, 518–525 (2004).

43. Ron D. Frostig *et al.* Cortical functional architecture and local coupling between neuronal activity and the microcirculation revealed by in vivo high-resolution optical imaging of intrinsic signals. *Proc. Natl. Acad. Sci. U. S. A.* **87**, 6082–6086 (1990).

44. Angélica Zepeda *et al.* Optical imaging of intrinsic signals: recent developments in the methodology and its applications. *J. Neurosci. Methods* **136**, 1–21 (2004).

45. Mark Tommerdahl *et al.* Optical imaging of intrinsic signals in somatosensory cortex. *Behav. Brain Res.* **135**, 83–91 (2002).

46. Sanjiv M. Narayan *et al.* Mapping Functional Activity in Rodent Cortex Using Optical Intrinsic Signals. *Cereb. Cortex* **4**, 195–204 (1994).

47. Elizabeth M. C. Hillman & Hillman, E. M. C. Optical brain imaging in vivo: techniques and applications from animal to man. *J. Biomed. Opt.* **12**, 051402–051402 (2007).

48. Hod Dana *et al.* High-performance calcium sensors for imaging activity in neuronal populations and microcompartments. *Nat. Methods* **16**, 649–657 (2019).

49. Andrew K. Dunn *et al.* Simultaneous imaging of total cerebral hemoglobin concentration, oxygenation, and blood flow during functional activation. *Opt. Lett.* **28**, 28–30 (2003).

50. Anna Devor *et al.* Coupling of total hemoglobin concentration, oxygenation, and neural activity in rat somatosensory cortex. *Neuron* **39**, 353–359 (2003).

51. Gao, Y. R. *et al.* Time to wake up: Studying neurovascular coupling and brain-wide circuit function in the un-anesthetized animal. *NeuroImage* **153**, 382 (2017).

52. Kazuto Masamoto, Masamoto, K., Iwao Kanno & Kanno, I. Anesthesia and the Quantitative Evaluation of Neurovascular Coupling. *J. Cereb. Blood Flow Metab.* **32**, 1233–1247 (2012).

53. Qingguang Zhang *et al.* Behavioral and physiological monitoring for awake neurovascular coupling experiments: a how-to guide. *Neurophotonics* **9**, (2022).

54. Konrad Juczewski *et al.* Stress and behavioral correlates in the head-fixed method: stress measurements, habituation dynamics, locomotion, and motor-skill learning in mice. *Sci. Rep.* **10**, 12245 (2020).

55. Rivera, D. Application of light to observe and manipulate physiological function in mouse models of neurological and cardiovascular disease. (Cornell University, 2023).

CHAPTER 2: NEURAL ACTIVITY IMPAIRMENTS IN ALZHEIMER'S DISEASE

2.1 Alzheimer's Disease and Cognitive Dysfunction

Alzheimer's disease (AD) is a progressive neurodegenerative disorder and the most common cause of dementia, accounting for 60–80% of dementia cases worldwide. It is characterized by a gradual decline in cognitive function, including memory loss, impaired reasoning, and difficulties with language and problem-solving. As the disease advances, individuals may lose the ability to perform daily tasks and eventually require full-time care.[1]

At the pathological level, AD is defined by two hallmark features: the accumulation of extracellular amyloid-beta (Aβ) plaques and intracellular neurofibrillary tangles composed of hyperphosphorylated tau protein [2,3]. These aggregates contribute to widespread neuronal dysfunction and synaptic loss, leading to progressive atrophy, particularly in regions critical for memory and cognition, such as the hippocampus and entorhinal cortex [4,5]. Beyond these hallmark pathologies, AD is also associated with neuroinflammation, oxidative stress, metabolic dysregulation, and vascular impairments, all of which contribute to the complexity of disease progression [6,7,8].

While most cases of AD occur sporadically with aging as the greatest risk factor, a small percentage of cases result from genetic mutations in the APP, PSEN1, or PSEN2 genes, leading to early-onset familial AD [9]. Other risk factors include APOE4 genotype, cardiovascular disease, diabetes, traumatic brain injury, and lifestyle factors such as diet and physical activity [10]. Despite extensive research, no cure currently exists for AD, though recent therapeutic strategies aim to slow disease progression by targeting Aβ pathology, tau aggregation, and neuroinflammation [11].

Emerging approaches also focus on restoring neural circuit function and modulating network activity to improve cognitive outcomes.

Cognitive impairments associated with AD arise from widespread disruptions in neural circuits, which are essential for information processing and learning [12,13]. While AD is often characterized by pathological hallmarks such as Aβ plaques and tau tangles, accumulating evidence suggests that disruptions in neural activity patterns — ranging from hyperexcitability to network desynchronization — play a central role in disease progression. These deficits are have been studied in depth using animal models of the disease, where in vivo techniques such as two-photon imaging and electrophysiology have provided mechanistic insights [14]. Studies in AD mouse models reveal profound disruptions in neural activity that correlate with cognitive decline [15,16,17,18,13]. Unlike human imaging studies, in vivo approaches allow for cell-type-specific and circuit-level investigation, enabling precise mechanistic understanding of neural network breakdown in AD. Understanding these activity impairments is critical for identifying mechanisms of cognitive decline and potential therapeutic interventions.

2.2 Neural Circuit Disruptions in AD: A Breakdown in Excitation-Inhibition Balance

A fundamental aspect of neural dysfunction in Alzheimer's disease (AD) is region-dependent alterations in network excitability [19,20]. Emerging evidence suggests that a major underlying mechanism of this dysfunction is an imbalance in the dynamic regulation between excitatory and inhibitory neural activity (E/I balance), which may be necessary to maintain normal circuit function [21,22,23,24,25]. Studies using AD mouse models indicate that Aβ-induced disruptions in E/I balance drive widespread impairments in neural activity across cortical and hippocampal circuits

[12,13]. These alterations include neuronal hyperactivity, a breakdown of slow-wave oscillations, and increased network synchrony, all of which emerge early in disease progression, even before the formation of Aβ plaques (Fig 2.1) [24]. This suggests that E/I imbalances may serve as an early marker of disease and a potential target for therapeutic intervention.

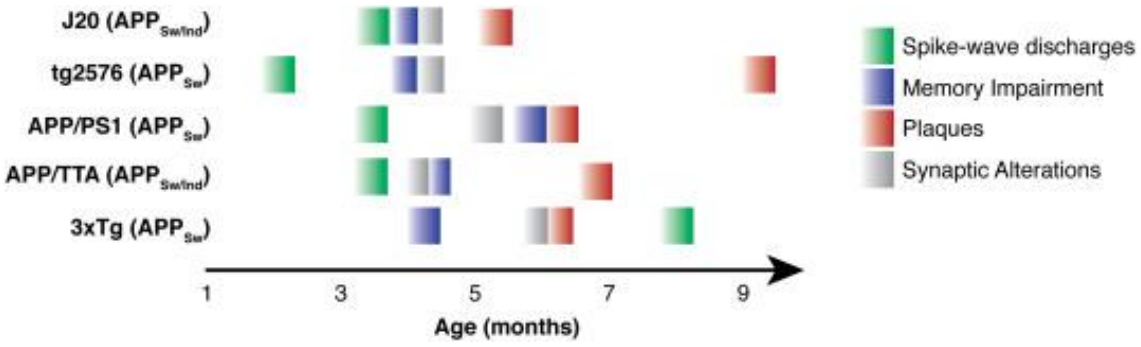

Figure 2.1 Timing of pathology in AD mouse models. 4 Comparing factors underlying or contributing to cognitive defects in specific AD mouse models as they age. All models carry the APP Swedish mutation, which increases overall Aβ levels, in conjunction with other mutations.[24] (Adapted from Varela 2019)

To develop effective treatments, a mechanistic understanding of what causes E/I imbalances in AD is necessary. One emerging hypothesis is that impairments in inhibitory interneuron function are a critical contributor to circuit dysregulation [13,26]. Dysfunction in inhibitory interneurons has been implicated in multiple neurological disorders associated with disrupted network activity, including epilepsy, schizophrenia, and AD [13,26,15,27,28]. A reduction in interneuron-mediated inhibition can lead to excessive excitatory neuron activity, increasing susceptibility to hyperexcitability and network hypersynchrony.

A key area of focus is the selective vulnerability of fast-spiking PV interneurons, which play a crucial role in maintaining network stability and synchrony [29]. These interneurons fire action potentials at high frequencies and exert rhythmic inhibitory control over pyramidal neurons, regulating fast oscillations such as gamma rhythms (30–200 Hz). Gamma oscillations are

essential for sensory processing, motor coordination, and memory formation, particularly within the hippocampus and neocortex. However, PV interneurons have exceptionally high metabolic demands due to their unique electrophysiological properties, including rapid action potential kinetics and specialized ion channel conductances. This makes them highly sensitive to metabolic stress, oxidative damage, and disruptions in glucose and oxygen supply — deficits that are prominent in AD (Fig 2.2) [30,31].

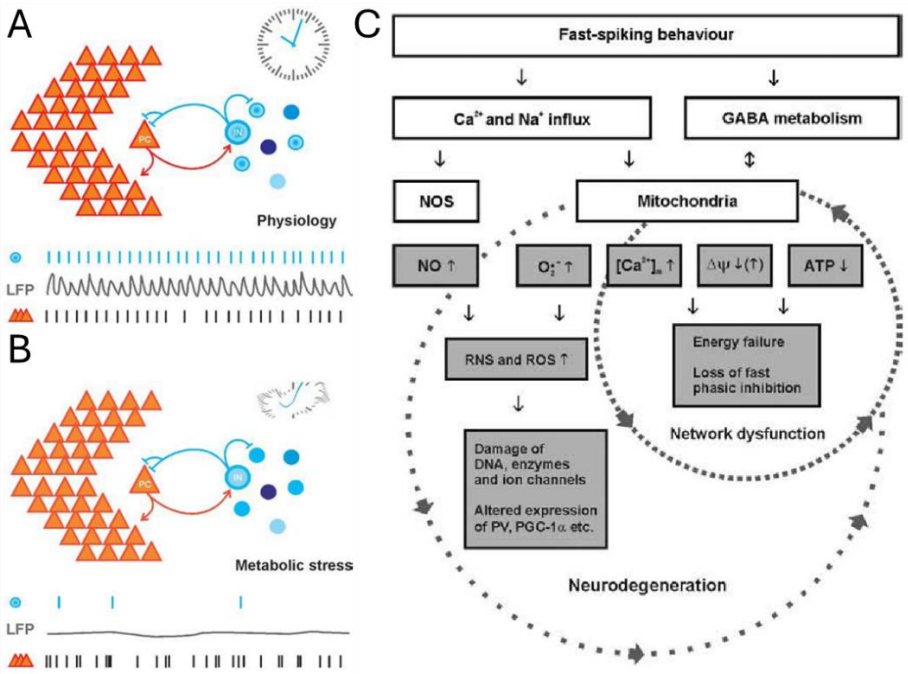

Figure 2.2 Fast spiking interneuron dysfunction with metabolic stress. 5A: Synchronized rhythmic activity of pyramidal cells highly depends on interactions with GABAergic interneurons. Fast-spiking interneurons are central for fast rhythmic synchronization pf pyramidal cell activity. **B:** Functional consequences of metabolic stress in fast-spiking interneurons. This is associated with a decrease of action potentials in fast-spiking interneurons, gamma oscillations in LFP, and precise temporal; sequence of information processing in the neuronal network. **C:** Perspective on metabolic and oxidative stress in fast-spiking, PV interneurons. [Ca2+]m, mitochondrial Ca2+-concentration; GABA, γ-aminobutyric acid; NO, nitric oxide; NOS, nitric oxide synthase; O2•−, superoxide anion; Δψ, mitochondrial membrane potential; RNS, reactive nitrogen species; ROS, reactive oxygen species; PGC-1α, peroxisome proliferator-activated receptor gamma coactivator 1-α PV, parvalbumin.[30] (Adapted from Kann 2014)

Given this metabolic vulnerability, one potential therapeutic strategy is to target interneuron energy deficiencies early in disease progression [32,33,34]. Zilberter et al. demonstrated that administering exogenous oxidative energy substrates can restore neuronal energy homeostasis, reduce Aβ-induced hyperactivity in vitro, and suppress epileptiform discharges in APP/PS1 mice in vivo [35]. These findings suggest that interventions aimed at bolstering interneuron energy metabolism could mitigate network dysfunction in AD.

Restoring E/I balance has been shown to improve both neural circuit function and behavioral outcomes in AD models. Several studies have demonstrated that enhancing inhibitory neuron activity can reduce network hyperexcitability and rescue cognitive impairments [36,37,38,39]. For instance, targeted restoration of PV interneuron function has been found to prevent memory loss and normalize network synchrony in AD mice. These results underscore the therapeutic potential of modulating inhibitory circuits as a means to counteract disease-related neural dysfunction.

Overall, addressing inhibitory neuron dysfunction could offer a valuable approach for intervention in AD. Restoring proper interneuron function and E/I balance may help support neural circuit integrity and cognitive function, potentially slowing disease progression. Future studies may benefit from further exploring metabolic interventions, interneuron-targeted therapies, and network-level strategies for modulating circuit activity in AD.

2.3 Functional Network Dysconnectivity and Disruptions

Stemming from these activity dysregulations is a series of network level disruptions to normal cognitive functioning. Higher brain functions such as learning and memory emerge from the interaction of many neurons across multiple hierarchical levels from local circuits to large-

scale network communication. Studies therefore have looked to see if dysfunction of individual neurons observed in AD mouse models can impair broader network brain connectivity.

2.3.1 Default Mode Network (DMN) Alterations

One of the earliest signs of network disruption is the impaired function of the Default Mode Network (DMN). The DMN is a collection of interconnected brain regions such as the hippocampus and posterior cingulate cortex, regions that are impacted by AD pathology. This network is most active during internally directed mental processes, such as self-referential thought, daydreaming, and mind-wandering. In contrast, the DMN is typically deactivated during externally focused cognitive tasks, such as learning and goal-directed behavior. This dynamic regulation of DMN activity is associated with efficient cognitive function. However, in Alzheimer's disease (AD) and other cognitive disorders, deactivation of DMN components during task engagement is altered and associated with deficits in cognitive flexibility and memory processing [40,41,42,43].

Network synchrony is critical for maintaining the DMN's role in cognition. Disruptions in the coordination of DMN activity are thought to contribute to cognitive dysfunction in AD, suggesting that impaired network synchrony underlies broader deficits in learning and memory. Notably, DMN alterations emerges early in AD progression, often preceding clinical symptoms and structural brain changes. Hippocampal hyperactivation and reduced deactivation of DMN components during memory encoding tasks have been observed in cognitively normal individuals with early risk factors for AD, including those with Aβ accumulation or genetic predispositions [44,45,46,47].

These findings suggest that abnormal DMN activity reflects underlying neural network changes in AD, contributing to deficits in memory formation and retrieval. Further research into DMN dysfunction may provide insights into early biomarkers of AD progression and potential therapeutic targets aimed at restoring network-level synchrony and cognitive function.

2.3.2 Network Hypersynchrony and Aberrant Synchronization

Neural networks generate specific oscillatory patterns that can be measured using electroencephalography (EEG), with fluctuations in network synchrony reflecting physiological changes in behavior and brain state. These oscillations play a fundamental role in cognitive functions by coordinating neuronal activity to support processes such as attention, working memory, and sensory perception. However, network hypersynchrony, a pathological state characterized by excessive and aberrant neuronal synchronization, has been frequently observed in Alzheimer's disease (AD) [12,13,26]. This phenomenon is linked to epileptiform discharges and an increased susceptibility to seizures, which have been widely reported across various AD mouse models [48,49,23]. EEG recordings from these models have demonstrated abnormalities in gamma oscillations, along with clustered occurrences of frequent spike discharges. Alterations in hippocampal network oscillations and theta-gamma coupling arise before Aβ overproduction [50,51]. Interestingly, these hypersynchronous events often occur in an inverse relationship with gamma activity, suggesting that disrupted inhibitory control contributes to both reduced gamma power and pathological network synchronization. Given the essential role of gamma oscillations in higher-order cognitive functions, such disruptions are likely to underly many of the cognitive deficits observed in AD. (Fig 2.3)

Another critical oscillatory pattern affected in AD is hippocampal Sharp Wave Ripples (SWRs) — high-frequency oscillations (~100–250 Hz) that play a crucial role in memory

consolidation by facilitating the replay of recent experiences during sleep and rest states [52,53]. SWRs are thought to be essential for stabilizing newly encoded memories by coordinating hippocampal-cortical interactions, a process that supports long-term storage and retrieval of information. However, studies in AD models have demonstrated a significant reduction in the occurrence and strength of SWRs, leading to impaired memory consolidation and retrieval [54,55,56,57,58].

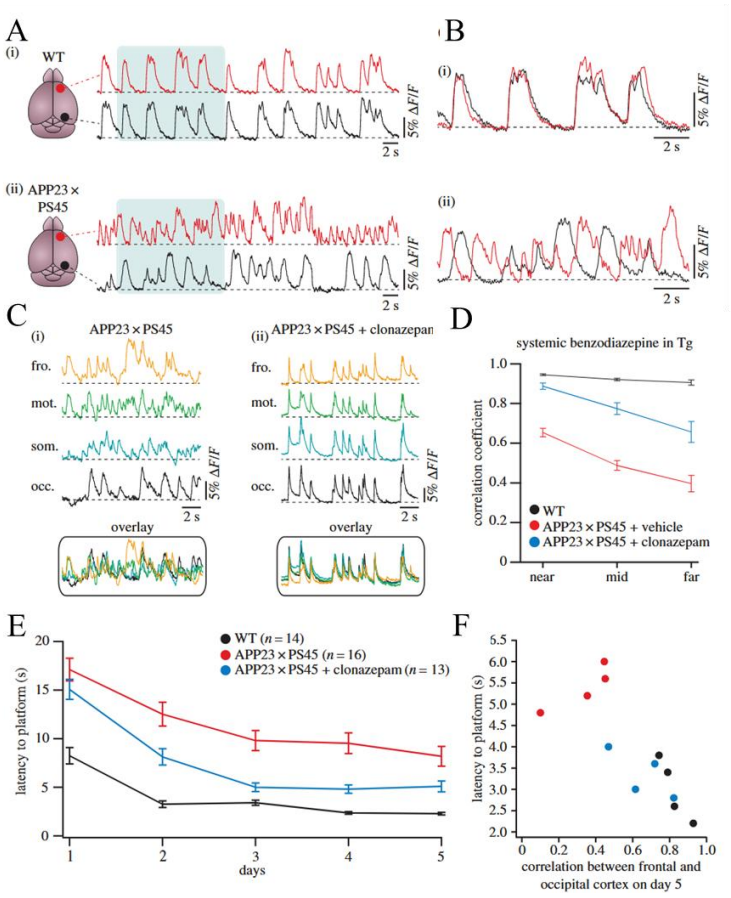

Figure 2.3 Impaired and restored slow-wave oscillations in mouse models of AD. A: Example slow-wave oscillation traces from the frontal (red) and occipital (black) cortex in WT (i) and APP23 × PS45 (ii) mice. **B:** Superimposed traces from the shaded areas in A. **C:** Slow-wave oscillations in untreated (i) and benzodiazepine-treated (ii) APP23 × PS45 mice. **D:** Average cross-correlation coefficients vs. cortical distance in WT (black), untreated (red), and treated (blue) APP23 × PS45 mice. **E:** Water maze performance showing latency to find the platform. **F:** Correlation between frontal-occipital activity and day 5 latency. Each circle represents an individual mouse; error bars indicate s.e.m. [12,83] (Adapted from Busche 2016 & Busche 2015)

Network synchrony and oscillatory brain rhythms are primarily regulated by inhibitory interneurons, particularly PV-expressing fast-spiking interneurons, which coordinate the timing of pyramidal neuron firing through rhythmic inhibition [59,60]. In AD, dysfunction in these interneurons leads to widespread network instability, further contributing to oscillatory

impairments and cognitive deficits, for example the disruption of SWRs further exacerbates memory impairments, providing another mechanism by which network instability contributes to cognitive decline [13]. Notably, dysfunction in PV interneurons is not unique to AD but is increasingly recognized as a shared mechanism underlying network dysrhythmias in multiple neurological disorders [61].

Given the central role of inhibitory interneurons in maintaining network stability, recent studies have explored therapeutic strategies aimed at restoring interneuron function to normalize oscillatory activity in AD. Enhancing inhibitory synaptic currents has been shown to reduce epileptiform discharges in AD mouse models[26]. Additional studies have demonstrated that optogenetic stimulation of PV interneurons, a technique that requires light delivery through fiber optics, or pharmacological enhancement of GABAergic signaling can mitigate network hypersynchrony and improve cognitive outcomes in AD models [62,26,39,34]. These findings suggest that targeting inhibitory network dysfunction could serve as a promising therapeutic avenue for early intervention in AD, potentially stabilizing network oscillations and preserving cognitive function.

2.4 Neural Activity Impairments in Specific Cognitive Domains

The disruptions in neural activity seen in AD — ranging from hyper- and hypoactivity to imbalances in excitation and inhibition — ultimately manifest as deficits across multiple cognitive domains. These impairments are not uniform but instead affect distinct brain regions and functions in ways that contribute to the hallmark symptoms of the disease. These deficits (such as spatial memory and olfactory changes) appear early in AD as the underlying brain systems are particularly vulnerable to AD-related pathology. Dysfunctional hippocampal circuits

underlie impairments in spatial memory encoding, while cortical dysregulation disrupts sensory processing and attentional control [13,12]. Moreover, abnormal oscillatory rhythms and network synchrony further degrade cognitive function by impairing communication between brain regions. Examining how these deficits emerge at the neural level provides critical insight into the cognitive decline associated with AD and potential intervention strategies.

2.4.1 Orientation and Direction Selectivity Decrease

A particular example of impaired sensory processing occurs in the primary visual cortex (V1). Simple cells are neurons in V1 that fire in response to specific sets of visual stimuli, including drifting gratings at specific orientations and directions within their receptive fields (Fig 2.4 A) [63]. The receptive fields of these neurons have distinct excitatory and inhibitory regions, meaning they only respond when a stimulus is placed in the correct location and orientation (Fig 2.4 B). The output of these cells is considered linear, meaning that their output is a weighted sum of inputs from the lateral geniculate nucleus (LGN). The response specificity of these neurons to particular drifting grating parameters plays a crucial role in edge detection and are thought to contribute to the initial stages of feature extraction in visual processing. This process occurs in a hierarchical manner, beginning in the retina and progressing through the LGN of the thalamus to V1 and beyond, a process critical for enabling perception and object recognition.

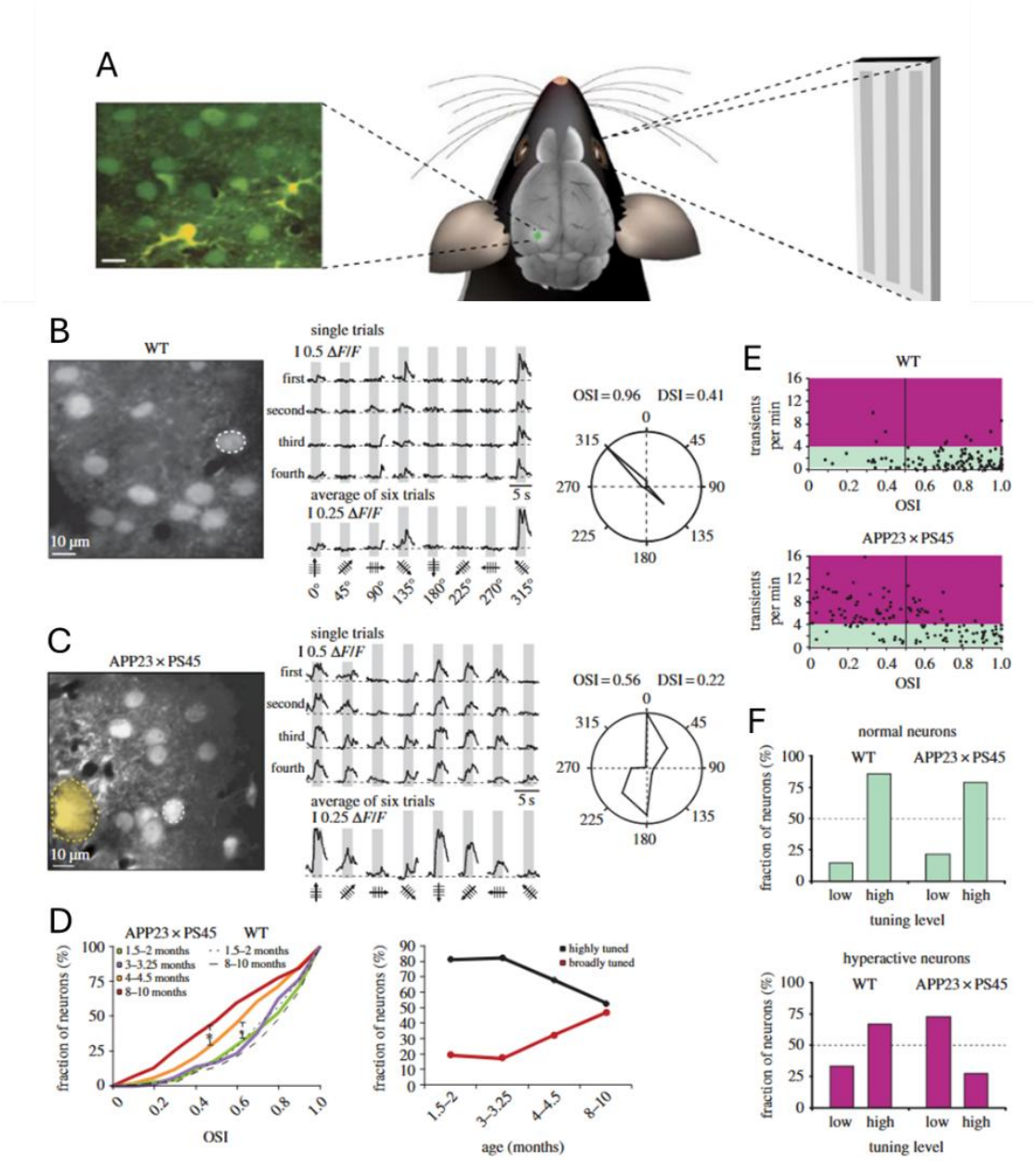

Figure 2.4 Impaired signal processing in the visual cortex of an AD mouse model. A: Experimental arrangement of in vivo two-photon calicum imaging of drifting grating stimulation-evoked neuronal activity. **B-C:** Two-photon imaging of layer 2/3 neurons in WT (B) and APP23 × PS45 (C) mice, with stimulus-evoked Ca^{2+} transients and polar plots of orientation selectivity. **D:** Orientation selectivity indices (OSIs) for WT and APP23 × PS45 mice at different ages. **E:** Relationship between OSI and spontaneous Ca^{2+}-transient frequency, with hyperactive neurons highlighted. **F:** Comparison of normal and hyperactive neurons with low vs. high orientation tuning across groups. [12,64] (Adapted from Busche 2016 & Grienberger 2012)

Grienberger et.al. demonstrated that in the APP23 x PS45 mouse model of AD, there is impaired orientation tuning in layer 2/3 V1 neurons (Fig 2.4) [64,12]. Using in vivo two-photon (2P) imaging, the authors track the progressive deterioration of neuronal tuning for the orientation of visual stimuli (calcium indicator OGB1-AM) as amyloid-B (AB) load increases with age. Mice were shown drifting grating visual stimuli in different orientations while neuronal responses were recorded, and neuronal tuning was quantified using orientation selectivity index (OSI) and a direction selectivity index (DSI). Their findings showed that young mice (1.5-3 months) show normal neuronal tuning and visual discrimination; at 4-4.5 months, as Aβ plaques begin to accumulate, neuronal tuning and visual discrimination start to decline; and by 8-10 months, tuning and discrimination deficits are severe (Fig 2.4 D). These mice fail to discriminate between fine visual patterns (22.5 degree) differences, while basic visual responses remain intact, indicating specific deficits in cortical processing rather than global vision loss.

In addition to tuning deficits, the study showed that a significant proportion of neurons become either hyperactive or hypoactive in their spontaneous activity patterns (Fig 2.4 F). Hyperactive neurons showed abnormal responses to multiple orientations of visual stimuli, and there was a trend for hyperactive neurons to be more abundant near plaques. These findings establish a direct link between Aβ load, neural circuit dysfunction, and sensory deficits, as well as supporting the idea that an imbalance in excitation/inhibition imbalance could be directly implicated in such impairments.

2.4.2 Spatial Memory Encoding Deficits: Place and Grid Cell Dysfunction

Visual and other sensory processing is critical to perception and interaction with one's external environment. These processes provide key input to other brain regions that coordinate information to learn and form new memories. In AD, this learning process is impaired, a deficit

particularly evident in spatial memory, which relies on precise encoding of environmental cues and spatial relationships.

The hippocampus and associated medial temporal lobe structures play a central role in spatial memory processing, utilizing specialized neurons to encode an animal's position, movement, and orientation within an environment [65]. Place cells in the hippocampus fire in specific locations, creating a dynamic cognitive map [66] (Fig 2.5 A). These representations are supported by grid cells in the entorhinal cortex, which generate a hexagonal coordinate system to measure distances and spatial relationships. Border cells respond to environmental boundaries, while head direction cells track an individual's orientation relative to external landmarks. Together, these systems allow for spatial navigation, memory retrieval, and goal-directed behavior.

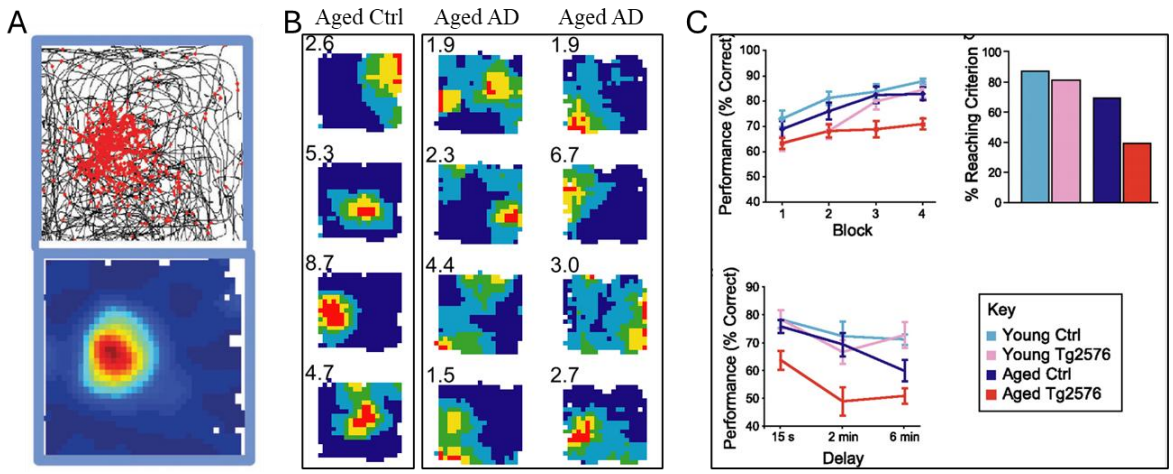

Figure 2.5 Place cell representation is degraded in an aged AD mouse model. 6A: Place cell firing pattern. (*Top*) Trajectory with spike locations. (*Bottom*) Color-coded rate map with red showing high activity and blue showing low acitvity. **B:** Degraded place fields in four representative place cells in two Tg2576 AD mice compared to an aged control mouse. **C:** Aged transgenic mice show impaired acquisition in the 15-s-delay task. Fewer aged transgenic mice reach the >80% correct criterion over three days. Performance declines with increasing delay, with aged mice performing worse than young mice, though no additional deficit is seen in the aged transgenic group. Error bars indicate SEMs. [65,67] (Adapted from Cacucci 2008 & Moser 2015)

In AD, degeneration of hippocampal and entorhinal circuits disrupts these encoding mechanisms [67,68,18,69,70]. Place cell spatial stability deteriorates (Fig 2.5 B), grid cell firing patterns become disorganized, and head direction cells lose precision. These impairments contribute to the characteristic spatial disorientation seen in AD patients and rodent models, affecting tasks such as maze navigation and object-location memory (Fig 2.5 C). Disruptions in synaptic plasticity, excitation-inhibition balance, and cholinergic signaling further degrade spatial encoding, making spatial memory deficits an early and prominent feature of AD-related cognitive decline. Optogenetic and neuromodulatory activation of medial septal inputs to the hippocampus has been shown to partially rescue these deficits, highlighting the role of disrupted oscillatory dynamics [71,72].

2.4.3 Attention and Executive Dysfunction

The ability to maintain attention and execute goal-directed behaviors relies on coordinated activity between the prefrontal cortex (PFC) and hippocampus, a network that is profoundly disrupted in Alzheimer's disease (AD) [55]. In AD mouse models, impairments in PFC-hippocampal communication have been observed using in vivo calcium imaging and electrophysiology, revealing weakened synchrony between these regions during cognitive tasks. Studies in 5xFAD and APP/PS1 mice indicate that amyloid pathology alters network coherence, leading to deficits in working memory, decision-making, and task flexibility [55,28]. Disruptions in theta-gamma coupling, a key mechanism for information transfer between the PFC and hippocampus, have been identified in AD models, further linking network dysfunction to cognitive impairment [73]. By exploring these changes in vivo, researchers aim to identify neural mechanisms underlying executive dysfunction and develop targeted interventions to restore network function.

2.5 Mechanisms Driving Neural Dysfunction: Metabolic and Neurovascular Vulnerabilities

Alzheimer's disease is not only characterized by synaptic and network dysfunction but also by metabolic and vascular impairments that exacerbate neuronal instability [8,74,75,7,6]. Recent in vivo studies using two-photon imaging and laser speckle contrast imaging have demonstrated that cerebral blood flow (CBF) is reduced in AD models, impairing the supply of oxygen and glucose necessary for normal neuronal activity [7]. This reduction in metabolic support may disproportionately affect fast-spiking interneurons, particularly parvalbumin (PV)-expressing inhibitory neurons, which have exceptionally high energy demands [31,30]. In APP/PS1 mice. These findings suggest that restoring metabolic and vascular function in AD models could help preserve interneuron function and prevent circuit-level dysfunction.

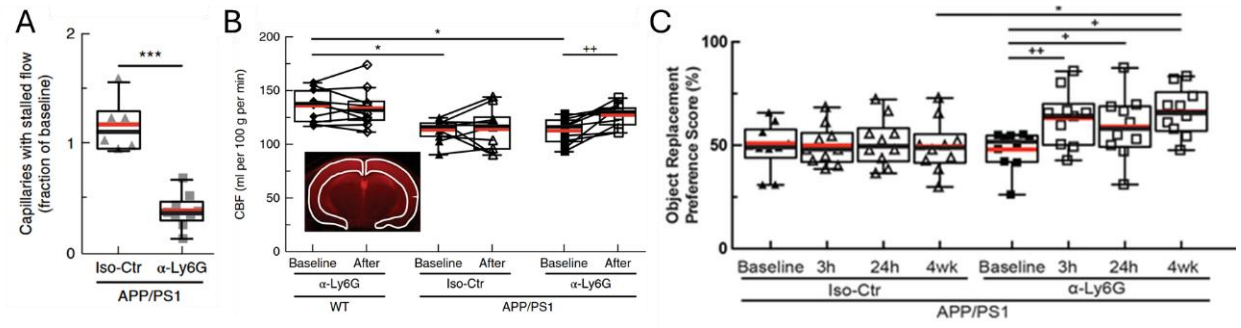

Figure 2.6 Administration of antibodies against Ly6G reduced the number of stalled capillaries, increased 7cCBF, and improved short-term memory in APP/PS1 mice. A: Capillaries with stalled blood flow decrease ~1 h after α-Ly6G administration. B: cCBF increases in APP/PS1 mice after α-Ly6G administration. Boxplots show median (black) and mean (red). C: Preference scores in the object replacement task.[7] (Adapted from Cruz-Hernandez 2019)

In Cruz-Hernandez et al., the authors investigated the role of capillary stalling as a mechanism underlying cerebral blood flow (CBF) reductions in Alzheimer's disease (AD) mouse models. Using in vivo two-photon microscopy in APP/PS1 mice, they found that an increased

fraction of capillaries exhibited stalled red blood cell flow, leading to a global decrease in CBF perfusion. This capillary stalling was associated with the adhesion of neutrophils, immune cells that became lodged in the microvasculature. Administration of an antibody against the neutrophil specific protein Ly6G resulted in an elimination of capillary stalling events (Fig 2.6 A), leading to a two-thirds recovery of the global CBF deficit (Fig 2.6 B). Notably, this increase in CBF corresponded with a significant improvement in cognitive performance on spatial memory tasks in APP/PS1 mice (Fig 2.6 C). These findings suggest that targeting vascular dysfunction and metabolic deficiencies early in disease progression could serve as a viable therapeutic strategy for mitigating cognitive decline in AD. The study highlights the critical interplay between neurovascular function and cognitive performance, reinforcing the idea that improving cerebral perfusion may help counteract neural circuit impairments in AD.

2.6 Restoring Neural Circuit Function in AD

Given the profound network disruptions in AD, significant research efforts have been directed toward developing interventions that restore neural circuit function in vivo [62,39,36,76,71,77,78,13,12]. Optogenetic and chemogenetic approaches have been used to selectively activate PV interneurons, successfully restoring gamma oscillations and reducing network hypersynchrony in AD mouse models [71,36]. Pharmacological interventions targeting GABAergic inhibition, metabolic support, and neurovascular function have also shown promise in preclinical studies, helping to rebalance E/I dynamics and improve cognitive outcomes [38,37,27,79]. Additionally, neuromodulation techniques, such as transcranial magnetic stimulation (TMS) applied in awake, behaving AD mice have been found to enhance gamma activity and improve

memory performance [78]. By leveraging these in vivo experimental approaches, researchers aim to identify translational strategies for restoring brain function in AD.

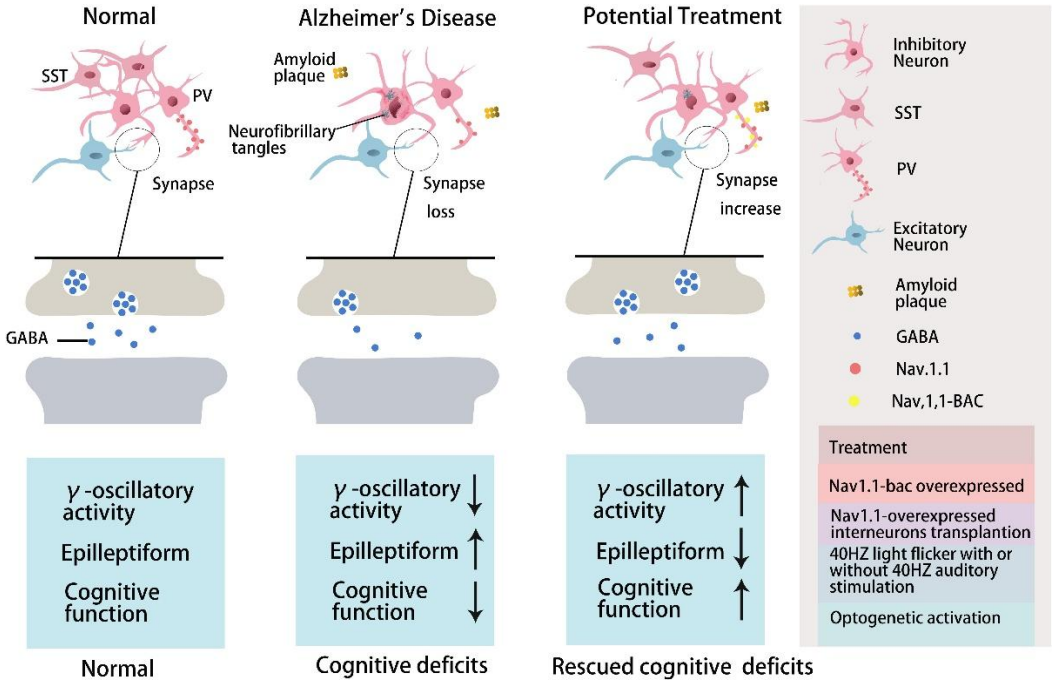

Figure 2.7 Dysfunction of GABAergic interneurons, particularly PV and SST neurons, in Alzheimer8's disease (AD) and their potential as therapeutic targets. Loss or dysfunction of these inhibitory neurons contributes to increased network excitability in AD. PV neuron deficits include reduced γ-oscillatory activity, Nav1.1 expression, and GABA release. Potential interventions include enhancing Nav1.1 expression, 40 Hz light and auditory stimulation, interneuron transplantation, and optogenetic activation of PV and SST neurons, which have been shown to restore network oscillations and mitigate cognitive deficits.[37] (Adapted from Xu 2020)

2.6.1 Optogenetic and Chemogenetic Interventions

One of the most powerful tools for restoring circuit function in AD models is the use of optogenetics and chemogenetics, which allow for precise manipulation of neuronal activity. These approaches have been particularly effective in modulating inhibitory interneuron dysfunction, restoring gamma oscillations, and reducing network hypersynchrony in AD models [71,36]. (Fig. 2.7)

Studies using optogenetic stimulation of PV-expressing inhibitory interneurons in AD mouse models have successfully rescued gamma power, reduced hyperexcitability, and improved memory performance. Targeted stimulation of PV interneurons in the hippocampus and prefrontal cortex has been shown to normalize network synchrony and reduce epileptiform activity, further supporting the role of interneuron dysfunction in AD pathology. [29,71]

Unlike optogenetics, chemogenetics enables systemic and localized activation or inhibition of neurons through DREADD (Designer Receptors Exclusively Activated by Designer Drugs) technology. Recent studies have used chemogenetic activation of PV or SST (somatostatin)-expressing interneurons in AD models to restore network balance and improve cognitive performance [36]. This approach is particularly promising for translational research, as it allows for non-invasive control of neural circuits.

Together, optogenetic and chemogenetic interventions offer valuable tools for investigating network dysfunction in AD and may pave the way for circuit-based therapies aimed at restoring cognitive function.

2.6.2 Pharmacological and Metabolic Interventions

Pharmacological strategies targeting synaptic function, inhibitory signaling, and brain metabolism have been explored as potential therapeutic interventions for AD [80,81,27,82,38,83]. These approaches aim to restore excitation-inhibition balance, enhance metabolic support for neurons, and modulate neurotransmitter systems to improve cognitive function.

Dysfunction in inhibitory interneurons contributes to hyperexcitability and cognitive deficits in AD [22,13]. Pharmacological agents that enhance GABAergic inhibition have shown promise in restoring E/I balance. Studies using benzodiazepines, positive allosteric modulators of GABA-A

receptors, or selective interneuron-targeting drugs have demonstrated improvements in network stability, reduced seizure susceptibility, and enhanced cognitive performance in AD mouse models [83].

Energy deficits in AD may disproportionately affect high-energy-demanding inhibitory interneurons, particularly PV cells. Metabolic interventions, such as exogenous ketones, lactate supplementation, and mitochondrial enhancers, have been tested to restore interneuron function and stabilize neural networks [35]. Studies in AD mouse models show that ketone-based metabolic therapies can improve PV interneuron function, enhance synaptic plasticity, and restore gamma oscillations, highlighting their potential as therapeutic interventions.

Other pharmacological approaches target cholinergic, glutamatergic, and serotonergic systems, which are dysregulated in AD. Acetylcholinesterase inhibitors (AChEIs), NMDA receptor modulators, and serotonin receptor agonists have been explored in preclinical models to assess their effects on neural circuit function, cognitive outcomes, and neuroprotection [81].

These pharmacological and metabolic approaches provide potential avenues for stabilizing neural circuits and improving cognitive deficits in AD.

2.6.3 Electrical and Magnetic Brain Stimulation

Neuromodulation strategies such as Transcranial Magnetic Stimulation (TMS) and Transcranial Alternating Current Stimulation (tACS) have been investigated for their potential to restore oscillatory activity and improve cognitive function in AD [78,84,77,85]. These techniques modulate cortical excitability and network connectivity without requiring direct intracranial interventions.

TMS is a non-invasive brain stimulation technique that delivers repetitive magnetic pulses to modulate cortical excitability. In AD models, TMS applied to the prefrontal cortex and hippocampus has been shown to enhance gamma power, improve synaptic plasticity, and restore PFC-hippocampal coordination [84,78]. This suggests that TMS could serve as a potential therapeutic tool for restoring cognitive function in AD.

tACS applies low-amplitude alternating electrical currents at specific frequencies to entrain neural oscillations. Studies suggest that gamma-frequency tACS enhances hippocampal-cortical communication and improves memory performance in AD mouse models [85,77]. By restoring network synchronization, tACS has been proposed as a novel approach for mitigating cognitive dysfunction in AD.

DBS involves the implantation of electrodes to deliver chronic electrical stimulation to specific brain regions. Although primarily used for movement disorders, DBS targeting the fornix and medial septum has been explored in AD models to enhance hippocampal function and slow neurodegeneration [72]. Studies suggest that DBS promotes synaptic plasticity, enhances glucose metabolism, and modulates network activity, though further research is needed to refine its application for AD treatment.

Neuromodulation techniques like TMS, tACS, and DBS show promise for improving network function and cognition in AD. While early findings are encouraging, further research is needed to refine these approaches and assess their long-term benefits.

2.7 Conclusion

Neural activity impairments in AD span from local circuit dysfunction to large-scale network disruptions, all of which have been extensively studied using in vivo techniques in animal models. Disruptions in E/I balance, aberrant oscillatory rhythms, and metabolic deficits in inhibitory neurons contribute to widespread cognitive impairments. Interventions that restore normal network activity — whether through optogenetic stimulation, metabolic enhancement, or pharmacological modulation — hold promise for improving cognitive function in AD. Future research should continue leveraging in vivo imaging and electrophysiology to unravel the mechanistic underpinnings of AD and develop effective therapeutic strategies.

References

1. 2024 Alzheimer's disease facts and figures. *Alzheimers Dement. J. Alzheimers Assoc.* (2024) doi:10.1002/alz.13809.
2. Mathias Jucker, Jucker, M., Lary C. Walker & Walker, L. C. Pathogenic protein seeding in Alzheimer disease and other neurodegenerative disorders. *Ann. Neurol.* **70**, 532–540 (2011).
3. A. Pichet Binette *et al.* Proteomic changes in Alzheimer's disease associated with progressive Aβ plaque and tau tangle pathologies. *Nat. Neurosci.* (2024) doi:10.1038/s41593-024-01737-w.
4. Jorge J. Palop, Palop, J. J., Lennart Mucke & Mucke, L. Amyloid-[beta]-induced neuronal dysfunction in Alzheimer's disease: from synapses toward neural networks. *Nat. Neurosci.* **13**, 812–818 (2010).

5. Sam Harris *et al.* Tipping the Scales: Peptide-Dependent Dysregulation of Neural Circuit Dynamics in Alzheimer's Disease. *Neuron* **107**, 417–435 (2020).

6. Kiyoshi Niwa *et al.* Alterations in cerebral blood flow and glucose utilization in mice overexpressing the amyloid precursor protein. *Neurobiol. Dis.* **9**, 61–68 (2002).

7. Jean C. Cruz Hernández *et al.* Neutrophil adhesion in brain capillaries reduces cortical blood flow and impairs memory function in Alzheimer's disease mouse models. *Nat. Neurosci.* **22**, 413–420 (2019).

8. Costantino Iadecola & Iadecola, C. Vascular and Metabolic Factors in Alzheimer's Disease and Related Dementias: Introduction. *Cell. Mol. Neurobiol.* **36**, 151–154 (2016).

9. Liyong Wu *et al.* Early-onset familial Alzheimer's disease (EOFAD). *Can. J. Neurol. Sci.* **39**, 436–445 (2012).

10. Richard A. Armstrong & Armstrong, R. A. Risk factors for Alzheimer's disease. *Folia Neuropathol.* **57**, 87–105 (2019).

11. J. Grill & J. Cummings. Novel targets for Alzheimer's disease treatment. (2014).

12. Marc Aurel Busche, Busche, M. A., Arthur Konnerth & Konnerth, A. Impairments of neural circuit function in Alzheimer's disease. *Philos. Trans. R. Soc. B* **371**, 20150429 (2016).

13. Jorge J. Palop, Palop, J. J., Lennart Mucke & Mucke, L. Network abnormalities and interneuron dysfunction in Alzheimer's disease: A multiscale perspective on abnormal neuronal activity in early AD. *Alzheimers Dement.* **16**, (2016).

14. Steven F. Grieco, Todd C. Holmes, & Xiangmin Xu. Probing neural circuit mechanisms in Alzheimer's disease using novel technologies. *Mol. Psychiatry* (2023) doi:10.1038/s41380-023-02018-x.

15. Lena Schmid *et al.* Dysfunction of Somatostatin-Positive Interneurons Associated with Memory Deficits in an Alzheimer's Disease Model. *Neuron* **92**, 114–125 (2016).

16. Antonio Mario Locci *et al.* Comparison of memory, affective behavior, and neuropathology in APPNLGF knock-in mice to 5xFAD and APP/PS1 mice. *Behav. Brain Res.* **404**, 113192–113192 (2021).

17. Sebastien Cayzac *et al.* Altered hippocampal information coding and network synchrony in APP-PS1 mice. *Neurobiol. Aging* **36**, 3200–3213 (2015).

18. Alexandra J. Mably *et al.* Impairments in spatial representations and rhythmic coordination of place cells in the 3xTg mouse model of Alzheimer's disease. *Hippocampus* **27**, 378–392 (2017).

19. Sean Tok *et al.* Functional Neurophysiological Biomarkers of Early-Stage Alzheimer's Disease: A Perspective of Network Hyperexcitability in Disease Progression. *J. Alzheimers Dis.* 1–28 (2021) doi:10.3233/jad-210397.

20. Marc Aurel Busche, Busche, M. A., Arthur Konnerth & Konnerth, A. Neuronal hyperactivity – A key defect in Alzheimer's disease? *BioEssays* **37**, 624–632 (2015).

21. Fernando Maestú *et al.* Neuronal excitation/inhibition imbalance: core element of a translational perspective on Alzheimer pathophysiology. *Ageing Res. Rev.* **69**, 101372–101372 (2021).

22. Helena Targa Dias Anastacio *et al.* Neuronal hyperexcitability in Alzheimer's disease: what are the drivers behind this aberrant phenotype? *Transl. Psychiatry* **12**, (2022).

23. Jorge J. Palop *et al.* Aberrant Excitatory Neuronal Activity and Compensatory Remodeling of Inhibitory Hippocampal Circuits in Mouse Models of Alzheimer's Disease. *Neuron* **55**, 697–711 (2007).

24. Eva Vico Varela *et al.* Excitatory-inhibitory imbalance in Alzheimer's disease and therapeutic significance. *Neurobiol. Dis.* **127**, 605–615 (2019).

25. Moustafa Algamal *et al.* Reduced excitatory neuron activity and interneuron-type-specific deficits in a mouse model of Alzheimer's disease. *Commun. Biol.* **5**, (2022).

26. Laure Verret *et al.* Inhibitory Interneuron Deficit Links Altered Network Activity and Cognitive Dysfunction in Alzheimer Model. *Cell* **149**, 708–721 (2012).

27. Yanfang Li *et al.* Implications of GABAergic Neurotransmission in Alzheimer's Disease. *Front. Aging Neurosci.* **8**, 31–31 (2016).

28. Anupam Hazra *et al.* Inhibitory Neuron and Hippocampal Circuit Dysfunction in an Aged Mouse Model of Alzheimer's Disease. *PLOS ONE* **8**, (2013).

29. Sara Hijazi, August B. Smit, & Ronald E. van Kesteren. Fast-spiking parvalbumin-positive interneurons in brain physiology and Alzheimer's disease. *Mol. Psychiatry* (2023) doi:10.1038/s41380-023-02168-y.

30. Oliver Kann *et al.* Highly energized inhibitory interneurons are a central element for information processing in cortical networks. *J. Cereb. Blood Flow Metab.* **34**, 1270–1282 (2014).

31. Oliver Kann & Kann, O. The interneuron energy hypothesis: Implications for brain disease. *Neurobiol. Dis.* **90**, 75–85 (2016).

32. Shu Shu *et al.* Prefrontal parvalbumin interneurons deficits mediate early emotional dysfunction in Alzheimer's disease. *Neuropsychopharmacology* (2022) doi:10.1038/s41386-022-01435-w.

33. Mei-Hong Lu *et al.* Transplantation of GABAergic Interneuron Progenitor Attenuates Cognitive Deficits of Alzheimer's Disease Model Mice. *J. Alzheimers Dis.* **75**, 245–260 (2020).

34. Sarah D. Benthem *et al.* Rescuing impaired cortical-hippocampal interactions during sleep with 40Hz stimulation targeted to hippocampus in 3xTg-AD/PVcre mice. *Alzheimers Amp Dement.* **18**, (2022).

35. Misha Zilberter *et al.* Dietary energy substrates reverse early neuronal hyperactivity in a mouse model of Alzheimer's disease. *J. Neurochem.* **125**, 157–171 (2013).

36. Sara Hijazi *et al.* Early restoration of parvalbumin interneuron activity prevents memory loss and network hyperexcitability in a mouse model of Alzheimer's disease. *Mol. Psychiatry* **25**, 3380–3398 (2020).

37. Yilan Xu *et al.* GABAergic Inhibitory Interneuron Deficits in Alzheimer's Disease: Implications for Treatment. *Front. Neurosci.* **14**, 660 (2020).

38. Mauricio O. Nava-Mesa *et al.* GABAergic neurotransmission and new strategies of neuromodulation to compensate synaptic dysfunction in early stages of Alzheimer's disease. *Front. Cell. Neurosci.* **8**, 167–167 (2014).

39. Magdalena Martínez-Losa *et al.* Nav1.1-Overexpressing Interneuron Transplants Restore Brain Rhythms and Cognition in a Mouse Model of Alzheimer's Disease. *Neuron* **98**, 75–895 (2018).

40. David T. Jones *et al.* Age-related changes in the default mode network are more advanced in Alzheimer disease. *Neurology* **77**, 1524–1531 (2011).

41. Michael D. Greicius *et al.* Default-mode network activity distinguishes Alzheimer's disease from healthy aging: Evidence from functional MRI. *Proc. Natl. Acad. Sci. U. S. A.* **101**, 4637–4642 (2004).

42. Federica Agosta *et al.* Resting state fMRI in Alzheimer's disease: beyond the default mode network. *Neurobiol. Aging* **33**, 1564–1578 (2012).

43. Alan Antičević *et al.* The role of default network deactivation in cognition and disease. *Trends Cogn. Sci.* **16**, 584–592 (2012).

44. Reisa A. Sperling *et al.* Amyloid deposition is associated with impaired default network function in older persons without dementia. *Neuron* **63**, 178–188 (2009).

45. Nicola Filippini *et al.* Distinct patterns of brain activity in young carriers of the APOE e4 allele. *NeuroImage* **47**, (2009).

46. Susan Y. Bookheimer *et al.* Patterns of brain activation in people at risk for Alzheimer's disease. *N. Engl. J. Med.* **343**, 450–456 (2000).

47. Jasmeer P. Chhatwal *et al.* Impaired default network functional connectivity in autosomal dominant Alzheimer disease. *Neurology* **81**, 736–744 (2013).

48. Ana M. García-Cabrero *et al.* Hyperexcitability and epileptic seizures in a model of frontotemporal dementia. *Neurobiol. Dis.* **58**, 200–208 (2013).

49. Meaghan Morris *et al.* Network dysfunction in α-synuclein transgenic mice and human Lewy body dementia. *Ann. Clin. Transl. Neurol.* **2**, 1012–1028 (2015).

50. Romain Goutagny *et al.* Alterations in hippocampal network oscillations and theta-gamma coupling arise before Aβ overproduction in a mouse model of Alzheimer's disease. *Eur. J. Neurosci.* **37**, 1896–1902 (2013).

51. Sitong Wang *et al.* Early-stage dysfunction of hippocampal theta and gamma oscillations and its modulation of neural network in a transgenic 5xFAD mouse model. *Neurobiol. Aging* **94**, 121–129 (2020).

52. György Buzsáki & Buzsáki, G. Hippocampal sharp wave-ripple: A cognitive biomarker for episodic memory and planning. *Hippocampus* **25**, 1073–1188 (2015).

53. Shantanu P. Jadhav *et al.* Awake hippocampal sharp-wave ripples support spatial memory. *Science* **336**, 1454–1458 (2012).

54. Anna K. Gillespie *et al.* Apolipoprotein E4 Causes Age-Dependent Disruption of Slow Gamma Oscillations during Hippocampal Sharp-Wave Ripples. *Neuron* **90**, 740–751 (2016).

55. Eun Joo Kim *et al.* Disruption of hippocampal-prefrontal neural dynamics and risky decision-making in a mouse model of Alzheimer's disease. *bioRxiv* (2024) doi:10.1101/2024.09.17.613376.

56. SD Cushing *et al.* Impaired Hippocampal-Cortical Interactions during Sleep in a Mouse Model of Alzheimer's Disease. *Curr. Biol. CB* (2024) doi:10.1016/j.cub.2024.03.040.

57. Emily A Aery Jones *et al.* Early Hippocampal Sharp-Wave Ripple Deficits Predict Later Learning and Memory Impairments in an Alzheimer's Disease Mouse Model. *bioRxiv* 596569 (2019) doi:10.1101/596569.

58. Gabrielle Girardeau *et al.* Selective suppression of hippocampal ripples impairs spatial memory. *Nat. Neurosci.* **12**, 1222–1223 (2009).

59. György Buzsáki, Buzsáki, G., Andreas Draguhn & Draguhn, A. Neuronal Oscillations in Cortical Networks. *Science* **304**, 1926–1929 (2004).

60. Vikaas S. Sohal *et al.* Parvalbumin neurons and gamma rhythms enhance cortical circuit performance. *Nature* **459**, 698–702 (2009).

61. Beulah Leitch. Parvalbumin Interneuron Dysfunction in Neurological Disorders: Focus on Epilepsy and Alzheimer's Disease. *Int. J. Mol. Sci.* (2024) doi:10.3390/ijms25105549.

62. Leslie M. Tong *et al.* Inhibitory interneuron progenitor transplantation restores normal learning and memory in ApoE4 knock-in mice without or with Aβ accumulation. *J. Neurosci.* **34**, 9506–9515 (2014).

63. David H. Hubel, Hubel, D. H., D. H. Hubel, Torsten N. Wiesel & Wiesel, T. N. Receptive fields of single neurones in the cat's striate cortex. *J. Physiol.* **148**, 574–591 (1959).

64. Christine Grienberger *et al.* Staged decline of neuronal function in vivo in an animal model of Alzheimer's disease. *Nat. Commun.* **3**, 774–774 (2012).

65. May-Britt Moser *et al.* Place Cells, Grid Cells, and Memory. *Cold Spring Harb. Perspect. Biol.* **7**, (2015).

66. O'Keefe, J. Place units in the hippocampus of the freely moving rat. *Exp. Neurol.* **51**, 78–109 (1976).

67. Francesca Cacucci *et al.* Place cell firing correlates with memory deficits and amyloid plaque burden in Tg2576 Alzheimer mouse model. *Proc. Natl. Acad. Sci. U. S. A.* **105**, 7863–7868 (2008).

68. Azul Silva & María Cecilia Martínez. Spatial memory deficits in Alzheimer's disease and their connection to cognitive maps' formation by place cells and grid cells. *Front. Behav. Neurosci.* **16**, (2023).

69. Jun, H. *et al.* Disrupted Place Cell Remapping and Impaired Grid Cells in a Knockin Model of Alzheimer's Disease. *Neuron* **107**, 1095-1112.e6 (2020).

70. Mariana Gil *et al.* Impaired path integration in mice with disrupted grid cell firing. *Nat. Neurosci.* **21**, 81–91 (2018).

71. Etter, G. *et al.* Optogenetic gamma stimulation rescues memory impairments in an Alzheimer's disease mouse model. *Nat. Commun.* **10**, 5322 (2019).

72. Da Un Jeong *et al.* Improvements in Memory after Medial Septum Stimulation Are Associated with Changes in Hippocampal Cholinergic Activity and Neurogenesis. *BioMed Res. Int.* **2014**, 568587 (2014).

73. Ryan A. Wirt *et al.* Altered theta rhythm and hippocampal-cortical interactions underlie working memory deficits in a hyperglycemia risk factor model of Alzheimer's disease. *Commun. Biol.* **4**, 1–16 (2021).

74. Rojas-Gutierrez, E. *et al.* Alzheimer's disease and metabolic syndrome: A link from oxidative stress and inflammation to neurodegeneration. *Synap. N. Y. N* **71**, (2017).

75. Mattson, M. P. & Arumugam, T. V. Cell Metabolism Perspective Hallmarks of Brain Aging: Adaptive and Pathological Modification by Metabolic States. (2018) doi:10.1016/j.cmet.2018.05.011.

76. D. Chan *et al.* Induction of specific brain oscillations may restore neural circuits and be used for the treatment of Alzheimer's disease. *J. Intern. Med.* **290**, 993–1009 (2021).

77. Linyan Wu *et al.* Transcranial Alternating Current Stimulation Improves Memory Function in Alzheimer's Mice by Ameliorating Abnormal Gamma Oscillation. *IEEE Trans. Neural Syst. Rehabil. Eng.* **31**, 2060–2068 (2023).

78. Tao Tan *et al.* Low-frequency (1Hz) repetitive transcranial magnetic stimulation (rTMS) reverses Aβ1–42-mediated memory deficits in rats. *Exp. Gerontol.* **48**, 786–794 (2013).

79. Ambrad Giovannetti, E. & Fuhrmann, M. Unsupervised excitation: GABAergic dysfunctions in Alzheimer's disease. *Brain Res.* **1707**, 216–226 (2019).

80. Danysz, W. & Parsons, C. G. Alzheimer's disease, β-amyloid, glutamate, NMDA receptors and memantine - searching for the connections. *Br. J. Pharmacol.* **167**, 324–352 (2012).

81. Ramesh Kandimalla, Kandimalla, R., P. Hemachandra Reddy, Reddy, P. P. & Reddy, P. H. Therapeutics of Neurotransmitters in Alzheimer's Disease. *J. Alzheimers Dis.* **57**, 1049–1069 (2017).

82. Bracko, O. *et al.* Increasing cerebral blood flow improves cognition into late stages in Alzheimer's disease mice. *J. Cereb. Blood Flow Metab.* **40**, 1441–1452 (2020).

83. Busche, M. A. *et al.* Rescue of long-range circuit dysfunction in Alzheimer's disease models. *Nat. Neurosci. 2015 1811* **18**, 1623–1630 (2015).

84. Mohammad Uzair *et al.* Transcranial magnetic stimulation in animal models of neurodegeneration. *Neural Regen. Res.* **17**, 251–265 (2022).

85. Linyan Wu *et al.* Long-term gamma transcranial alternating current stimulation improves the memory function of mice with Alzheimer's disease. *Front. Aging Neurosci.* **14**, (2022).

CHAPTER 3: THE THERAPEUTIC POTENTIAL AND MECHANSIMS OF PSYCHEDELIC DRUGS

3.1 Introduction to Psychedelics

The term “psychedelic”, meaning “mind-manifesting”, was coined in 1957 by Humphrey Osmond to describe a class of compounds that induce emotional shifts, vivid sensory distortions, altered self-awareness, and, in some cases, hallucinations [1]. Despite their relatively modern description by Western society, it should be noted that these substances have been used for centuries in spiritual, religious, and medicinal contexts by indigenous cultures for thousands of years [2]. In Mesoamerica for instance, psilocybin-containing mushrooms were incorporated into ceremonial rituals of the Aztec and Mayan empires, while to this day, folk healers from various indigenous South American cultures utilize ayahuasca, a DMT-containing brew with psychoactive properties. The systemic investigation of psychedelics’ therapeutic potential by Western scientists began in the mid-20th century, with early studies suggesting efficacy in treating mood disorders and addiction. However, increasing concerns over recreational use and government regulation led to their classification as Schedule I substances in the 1970s, effectively halting most clinical research [3,2].

Interest in psychedelics resurged in the early 2000s, driven by advancements in neuroimaging, neuroscience, and clinical trials demonstrating potential therapeutic effects. Today, psychedelics are at the forefront of psychiatric and neurological research, with efforts to integrate them into treatments for addiction, anxiety, depression, and post-traumatic stress disorder (PTSD). The most widely studied approach, known as psychedelic-assisted therapy (PAT), involves administering psychedelics in controlled clinical settings alongside therapeutic

guidance [4]. While clinical trials have shown compelling evidence of efficacy, these substances remain controversial due to variability in patient response, potential adverse effects (e.g., anxiety, disorientation), and uncertainties regarding long-term safety. As such, there is an urgent need to understand the mechanisms by which these drugs elicit both beneficial and adverse effects. Preclinical studies using animal models seek to unravel how psychedelics modulate network-level activity, cell-type-specific interactions, and changes in neuromodulation, providing key insights into these questions [5]. Notably, this research has led to the development of non-hallucinogenic psychedelic derivatives, which aim to retain therapeutic benefits while eliminating perceptual distortions [6,7,8].

However, despite growing enthusiasm surrounding psychedelic research, the precise mechanisms underlying their therapeutic effects remain poorly understood. Further research is essential to refining their clinical use, addressing safety concerns, and developing targeted interventions. Understanding both clinical and preclinical aspects of psychedelic action is critical for harnessing their full therapeutic potential while minimizing risks, ultimately paving the way for novel treatments for psychiatric and neurological disorders.

3.2 Types of Psychedelics

Psychedelics have been previously classified using various frameworks based on chemical structure, subjective effects, and clinical applications. Here, they are categorized by their pharmacological mechanisms, which dictate their effects on consciousness and brain function. The first of these categories is that of classical serotonergic psychedelics, which includes compounds such as psilocybin, LSD, DMT, and mescaline. The common mechanism of these

drugs Is their action as 5-HT_2A receptor agonists, leading to altered perception, cognition, and dissolution of the self [2,9,10]. These substances profoundly impact brain connectivity, increasing entropy (the complexity and variability of neural activity patterns), and reducing activity in the default mode network (DMN). The second category is that of dissociatives, which includes ketamine and PCP. These substances block NMDA receptors, disrupting sensory integration and inducing out-of-body experiences [11]. The last category, entactogens, describes drugs such as MDMA, which enhance serotonin release, leading to increased emotional openness rather than classic hallucinogenic effects. While classical psychedelics, dissociatives, and entactogens all differ in their neuropharmacology and subjective experiences, all share the ability to induce altered states of consciousness and show promise in the treatment of psychiatric and neurological conditions.

3.2.1 Classical serotonergic psychedelics

The defining feature of classical psychedelics is their structural similarity to serotonin (5-HT), which allows them to bind to 5-HT_2A receptors with high affinity [12]. These are G protein-coupled receptors (GPCR), which are highly expressed in the cortex, thalamus, and limbic system, where they play roles in modulating perception, cognition, and mood [13]. Psychedelics such as psilocybin, LSD, DMT, and mescaline exert their hallucinogenic effects primarily via 5-HT_2A receptor agonism, though they also interact with other serotonin and dopamine receptors, leading to variability in their effects [14,15,16]

Psilocybin, the active compound in magic mushrooms, is metabolized in the body into psilocin, which acts on serotonin receptors to induce altered states of consciousness. These experiences typically last 4–6 hours and are associated with visual distortions, emotional introspection, and a sense of unity with the environment. [17,18]

LSD (lysergic acid diethylamide), first synthesized by Albert Hofmann in 1938, is a potent synthetic psychedelic that produces profound visual distortions, time dilation, and ego dissolution. LSD is unique in that it is active at microgram doses and has a long duration of action, lasting 8–12 hours. [17,19]

DMT (dimethyltryptamine), found in ayahuasca and various plants, produces intense but short-lived psychedelic effects, typically lasting 5–20 minutes when injected or vaporized. DMT experiences are often described as highly immersive, involving vivid geometric patterns, entity encounters, and ego disintegration. [20,21,22]

Mescaline, derived from peyote and San Pedro cacti, has a long-lasting psychedelic effect (8–12 hours) and is known for geometric visuals, enhanced sensory perception, and deep emotional introspection. [17]

Despite their shared 5-HT_2A agonism, these compounds exhibit unique binding affinities, pharmacokinetics, and subjective effects, leading to variability in psychedelic experiences.

	Name	Psychoactive component	Effects	Brain chemicals affected	Use in treatment	Chemical structure
			Tryptamines			
Classic Psychedelics	**LSD/Acid**	Lysergic acid diethylamide	Increase in blood pressure, changes in body temperature, loss of appetite	Serotonin	Depression, anxiety, alcohol use disorder	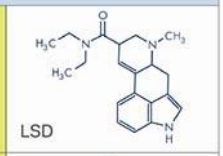 LSD
	Psilocybin/Mushrooms	4-phosphoryloxy-N, N-dimethyltryptamine	Feelings of relaxation, nervousness, introspective/spiritual experiences	Serotonin	Depression, anxiety, substance use disorders, illness-related anxiety, cancer-related depression, obsessive-compulsive disorder	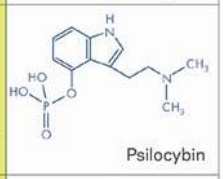 Psilocybin
	Ayahuasca	N,N-dimethyltryptamine (DMT)	Increased heart rate, altered state of awareness	Serotonin	Alcohol use disorder	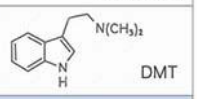 DMT
			Phenethylamines			
	Peyote	Mescaline	Increased body temperature and heart rate, hallucinations, agitation	Serotonin, dopamine	Substance use disorder	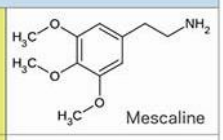 Mescaline
Non-Classic	**MDMA/Ecstasy**	3,4-Methylenedioxy-methamphetamine	Altered state of consciousness: euphoria, empathy, positive mood. Anxiety, increase in heart rate, body temperature and blood pressure.	Dopamine, Norepinephrine, Serotonin	Post-traumatic stress disorder (PTSD)	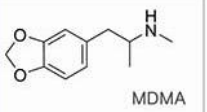 MDMA

Table 3.1 List of Classic and Non-Classic Psychedelics. Comparison of the psychoactive component, effects, brain chemicals affected, use in treatment, and chemical structure of classic and non-classic psychedelics, including LSD, Psilocybin, Ayahuasca, Peyote, and MDMA.[23] (Adapted from

Table 3.1

Shows a list of "classic psychedelics," which includes LSD, Psilocybin, Ayahuasca (DMT), and Peyote (Mescaline), and one "non-classic psychedelic," MDMA/Ecstasy. Although all these substances affect the brain's serotonin receptors, researchers have found that they affect other neural receptors and regions as well.

3.2.2 Entactogens/Empathogens

Entactogens (meaning "to touch within") and empathogens ("to generate empathy") refer to substances that enhance emotional connection, sociability, and introspection [10]. While these

terms are often used interchangeably, “entactogen” is the preferred scientific term. The most well-known entactogen is MDMA (3,4-methylenedioxymethamphetamine), commonly known as Ecstasy or Molly, with others including MDA (Sassafras) and Methylone (bk-MDMA). [24]

Unlike classical psychedelics, which act primarily on 5-HT_2A receptors, entactogens increase serotonin, dopamine, and norepinephrine release. They achieve this as monoamine releasers by inhibiting serotonin reuptake (SERT inhibition), reversing serotonin transporters (SERT reversal), and enhancing dopamine/norepinephrine activity [25,26]. This results in euphoria, increased emotional openness, reduced fear responses, and enhanced sensory perception, making MDMA particularly useful in psychedelic-assisted therapy for PTSD and social anxiety, however also leading to high potential for abuse.

Entactogens generally lack hallucinogenic effects but can still induce mild visual distortions at high doses. While promising for clinical applications, concerns about serotonin depletion, neurotoxicity, and potential for abuse remain key areas of research [25,26].

3.2.3 Dissociatives

Dissociatives are psychoactive substances that disrupt sensory integration and induce a sense of detachment from the body and environment. Unlike serotonergic psychedelics, dissociatives act primarily as NMDA receptor antagonists, reducing glutamatergic signaling and disrupting thalamocortical connectivity [11]. This results in altered perception, out-of-body experiences, and sedation, rather than the geometric visuals and cognitive expansion seen with classic psychedelics.[27]

Ketamine, a well-known dissociative, has been extensively studied for its rapid antidepressant effects [28], with clinical trials demonstrating its ability to alleviate treatment-

resistant depression within hours [29,30]. Ketamine induces hallucinatory states, time dilation, and dissociation, making it a substance of both therapeutic and recreational interest. However, at high doses, ketamine is an anesthetic. The drastic difference in dose effects is thought to be through inhibition of interneurons at low doses, leading to spikes in glutamate, and inhibition of NMDA receptors at high doses [31].

Phencyclidine (PCP), another dissociative, was originally developed as an anesthetic but was later discontinued due to severe psychiatric side effects, including hallucinations and psychosis. Compared to ketamine, PCP has a higher potential for addiction and cognitive impairment [32].

While dissociatives and classical psychedelics are often grouped together as "hallucinogens," their effects are fundamentally different. Classical psychedelics enhance connectivity and increase entropy in brain activity, while dissociatives disrupt sensory processing and have variable effects on brain activity at different doses [11].

Psychedelics, entactogens, and dissociatives represent distinct but overlapping classes of psychoactive substances, each with unique mechanisms of action, therapeutic applications, and subjective effects. While they all have the potential to alter consciousness and cognition, they vary significantly in trip duration, receptor binding, and risk profiles. Current research aims to further delineate these differences, ensuring that each compound is appropriately studied for its therapeutic potential in treating psychiatric and neurological disorders.

3.3 Therapeutic Potential of Psychedelics

A growing body of evidence suggests that psychedelics have therapeutic potential in treating depression, PTSD, addiction, and anxiety disorders. Clinical trials have demonstrated that

psychedelics, when administered in a controlled setting, can lead to long-lasting reductions in symptoms, potentially through mechanisms such as enhanced neuroplasticity, reduced amygdala hyperactivity, and increased emotional openness [10,33]. While the results are promising, questions remain about the underlying neural mechanisms, the role of set and setting, and the long-term safety of repeated use.

3.3.1 Psychedelic-Assisted Therapy (PAT): Mechanisms and Rationale

Psychedelic-assisted therapy (PAT) is an emerging treatment model that integrates psychedelic substances with psychotherapy to facilitate profound psychological and emotional breakthroughs [4]. Unlike traditional psychiatric medications, which require chronic daily use, psychedelics such as psilocybin, LSD, and MDMA are administered in a limited number of controlled sessions, often producing long-lasting effects after just one or a few treatments. The therapeutic rationale behind PAT is based on enhancing neuroplasticity, disrupting maladaptive thought patterns, and fostering emotional processing in a way that traditional therapies struggle to achieve.

Clinical research suggests that psychedelics temporarily weaken rigid neural patterns (e.g., those underlying depression, PTSD, or addiction) while enhancing brain connectivity and emotional openness, allowing for deep psychological processing [34,35,36,37]. Studies on psilocybin-assisted therapy have demonstrated that patients often experience reduced fear, increased cognitive flexibility, and a sense of personal meaning, which contribute to lasting symptom relief. Preclinical research using animal models and neuroimaging has provided insight into the biological underpinnings of psychedelic-assisted therapy.

Together, clinical and preclinical findings support the hypothesis that psychedelics promote cognitive flexibility, emotional regulation, and long-term neural adaptation, making them uniquely suited for therapeutic interventions in mood, trauma-related, and substance use disorders.

3.3.2 Depression and Anxiety Disorders

Clinical evidence strongly supports the use of psychedelics in the treatment of depression and anxiety disorders. Multiple studies have demonstrated that psilocybin and LSD produce substantial and sustained reductions in depressive and anxiety symptoms, particularly in patients with life-threatening cancer [38,39,40,41].

A randomized controlled trial comparing psilocybin to escitalopram (a selective serotonin reuptake inhibitor, SSRI) for depression found that psilocybin led to greater reductions in depressive symptom severity than escitalopram, with effects sustained for up to six weeks post-treatment [42]. Notably, the authors' primary outcome measure was not statistically significant, suggesting that psilocybin did not outperform escitalopram in terms of reducing depressive symptoms. Longer-term follow-ups further support these findings — a 12-month post-psilocybin study reported that participants continued to experience decreased depressive symptoms, with 72% showing a significant clinical response and 58% achieving remission [43].

Beyond psilocybin, other psychedelics have shown similar therapeutic potential. A double-blind, placebo-controlled study on LSD in patients with anxiety disorders — both with and without life-threatening illness — found significant reductions in anxiety scores that persisted for up to 16 weeks post-treatment [44]. Similar effects were observed for comorbid depressive symptoms, further supporting LSD's potential as an anxiolytic treatment.

Preclinical research has provided valuable mechanistic insights into the antidepressant and anxiolytic effects of psychedelics. Animal models of risk factors for depression and anxiety allow researchers to assess therapeutic efficacy in a controlled environment, while simultaneously investigating in vivo physiological changes underlying these effects. Studies in rodents have demonstrated that psychedelics such as psilocybin, DMT, and LSD reduce anxiety-like and depressive behaviors, reinforcing their potential as rapid-acting antidepressants [45,46,47].

It Is Important to note that various issues that arise with these clinical trials. For example, unblinding due to drug effects, and thereby expectancy effects, are key challenges in such studies. Almost 100% of patients in the psychedelic groups correctly guess their treatment.

In addition to their behavioral effects, preclinical studies have revealed possible mechanisms driving psychedelic-induced mood improvements. These include enhanced synaptic plasticity, increased dendritic spine density, and modulation of stress-related neural circuits. Such mechanisms have been shown to be critical in mood disorders such as depression and anxiety [48,49,50,28]. However, the precise mechanisms remain an ongoing area of debate and investigation. Future studies should focus on elucidating these pathways to optimize therapeutic strategies for mood disorders while minimizing risks and side effects.

Study	Population/indication and sample size	Drug and design	Main efficacy outcome
Moreno et al (2006)	Obsessive compulsive disorder, *n*=9	Psilocybin: single-arm, within subjects, variable doses. Up to four doses of psilocybin	All patients showed improvements within 24 h of a treatment but no effect of dose
Grob et al (2011)	Anxiety and depression in end-stage cancer, *n*=12	Psilocybin: DB-RCT, crossover, inert placebo. Single dose of psilocybin	Significant reductions in trait anxiety at 3 months and depression at 6 months
Johnson et al (2014)	Long-term chronic tobacco smoking, *n*=15	Psilocybin: open-label. Up to three doses of psilocybin after four CBT sessions	80% of sample abstinent at 6 month follow-up
Gasser et al (2014)	Anxiety related to life-threatening disease, *n*=12	LSD: DB-RCT, crossover, very low dose (VLD) LSD=control. Single dose of LSD	Significant decreases in state and trait anxiety *vs* VLD at 2 months and sustained for 12 months
Bogenschutz et al (2015)	Alcohol dependence, *n*=10	Psilocybin: open-label. Up to two doses after seven motivational therapy sessions	Significant decrease in drinking behaviors for up to 9 months
Osorio Fde et al (2015) and Sanches *et al* (2016)	Major depressive disorder (MDD), *n*=6+study extension to *n*=17	Ayahuasca: open-label. Single dose of ayahuasca	Significant decreases in depressive symptoms for up to 21 days
Carhart-Harris et al (2016a, b)	Treatment-resistant MDD, *n*=12+study extension to *n*=20	Psilocybin: open-label. Two doses of psilocybin	Significant decreases in depressive symptoms for up to 6 months
Ross et al (2016)	Anxiety and depression related to life-threatening cancer, *n*=29	Psilocybin: DB-RCT, crossover, niacin=active placebo. Single dose of psilocybin	Significant decreases in anxiety and depression *vs* niacin at 7 weeks (pre crossover) and sustained for 6.5 months
Griffiths et al (2016)	Anxiety and depression related to life-threatening cancer, *n*=51	Psilocybin: DB-RCT, crossover, VLD psilocybin=control. Single dose of psilocybin	Significant decreases in anxiety and depression *vs* VLD at 5 weeks (pre crossover). Effects sustained for 6 months

Table 3.2 Clinical Trials Involving Psychedelics Published During the Present 'Second Wave' of Psychedelic Research A comparison of recent clinical trials investigating the therapeutic efficacy of psychedelic drugs. Factors included population/indication and sample size, drug and design, and main efficacy outcome. [51] (Adapted from

3.3.3 PTSD and Trauma-Related Disorders

Post-traumatic stress disorder (PTSD) has become a primary focus of PAT research. While MDMA showed promising results in clinical trials for PTSD [52,53], recent FDA review of the drug led to its rejection due to concerns about trial methodology, particularly placebo controls and biases, misconduct allegations, safety concerns, and unclear long-term effects.

MDMA is believed to enhance the therapeutic process by reducing fear responses during trauma processing and promoting extinction learning. This effect is thought to occur through increased serotonin and oxytocin release, facilitating emotional openness, trust, and cognitive flexibility, which may help individuals reprocess traumatic memories more effectively, especially through facilitation of the therapeutic alliance between patient and provider [10].

Prolonged exposure therapy is the gold-standard treatment for PTSD, being one of the best evidenced and most effective psychological interventions in use today. MDMA may be a beneficial addition to facilitate such therapeutics, however further research is needed to optimize treatment protocols, determine long-term efficacy, and explore how psychedelics may be integrated into broader trauma-informed care strategies.

3.3.4 Addiction Treatment: Alcohol, Nicotine, and Opioid Use Disorders

Beyond their potential for treating mood and anxiety disorders, psychedelics have shown promising effects in addiction treatment, particularly for alcohol, nicotine, and opioid use disorders. Clinical and preclinical research suggests that PAT may reduce substance dependence and craving while promoting long-term behavioral change .

A landmark study on psilocybin-facilitated smoking cessation found that, at a 6-month follow-up, 67% of participants remained abstinent, as confirmed by biological markers [54]. Similarly, a clinical trial investigating psilocybin for alcohol use disorder (AUD) found that participants receiving psilocybin showed a significant reduction in heavy drinking days and overall alcohol consumption compared to placebo controls. These effects were sustained for up to 36 weeks post-treatment [55], suggesting that psychedelics may produce long-term behavioral and neurobiological changes that support addiction recovery.

While human trials have demonstrated the efficacy of psychedelics in addiction treatment, preclinical studies investigating classical psychedelics in addiction models remain limited [56]. However, available research has shown promising effects.

In opioid addiction models, ketamine was found to block morphine-induced conditioned place preference (CPP) and reduce anxiety-like behaviors in mice, indicating a potential role in preventing relapse and withdrawal-related distress [57].

For alcohol use disorder, most preclinical studies have used the two-bottle choice paradigm, where rodents select between alcohol and water. Notably, Apler et al. demonstrated that psilocybin sex-dependently reduced alcohol consumption in C57BL/6J mice, highlighting the need for further research on sex-dependent differences in psychedelic effects on addiction-related behaviors [58]. Additional studies found that a single dose of LSD significantly reduced alcohol intake, while DOI (a selective 5-HT_2A agonist) attenuated ethanol consumption and conditioned place preference in male mice [59,60].

While more research is needed to fully understand the mechanisms underlying psychedelic-assisted addiction treatment, current findings indicate that psychedelics may help disrupt maladaptive reward pathways, enhance cognitive flexibility, and reduce substance craving. Future studies should focus on optimizing dosing strategies, assessing long-term safety, and understanding individual differences in response to psychedelic treatment for addiction recovery.

3.3.5 Neurodegenerative and Cognitive Disorders

While much of the focus on psychedelics has been on their potential for treating psychiatric conditions such as depression, PTSD, and addiction, a growing area of interest is their therapeutic application for neurodegenerative and cognitive disorders [61,62.] Compounds such as

psilocybin and LSD are being explored as potential treatments for early-stage Alzheimer's disease (AD) and age-related cognitive decline due to their effects on neuroplasticity, inflammation, and cognitive function.

A clinical trial investigating psilocybin in AD patients aims to determine whether it can alleviate depression and cognitive decline, symptoms that often co-occur in neurodegenerative diseases [61]. Additionally, a 2018 study on microdosing psilocybin found that it improves cognitive flexibility and verbal fluency in older adults, suggesting a potential role in counteracting age-related cognitive decline [63].

PET imaging studies have revealed reduced 5-HT_2A receptor density in AD patients, suggesting that serotonergic dysfunction may contribute to cognitive impairment and neuropsychiatric symptoms associated with the disease [64,65]. Since serotonergic psychedelics act as 5-HT_2A agonists, they may help restore serotonergic signaling and counteract some of the cognitive and emotional deficits seen in AD.

Activation of 5-HT_2A receptors is known to enhance synaptic plasticity and long-term potentiation (LTP), both of which are essential for learning and memory formation. Rodent studies have demonstrated that psychedelics promote dendritic spine growth and increase brain-derived neurotrophic factor (BDNF) expression, key processes involved in neuroprotection and synaptic resilience [66]. In the context of neurodegenerative disease, these findings suggest that psychedelics could support synaptic integrity and cognitive function, possibly slowing disease progression.

Neuroinflammation is a hallmark of AD and other neurodegenerative diseases, contributing to synaptic dysfunction, oxidative stress, and neuronal death. Emerging evidence suggests that

serotonergic psychedelics can modulate inflammatory pathways, leading to reduced pro-inflammatory cytokines and oxidative stress [67]. Differences in pharmacological properties, signaling dynamics, and intracellular effects between serotonin and psychedelics contribute to variable inflammatory properties. By attenuating neuroinflammation, psychedelics may help slow disease progression and preserve cognitive function.

Despite promising preclinical findings and early human trials, much research is still needed to determine the long-term safety, efficacy, and mechanisms of psychedelics in treating neurodegenerative diseases. Large-scale clinical trials are essential to validate their therapeutic potential and establish protocols for safe implementation in aging and neurodegenerative care. If successful, psychedelics could represent a novel class of therapeutics for not only treating neuropsychiatric symptoms in AD but also potentially modifying disease progression by enhancing plasticity and neuroprotection.

3.3.6 Risks, Challenges, and Ethical Considerations

While psychedelics show tremendous promise for treating neuropsychiatric and neurodegenerative disorders, their clinical use remains controversial due to safety concerns, regulatory hurdles, and ethical considerations [68,40,43,69,70]. Although many studies report positive therapeutic outcomes, psychedelics also pose risks related to adverse psychological effects, individual variability in response, and long-term safety. Additionally, their historical stigma, potential for misuse, and the commercialization of psychedelic therapy raise ethical questions about equitable access and responsible medical use.

Despite generally low physiological toxicity, psychedelics can cause acute psychological distress, anxiety, and hallucinations that may be overwhelming or dysphoric [69]. In rare cases,

individuals may experience Hallucinogen-Persisting Perception Disorder (HPPD) — a condition where users experience flashbacks or lingering visual disturbances long after use[71], psychedelic-induced psychosis — individuals with underlying schizophrenia or bipolar disorder may be at heightened risk of prolonged psychotic episodes [68], or dissociation and depersonalization — some individuals report loss of identity or difficulty reintegrating into daily life after intense psychedelic experience [72]. While these risks are mitigated in controlled clinical settings, they highlight the need for screening protocols and trained facilitators in PAT.

In attempt to avoid such adverse effects, ongoing studies aim to isolate the therapeutic effects of these drugs without the need for the hallucinogenic experience. This area is heavily debated in the field, with some suggesting that the subjective experience is essential for therapeutic outcomes, while others show supporting preclinical evidence for the opposite [73,74,33]. A recent study demonstrated the ability to isolate psychedelic responsive neurons underlying anxiolytic behavioral states, suggesting promising targets for future research [75].

Most psychedelics remain Schedule I substances, classified as having no accepted medical use and a high potential for abuse in many countries. While research efforts are shifting perceptions, regulatory approval remains a significant obstacle. On top of this, the rapid commercialization of psychedelics raises ethical concerns about profit-driven models overtaking scientific integrity. Such growth has been recent, and despite promising early results, long-term safety remains poorly understood, raising another point of consideration.

While psychedelics represent a paradigm shift in mental health treatment, their clinical use must be approached with caution, rigorous oversight, and ethical responsibility. Addressing safety, regulatory, and equity concerns will be critical in ensuring these compounds can be responsibly integrated into mainstream medicine.

3.4 Mechanisms of Psychedelic Drug Action: From Molecules to Networks

Understanding how psychedelics alter consciousness and promote therapeutic effects requires a comprehensive exploration that spans multiple levels — from molecular interactions to large-scale brain networks. In this section, we integrate evidence from both clinical neuroimaging and preclinical in vivo studies to elucidate how psychedelics act at the molecular, cellular, circuit, and whole-brain levels. At the molecular and cellular scale, psychedelics primarily engage with receptors like 5-HT_2A to trigger intracellular cascades that enhance neuroplasticity and synaptic remodeling. These changes set the stage for alterations in neural circuits, which have been observed as modifications in firing patterns, oscillatory dynamics, and functional connectivity across brain regions. Clinical studies using fMRI and EEG complement these findings by revealing how these substances modulate network synchrony. Together, these multi-scale insights not only deepen our understanding of the psychedelic state but also inform the development of targeted interventions for psychiatric and neurological disorders.

3.4.1 Molecular and Cellular Mechanisms

At the molecular level, psychedelics primarily exert their effects through high-affinity binding to serotonin 5-HT_2A receptors, which are widely expressed in the cortex, thalamus, and limbic system [33,76,77]. Activation of these G protein-coupled receptors (GPCRs) initiates intracellular signaling cascades, such as the phospholipase C (PLC) pathway, leading to an increase in intracellular calcium levels. This calcium influx triggers downstream kinases — including protein kinase C (PKC), extracellular signal-regulated kinase (ERK), and the mechanistic target of rapamycin (mTOR) pathway — that collectively promote neuroplasticity by regulating various cellular functions, including neurotransmitter release, dendritic remodeling,

and synaptic signaling. These cascades result in enhanced dendritic spine growth, upregulation of synaptic proteins, and increased expression of neurotrophic factors such as brain-derived neurotrophic factor (BDNF) [2,78].

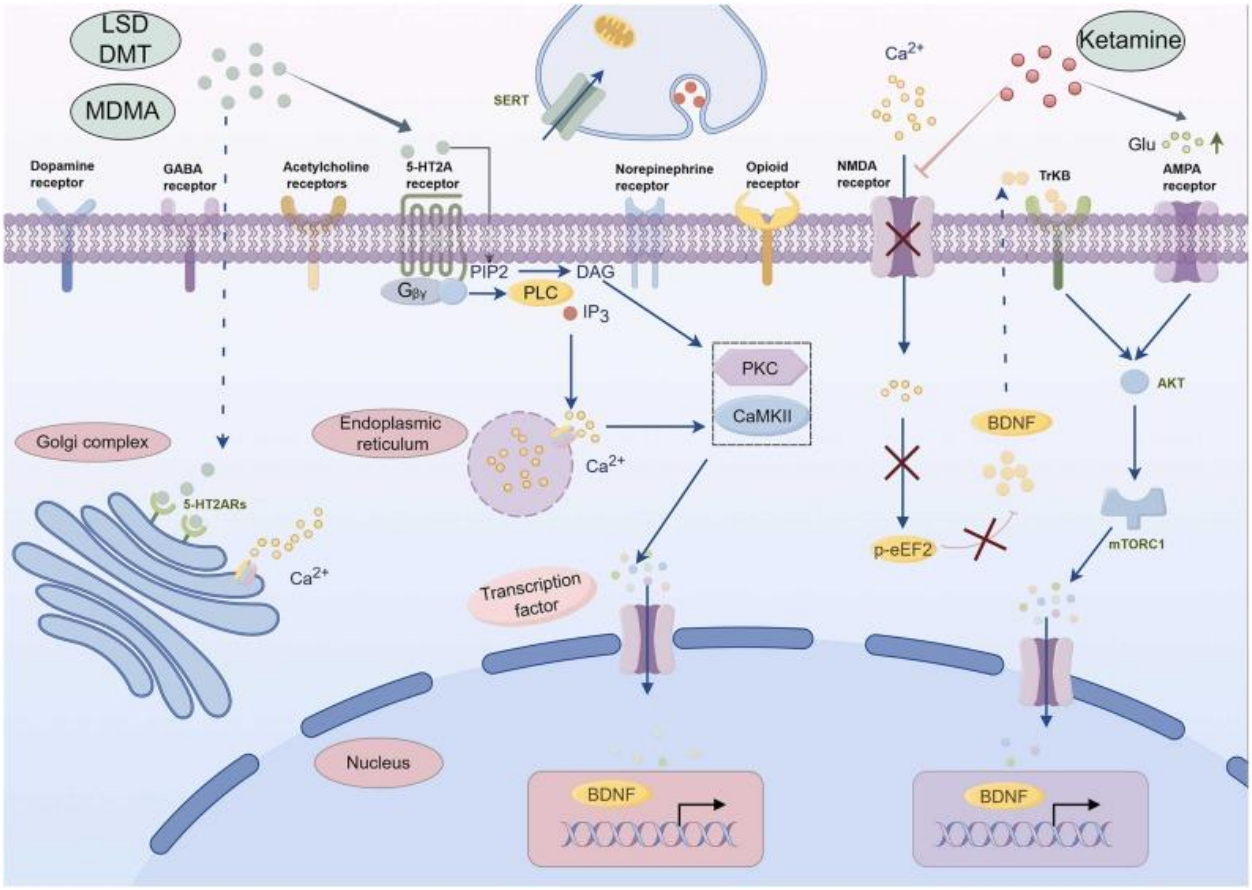

Figure 3.1 59-HT$_2$AR signaling pathways involved in the mechanisms of action of psychedelics. Classic psychedelics primarily act through the 5-HT$_2$A receptor, which recent studies suggest is located on the Golgi membrane rather than the cell membrane. Activation of 5-HT$_2$A receptors triggers Gq-mediated signaling, leading to Ca^{2+} release and downstream gene regulation. In contrast, ketamine blocks NMDA receptors, indirectly activating AMPA and TRKB receptors to engage the mTOR pathway. Additionally, psychedelics influence dopamine, norepinephrine, and acetylcholine receptor activity, contributing to their broad neurobiological effects. [79]

A major effect of psychedelic-induced 5-HT$_2$A receptor activation is its ability to enhance synaptic plasticity [80,76,81,46]. In vitro studies with rodent neuronal cultures have demonstrated that even low doses of classical psychedelics like psilocybin and LSD can induce rapid and sustained structural changes, including increased dendritic spine density and alterations in synaptic

connectivity [66]. These structural modifications are accompanied by changes in gene expression, such as the upregulation of immediate early genes like Arc and c-Fos, which are markers of neuronal activation and synaptic remodeling [82,83].

In in vivo animal studies, two-photon microscopy imaging has revealed that psychedelics promote dendritic spine growth in the prefrontal cortex (PFC) within hours of administration, with some structural changes persisting for weeks after a single dose [84]. These findings suggest that psychedelics may induce long-term enhancements in synaptic strength, potentially contributing to their sustained antidepressant and anxiolytic effects. Additionally, electrophysiological studies have shown that psychedelics increase synaptic excitability and glutamatergic neurotransmission, particularly in layer 5 pyramidal neurons of the PFC, a key region implicated in cognitive flexibility and emotional regulation [85].

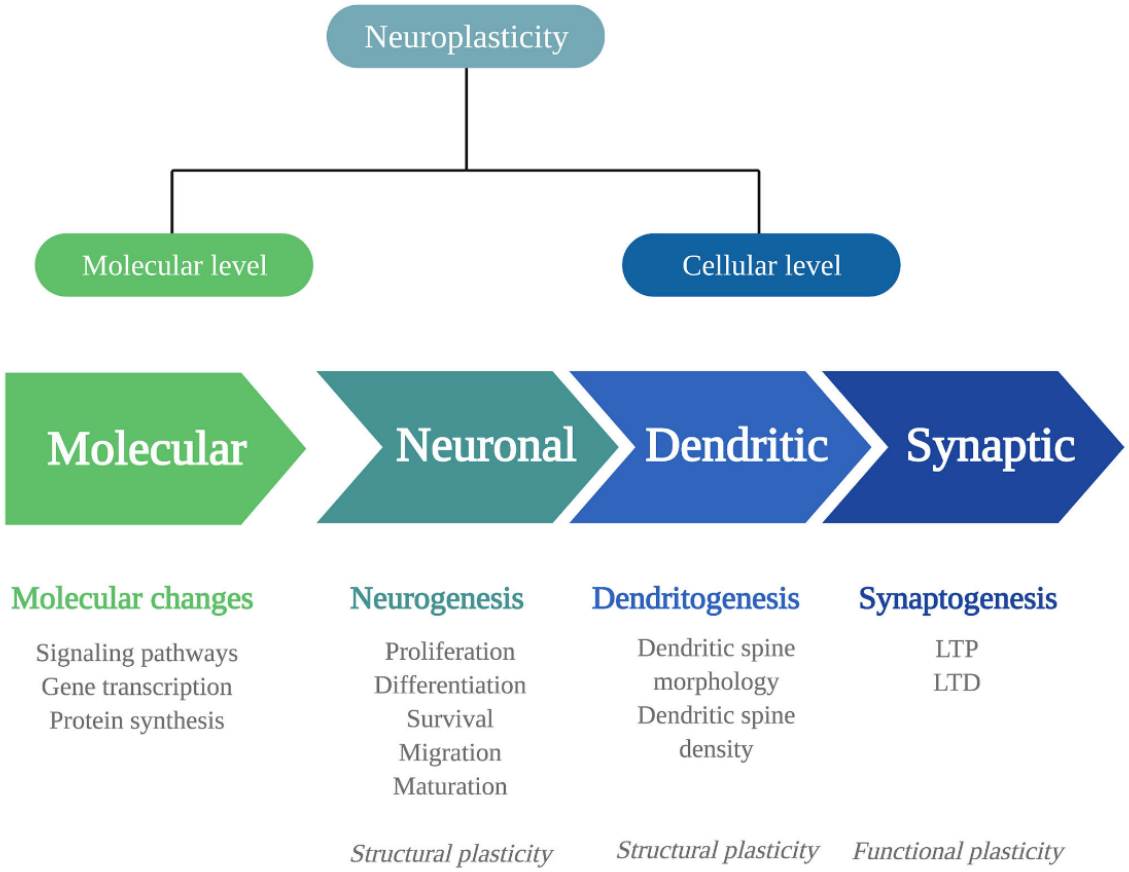

Figure 3.102 Molecular and cellular mechanisms of neuroplasticity. Neuroplasticity occurs at multiple levels, including intracellular signaling pathways, gene transcription, and protein synthesis. Structural plasticity involves neurogenesis and dendritic remodeling, altering neuronal morphology, while functional plasticity is driven by synaptogenesis, affecting synaptic strength and connectivity. Long-term potentiation (LTP) and long-term depression (LTD) modulate synaptic efficacy, contributing to learning and memory. [86] (Adapted from

In addition to Gq-mediated signaling, 5-HT$_2$A activation can recruit β-arrestin, influencing receptor internalization and downstream signaling pathways, such as mitogen-activated protein kinase (MAPK) cascades [13,87]. This has led to growing interest in biased agonism, where different psychedelics may preferentially activate specific intracellular pathways, leading to potentially dissociable effects on plasticity and cognition. Some evidence suggests that certain downstream plasticity-related effects — such as dendritic spine growth — could occur

independently of the hallucinogenic experience, raising the possibility of developing non-hallucinogenic psychedelics with therapeutic benefits [76].

Although 5-HT_2A receptor agonism is essential for the hallucinogenic effects of psychedelics, these compounds exhibit complex polypharmacology, interacting with multiple biogenic amine receptors [88]. For instance, LSD binds with high affinity not only to 5-HT_2A receptors but also to 5-HT_1A, 5-HT_2B, and 5-HT_2C, as well as dopamine (D1–D4) and adrenergic (α1, α2) receptors [89]. Some studies suggest that D2 receptor activation may contribute to LSD's prolonged effects [90], while 5-HT1A receptor agonism may play a role in mood modulation [91]. However, the precise functional contributions of these additional receptor interactions remain unclear, and it is uncertain whether 5-HT_2A activation alone accounts for the full therapeutic potential of psychedelics [92].

Recent advances in structural biology have provided high-resolution insights into psychedelic receptor interactions. Studies using X-ray crystallography and cryo-electron microscopy (cryo-EM) have revealed how psychedelics engage 5-HT_2A receptors via a combination of hydrophobic, ionic, and π-π interactions [77,93]. Structural studies on LSD-bound 5-HT_2B receptors have provided insights into prolonged receptor engagement, while cryo-EM structures of active-state 5-HT_2A suggest key determinants of psychedelic pharmacology [94]. These findings are informing rational drug design, including efforts to develop non-hallucinogenic psychedelics that retain therapeutic efficacy while avoiding undesirable effects, such as 5-HT_2B-mediated cardiac valvulopathy [95].

Beyond their direct effects on serotonin receptors, recent research suggests that some psychedelics may act through receptor-independent mechanisms. For instance, psilocybin and LSD have been found to allosterically modulate the TrkB receptor, which is the main receptor for

BDNF [92]. By enhancing TrkB dimerization, psychedelics potentiate BDNF signaling, further promoting neuronal plasticity and synaptic remodeling. This 5-HT_2A-independent mechanism may contribute to the long-term neural adaptations associated with psychedelic therapy and could be leveraged to develop novel neuroplasticity-promoting compounds.

Psychedelics trigger intracellular signaling pathways that promote neuroplasticity, enhance synaptic connectivity, and induce long-term structural changes in the brain. These molecular and cellular changes set the stage for larger-scale alterations in neural circuits and brain networks, which likely underlie both the subjective psychedelic experience and the therapeutic effects observed in clinical trials. A deeper understanding of these mechanisms of action will be crucial for optimizing psychedelic-based therapies and developing novel pharmacological interventions for mood and psychiatric disorders.

3.4.2 Circuit-Level and Whole-Brain Mechanisms

While molecular and cellular changes induced by psychedelics set the foundation for neuroplasticity, their effects on neural circuits and large-scale brain networks explain the profound alterations in perception, cognition, and emotion associated with these substances. Neuroimaging and electrophysiological studies show that psychedelics induce widespread reorganization of brain activity by disrupting canonical network structures and increasing global connectivity [77].

One of the most well-documented effects of psychedelics is the disruption of the default mode network (DMN), a system of interconnected brain regions involved in self-referential thought, introspection, and ego maintenance. fMRI studies have demonstrated that psychedelics such as psilocybin and LSD reduce within-network DMN connectivity while enhancing

connectivity between the DMN and other brain regions [96]. This network disintegration is believed to underlie ego dissolution, altered self-perception, and heightened emotional processing [77].

At the circuit level, psychedelics increase excitatory drive onto pyramidal neurons in the prefrontal cortex (PFC), a region essential for cognitive flexibility and decision-making. Electrophysiological recordings in rodents show that psychedelics induce increased cortical firing rates [77], differentially modified gamma oscillations [97], and disrupted thalamocortical sensory gating [77]. These changes contribute to heightened sensory perception, altered consciousness, and enhanced cognitive flexibility during the psychedelic state.

Beyond the PFC, psychedelics also modulate hippocampal and amygdala dynamics, regions crucial for memory processing and emotional regulation [98]. Increased hippocampal-cortical connectivity following psilocybin administration has been observed in both rodents and humans, supporting the idea that psychedelics may restore dysfunctional connectivity in conditions such as PTSD and depression, where hippocampal-prefrontal interactions are often impaired [35].

Psychedelics are also thought to alter predictive coding processes, shifting the balance between bottom-up sensory input and top-down cognitive control. Recent EEG and fMRI studies suggest that psychedelics increase neural entropy and weaken top-down control, allowing for more flexible perception and cognition [99]. This could help disrupt rigid thought patterns observed in psychiatric conditions such as depression, OCD, and addiction. Such alterations have been corroborated by in vivo preclinical research in rodents [100,10].

Several models attempt to explain how psychedelics alter brain function and cognition by disrupting normal network coordination and sensory processing.

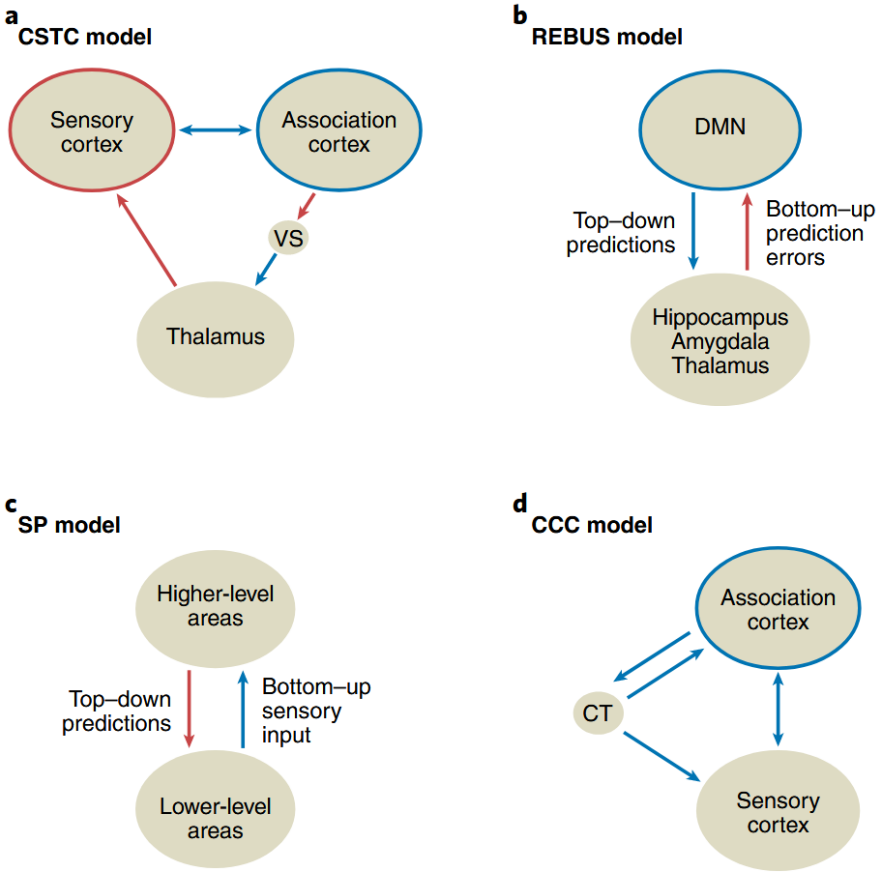

Figure 3.3 Network-level models of psychedelic action. 11(a) The CSTC model suggests psychedelics alter thalamic gating, shifting sensory versus associative processing. (b) The REBUS model proposes increased bottom-up signaling and reduced top-down control, leading to cognitive disintegration. (c) The SP model attributes psychedelic effects to reduced sensory input and heightened reliance on prior expectations. (d) The CCC model focuses on disrupted claustrum activity, leading to cortical desynchronization. Red arrows indicate increased connectivity, blue arrows indicate decreased connectivity, and circles represent integration changes.[77] (Adapted from Kwan 2022)

The Cortico–Striato–Thalamocortical (CSTC) Model suggests that psychedelics impair thalamic gating, allowing excess sensory input to reach the cortex [36,101]. Activation of 5-HT$_2$A receptors within thalamocortical loops weakens normal sensory filtering, contributing to hallucinations and perceptual distortions. This theory is supported by increased thalamocortical connectivity and impaired sensorimotor gating in both human and animal studies following psychedelic administration.

The Relaxed Beliefs Under Psychedelics (REBUS) Model proposes that psychedelics reduce the precision of prior beliefs, increasing bottom-up sensory processing and neural entropy [34]. This weakened top-down control results in disintegration of resting-state networks like the DMN, facilitating ego dissolution and altered self-referential thought.

The Strong Prior (SP) Model challenges REBUS by suggesting that hallucinations arise not from excess sensory input, but from an over-reliance on internally generated expectations [102]. Animal studies indicate that psychedelics suppress stimulus-evoked responses, implying a reduction in bottom-up sensory input rather than an increase.

The Cortico–Claustro–Cortical (CCC) Model focuses on the claustrum, a brain region rich in 5-HT_2A receptors and believed to play a key role in integrating sensory and cognitive processes [103]. Psychedelics have been shown to weaken functional connectivity between the claustrum and cortical regions, which may contribute to disorganized thought patterns and altered conscious states.

While the CSTC and CCC models emphasize neural circuit disruptions, the REBUS and SP models focus on predictive coding and cognitive constraints. A unified model may integrate both perspectives, acknowledging that psychedelics disrupt top-down control while altering reliance on internally generated perceptions.

Taken together, psychedelics exert their effects by enhancing synaptic plasticity, increasing global brain connectivity, and disrupting maladaptive network activity. These changes provide a strong mechanistic basis for their therapeutic potential in treating depression, PTSD, addiction, and other neuropsychiatric disorders. Further research combining neuroimaging,

electrophysiology, and computational modeling will be essential in refining our understanding of how psychedelics reshape brain networks and influence long-term mental health outcomes.

3.4.3 Neurovascular Coupling and the Limitations of fMRI in Psychedelic Research

With the growing recognition of psychedelics' therapeutic potential, there has been a surge in clinical trials aimed at understanding their mechanisms of action. A central tool in these investigations is functional magnetic resonance imaging (fMRI), which provides a noninvasive method to examine brain activity. However, fMRI does not directly measure neuronal activity; instead, it relies on changes in blood oxygenation levels as a proxy for neural activation — a relationship governed by neurovascular coupling (NVC). Since psychedelics have high affinity for serotonin receptors, many of which directly affect vascular function, their impact on NVC dynamics may confound fMRI-based interpretations of neural activity, raising important considerations for clinical research.

fMRI relies on the assumption that changes in blood flow accurately reflect changes in neural activity. This technique measures the blood-oxygen-level-dependent (BOLD) signal, which is driven by hemodynamic responses to local neuronal activation [104,105]. In typical conditions, increased neuronal firing leads to greater oxygen demand, resulting in vasodilation and enhanced blood flow to active brain regions. However, psychedelics, due to their serotonergic receptor agonism, may independently alter cerebrovascular responses, disrupting this tight neuronal-hemodynamic relationship and introducing potential artifacts into fMRI analyses.

Psychedelics act on multiple serotonin receptors, several of which are directly involved in regulating vascular tone [106,107]. 5-HT_2A receptor activation has been shown to dilate blood vessels, increasing regional cerebral blood flow (CBF) independently of local neuronal activity.

5-HT_1A receptor activation, in contrast, can cause vasoconstriction, potentially reducing CBF in certain areas. Serotonergic modulation of astrocytes can also influence vessel diameter, further altering the relationship between neuronal activation and blood supply.

Because psychedelics simultaneously engage these receptors across different brain regions, their effects on blood flow are highly context-dependent, leading to regional increases or decreases in CBF that may not correlate directly with underlying neural firing. This disrupts the fundamental assumption of fMRI — that BOLD signal changes accurately reflect neuronal activation — making it difficult to disentangle drug-induced vascular effects from actual changes in brain activity.

To improve the accuracy of fMRI-based psychedelic research, it is essential to integrate alternative imaging techniques that can directly measure both neural activity and vascular responses. Promising approaches include simultaneous fMRI and EEG/MEG – EEG and magnetoencephalography (MEG), which provide direct electrophysiological recordings of neural activity, allowing researchers to distinguish genuine neuronal effects from vascular artifacts in BOLD signals [108]. Methods like two-photon microscopy, laser speckle contrast imaging (LSCI), and optical intrinsic signal imaging (OISI) allow for high-resolution in vivo measurements of neurovascular responses, clarifying how psychedelics alter blood flow at the microvascular level (Fig 3.4) [109,110]. Finally, unlike standard BOLD fMRI, arterial spin labeling (ASL) fMRI directly measures cerebral blood flow, helping differentiate neuronal-driven perfusion changes from drug-induced vascular effects.

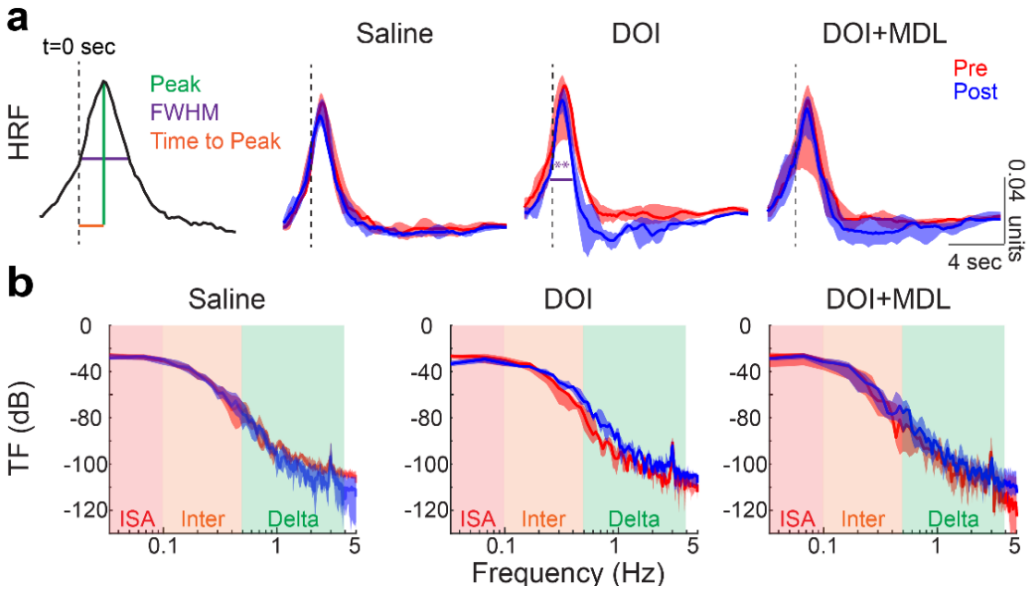

Figure 3.4 Hallucinogenic 5-HT12$_2$A receptor agonism alters stimulus-evoked neurovascular coupling. (a) Hemodynamic response functions (HRFs) estimated from whisker stimulation reveal that DOI significantly reduces the full width at half maximum (FWHM) of the HRF. (b) Transfer function analysis shows a trend toward increased transduction at frequencies above 0.5 Hz under DOI. Data are presented as medians with 25th and 75th percentiles across mice, highlighting altered neurovascular dynamics following hallucinogenic modulation. *p<0.01. [109] (Adapted from Padawer-Curry 2023)

Although fMRI has been instrumental in advancing our understanding of psychedelic effects on brain function, its reliance on neurovascular coupling introduces significant limitations due to the vasoactive properties of psychedelics. By independently modulating cerebral blood flow, psychedelics may confound fMRI interpretations, potentially leading to misrepresentations of neural activity and functional connectivity. To mitigate these confounds, future research should incorporate multi-modal imaging approaches that provide a more precise characterization of both neural and vascular effects. These advancements will be crucial for ensuring that fMRI-based findings accurately reflect the true mechanisms underlying psychedelic-induced changes in brain function.

3.5 Conclusion

Psychedelics have re-emerged as a significant focus of neuroscience and psychiatry, offering unique insights into brain function and potential therapeutic applications. Their ability to profoundly alter perception, cognition, and emotion is primarily driven by their interaction with the serotonin system, particularly through 5-HT_2A receptor activation. These effects extend beyond transient changes in consciousness, influencing neuroplasticity, large-scale brain network dynamics, and long-term psychological outcomes.

Despite historical challenges in psychedelic research due to regulatory restrictions, recent advancements in neuroimaging, circuit-level analyses, and clinical trials have revitalized the field. Studies continue to uncover the mechanisms by which psychedelics promote synaptic remodeling, enhance network flexibility, and disrupt maladaptive thought patterns. These findings support their potential in treating psychiatric disorders such as depression, PTSD, and addiction, though many questions remain about their safety, efficacy, and individual variability in response.

Future research must further delineate the neural circuits and molecular pathways underlying psychedelic effects while refining clinical protocols to maximize therapeutic benefits. By integrating basic science with translational applications, the next generation of psychedelic research will help determine their role in modern psychiatry and cognitive neuroscience, ultimately shaping how these compounds are understood and utilized in medicine.

References

1. Humphry Osmond & Osmond, H. A review of the clinical effects of psychotomimetic agents. *Ann. N. Y. Acad. Sci.* **66**, 418–434 (1957).

2. David E. Nichols & David E. Nichols. Psychedelics. *Pharmacol. Rev.* **68**, 264–355 (2016).

3. Lester Grinspoon, Bakalar, J. B., James B. Bakalar, Grinspoon, L. & Grinspoon, L. Psychedelic Drugs Reconsidered. (1979).

4. Gregory S. Barber, Gregory Barber, Scott T. Aaronson, & Scott T. Aaronson. The Emerging Field of Psychedelic Psychotherapy. *Curr. Psychiatry Rep.* (2022) doi:10.1007/s11920-022-01363-y.

5. Gumpper, R. H. & Roth, B. L. Psychedelics: preclinical insights provide directions for future research. *Neuropsychopharmacol. 2023* 1–9 (2023) doi:10.1038/s41386-023-01567-7.

6. Lindsay P. Cameron *et al.* A non-hallucinogenic psychedelic analogue with therapeutic potential. *Nature* **589**, 474–479 (2020).

7. Dongmei Cao *et al.* Structure-based discovery of nonhallucinogenic psychedelic analogs. *Science* **375**, 403–411 (2022).

8. Vern Lewis *et al.* A non-hallucinogenic LSD analog with therapeutic potential for mood disorders. *Cell Rep.* **42**, 112203–112203 (2023).

9. Franz X. Vollenweider & Vollenweider, F. X. Brain mechanisms of hallucinogens and entactogens. *Dialogues Clin. Neurosci.* **3**, 265–279 (2001).

10. Heifets, B. D. & Olson, D. E. Therapeutic mechanisms of psychedelics and entactogens. *Neuropsychopharmacology* **49**, 104–118 (2024).

11. Mark Petersen *et al.* Hallucinogens — psychedelics and dissociative drugs. 295–303 (2020) doi:10.1016/b978-0-12-815846-3.00016-8.

12. G K Aghajanian, Aghajanian, G. K., Marek Gj & Marek, G. J. Serotonin and hallucinogens. *Neuropsychopharmacology* **21**, 16–23 (1999).

13. López-Giménez, J. F. & González-Maeso, J. Hallucinogens and Serotonin 5-HT2A Receptor-Mediated Signaling Pathways. *Curr. Top. Behav. Neurosci.* **36**, 45 (2018).

14. Franz X. Vollenweider *et al.* Psilocybin induces schizophrenia-like psychosis in humans via a serotonin-2 agonist action. *Neuroreport* **9**, 3897–3902 (1998).

15. Michael Kometer *et al.* Activation of serotonin 2A receptors underlies the psilocybin-induced effects on α oscillations, N170 visual-evoked potentials, and visual hallucinations. *J. Neurosci.* **33**, 10544–10551 (2013).

16. Javier González-Maeso *et al.* Hallucinogens Recruit Specific Cortical 5-HT2A Receptor-Mediated Signaling Pathways to Affect Behavior. *Neuron* **53**, 439–452 (2007).

17. Laura Ley *et al.* Comparative acute effects of mescaline, lysergic acid diethylamide, and psilocybin in a randomized, double-blind, placebo-controlled cross-over study in healthy participants. *Neuropsychopharmacology* **48**, 1659–1667 (2023).

18. Mogens Madsen *et al.* Psychedelic effects of psilocybin correlate with serotonin 2A receptor occupancy and plasma psilocin levels. *Neuropsychopharmacology* **44**, 1328–1334 (2019).

19. Yasmin Schmid *et al.* Acute Effects of Lysergic Acid Diethylamide in Healthy Subjects. *Biol. Psychiatry* **78**, 544–553 (2015).

20. C. Timmermann, R. Zeifman, D. Erritzoe, D. J. Nutt, & R. Carhart-Harris. Effects of DMT on mental health outcomes in healthy volunteers. *Sci. Rep.* (2024) doi:10.1038/s41598-024-53363-y.

21. Ruck J. Strassman *et al.* Dose-Response Study of N,N-Dimethyltryptamine in Humans: II. Subjective Effects and Preliminary Results of a New Rating Scale. *Arch. Gen. Psychiatry* **51**, 98–108 (1994).

22. Severin B. Vogt *et al.* Acute effects of intravenous DMT in a randomized placebo-controlled study in healthy participants. *Transl. Psychiatry* **13**, (2023).

23. Butler Center for Research. Psychedelics as Therapeutic Treatment. *Research Update* https://www.hazeldenbettyford.org/research-studies/addiction-research/psychedelic-therapeutic-treatment (2022).

24. Erin A. Kolbrich *et al.* Physiological and subjective responses to controlled oral 3,4-methylenedioxymethamphetamine administration. *J. Clin. Psychopharmacol.* **28**, 432–440 (2008).

25. Nor Suliana Mustafa *et al.* MDMA and the Brain: A Short Review on the Role of Neurotransmitters in Neurotoxicit. *Basic Clin. Neurosci.* **11**, 381–388 (2019).

26. Susan Schenk, Schenk, S., Quenten Highgate & Highgate, Q. Methylenedioxymethamphetamine (MDMA): Serotonergic and dopaminergic mechanisms related to its use and misuse. *J. Neurochem.* **157**, 1714–1724 (2021).

27. Marieke Niesters *et al.* Ketamine for chronic pain: risks and benefits. *Br. J. Clin. Pharmacol.* **77**, 357–367 (2014).

28. Ronald S. Duman *et al.* Synaptic plasticity and depression: new insights from stress and rapid-acting antidepressants. *Nat. Med.* **22**, 238–249 (2016).

29. James W. Murrough *et al.* Antidepressant Efficacy of Ketamine in Treatment-Resistant Major Depression: A Two-Site Randomized Controlled Trial. *Am. J. Psychiatry* **170**, 1134–1142 (2013).

30. John H. Krystal, Ege T. Kavalali, & Lisa M. Monteggia. Ketamine and rapid antidepressant action: new treatments and novel synaptic signaling mechanisms. *Neuropsychopharmacology* (2023) doi:10.1038/s41386-023-01629-w.

31. Daniel S. Lorrain *et al.* Effects of ketamine and N-methyl-D-aspartate on glutamate and dopamine release in the rat prefrontal cortex: modulation by a group II selective metabotropic glutamate receptor agonist LY379268. *Neuroscience* **117**, 697–706 (2003).

32. Tareg Bey, Bey, T., Anar Patel & Patel, A. Phencyclidine Intoxication and Adverse Effects: A Clinical and Pharmacological Review of an Illicit Drug. *West. J. Emerg. Med.* **8**, 9–14 (2007).

33. Jaster, A. M. & González-Maeso, J. Mechanisms and molecular targets surrounding the potential therapeutic effects of psychedelics. *Mol. Psychiatry 2023* 1–18 (2023) doi:10.1038/s41380-023-02274-x.

34. Robin Carhart-Harris, Carhart-Harris, R. L., Karl J. Friston & Friston, K. J. REBUS and the Anarchic Brain: Toward a Unified Model of the Brain Action of Psychedelics. *Pharmacol. Rev.* **71**, 316–344 (2019).

35. Richard E. Daws *et al.* Increased global integration in the brain after psilocybin therapy for depression. *Nat. Med.* (2022) doi:10.1038/s41591-022-01744-z.

36. Katrin H. Preller *et al.* Changes in global and thalamic brain connectivity in LSD-induced altered states of consciousness are attributable to the 5-HT2A receptor. *eLife* **7**, (2018).

37. J. Siegel *et al.* Psilocybin desynchronizes the human brain. *Nature* (2024) doi:10.1038/s41586-024-07624-5.

38. Gabrielle Agin-Liebes *et al.* Long-term follow-up of psilocybin-assisted psychotherapy for psychiatric and existential distress in patients with life-threatening cancer: *J. Psychopharmacol. (Oxf.)* **34**, 155–166 (2020).

39. Roland R. Griffiths *et al.* Psilocybin produces substantial and sustained decreases in depression and anxiety in patients with life-threatening cancer: A randomized double-blind trial. *J. Psychopharmacol. (Oxf.)* **30**, 1181–1197 (2016).

40. Peter Gasser *et al.* Safety and efficacy of lysergic acid diethylamide-assisted psychotherapy for anxiety associated with life-threatening diseases. *J. Nerv. Ment. Dis.* **202**, 513–520 (2014).

41. Nina Schimmel *et al.* Psychedelics for the treatment of depression, anxiety, and existential distress in patients with a terminal illness: a systematic review. *Psychopharmacology (Berl.)* 1–19 (2021) doi:10.1007/s00213-021-06027-y.

42. Robin Carhart-Harris *et al.* Trial of Psilocybin versus Escitalopram for Depression. *N. Engl. J. Med.* **384**, 1402–1411 (2021).

43. Gukasyan, N. *et al.* Efficacy and safety of psilocybin-assisted treatment for major depressive disorder: Prospective 12-month follow-up. *J. Psychopharmacol. (Oxf.)* **36**, 151–158 (2022).

44. Friederike Holze *et al.* Lysergic acid diethylamide-assisted therapy in patients with anxiety with and without a life-threatening illness A randomized, double-blind, placebo-controlled Phase II study. *Biol. Psychiatry* (2022) doi:10.1016/j.biopsych.2022.08.025.

45. Natalie Hesselgrave *et al.* Harnessing psilocybin: antidepressant-like behavioral and synaptic actions of psilocybin are independent of 5-HT2R activation in mice. *Proc. Natl. Acad. Sci. U. S. A.* **118**, (2021).

46. Lindsay P. Cameron *et al.* Chronic, Intermittent Microdoses of the Psychedelic N,N-Dimethyltryptamine (DMT) Produce Positive Effects on Mood and Anxiety in Rodents. *ACS Chem. Neurosci.* **10**, 3261–3270 (2019).

47. Lindsay P. Cameron *et al.* 5-HT2ARs Mediate Therapeutic Behavioral Effects of Psychedelic Tryptamines. *ACS Chem. Neurosci.* **14**, 351–358 (2023).

48. Maurizio Popoli *et al.* The stressed synapse: the impact of stress and glucocorticoids on glutamate transmission. *Nat. Rev. Neurosci.* **13**, 22–37 (2012).

49. Scott M. Thompson *et al.* An excitatory synapse hypothesis of depression. *Trends Neurosci.* **38**, 279–294 (2015).

50. Jessica M. McKlveen *et al.* Chronic Stress Increases Prefrontal Inhibition: A Mechanism for Stress-Induced Prefrontal Dysfunction. *Biol. Psychiatry* **80**, 754–764 (2016).

51. Robin Carhart-Harris, Carhart-Harris, R. L., Guy M. Goodwin & Goodwin, G. M. The Therapeutic Potential of Psychedelic Drugs: Past, Present, and Future. *Neuropsychopharmacology* **42**, 2105–2113 (2017).

52. Jennifer Mitchell *et al.* MDMA-assisted therapy for moderate to severe PTSD: a randomized, placebo-controlled phase 3 trial. *Nat. Netw. Boston* **29**, 2473–2480 (2023).

53. Scott Singleton *et al.* Altered brain activity and functional connectivity after MDMA-assisted therapy for post-traumatic stress disorder. *Front. Psychiatry* **13**, (2023).

54. Matthew W. Johnson *et al.* Long-term Follow-Up of Psilocybin-Facilitated Smoking Cessation. *Am. J. Drug Alcohol Abuse* **43**, 55–60 (2017).

55. Michael P. Bogenschutz *et al.* Percentage of Heavy Drinking Days Following Psilocybin-Assisted Psychotherapy vs Placebo in the Treatment of Adult Patients With Alcohol Use Disorder. *JAMA Psychiatry* (2022) doi:10.1001/jamapsychiatry.2022.2096.

56. Fúlvio Rieli Mendes *et al.* Classic and non-classic psychedelics for substance use disorder: a review of their historic, past and current research. *Addict. Neurosci.* 100025–100025 (2022) doi:10.1016/j.addicn.2022.100025.

57. Greer McKendrick *et al.* Ketamine Blocks Morphine-Induced Conditioned Place Preference and Anxiety-Like Behaviors in Mice. *Front. Behav. Neurosci.* **14**, 75 (2020).

58. Kenneth Alper *et al.* Psilocybin sex-dependently reduces alcohol consumption in C57BL/6J mice. *Front. Pharmacol.* **13**, (2023).

59. Kenneth Alper *et al.* LSD Administered as a Single Dose Reduces Alcohol Consumption in C57BL/6J Mice. *Front. Pharmacol.* **9**, 994–994 (2018).

60. Aboagyewaah Oppong-Damoah *et al.* Effects of the synthetic psychedelic 2,5-dimethoxy-4-iodoamphetamine (DOI) on ethanol consumption and place conditioning in male mice. *Psychopharmacology (Berl.)* **236**, 3567–3578 (2019).

61. Simon Vann Jones, Jones, S. A. V., Allison O'Kelly & O'Kelly, A. Psychedelics as a Treatment for Alzheimer's Disease Dementia. *Front. Synaptic Neurosci.* **12**, 34 (2020).

62. Sinha, J. K. *et al.* Psychedelics for alzheimer's disease-related dementia: Unveiling therapeutic possibilities and pathways. *Ageing Res. Rev.* **96**, 102211 (2024).

63. Luisa Prochazkova *et al.* Exploring the effect of microdosing psychedelics on creativity in an open-label natural setting. *bioRxiv* 384412 (2018) doi:10.1101/384412.

64. Albert Garcia-Romeu *et al.* Psychedelics as Novel Therapeutics in Alzheimer's Disease: Rationale and Potential Mechanisms. *Curr. Top. Behav. Neurosci.* (2021) doi:10.1007/7854_2021_267.

65. Lisbeth Marner *et al.* Loss of serotonin 2A receptors exceeds loss of serotonergic projections in early Alzheimer's disease: a combined [11C]DASB and [18F]altanserin-PET study. *Neurobiol. Aging* **33**, 479–487 (2012).

66. Ly, C. *et al.* Psychedelics Promote Structural and Functional Neural Plasticity. *Cell Rep.* **23**, 3170 (2018).

67. Thomas W. Flanagan, Flanagan, T. W., Charles D. Nichols & Nichols, C. D. Psychedelics as anti-inflammatory agents. *Int. Rev. Psychiatry* **30**, 363–375 (2018).

68. Breeksema, J. J. *et al.* Adverse events in clinical treatments with serotonergic psychedelics and MDMA: A mixed-methods systematic review. *J. Psychopharmacol. (Oxf.)* 026988112211169–026988112211169 (2022) doi:10.1177/02698811221116926.

69. David Bender, David A. Bender, Hellerstein, D. J., & David J. Hellerstein. Assessing the risk-benefit profile of classical psychedelics: a clinical review of second-wave psychedelic research. *Psychopharmacology (Berl.)* (2022) doi:10.1007/s00213-021-06049-6.

70. Sarah Naher. The Potential Therapeutic Benefits and Safety of Psychedelics in the Treatment of Mental Health Conditions: A Systematic Review. *J. Sociol. Psychol. Amp Relig. Stud.* **5**, 20–39 (2023).

71. Laura Orsolini *et al.* The 'Endless Trip' among the NPS Users: Psychopathology and Psychopharmacology in the Hallucinogen-Persisting Perception Disorder. A Systematic Review. *Front. Psychiatry* **8**, 240–240 (2017).

72. Jules Evans *et al.* Extended difficulties following the use of psychedelic drugs: A mixed methods study. *PLoS ONE* **18**, e0293349–e0293349 (2023).

73. David B. Yaden, David B. Yaden, Yaden, D. B., Roland R. Griffiths & Griffiths, R. R. The Subjective Effects of Psychedelics Are Necessary for Their Enduring Therapeutic Effects. *ACS Pharmacol. Transl. Sci.* **4**, 568–572 (2020).

74. David E. Olson & Olson, D. E. The Subjective Effects of Psychedelics May Not Be Necessary for Their Enduring Therapeutic Effects. *ACS Pharmacol. Transl. Sci.* **4**, 563–567 (2020).

75. Muir, J. *et al.* Isolation of psychedelic-responsive neurons underlying anxiolytic behavioral states. *Science* **386**, 802–810 (2024).

76. Olson, D. E. & David E. Olson. Biochemical Mechanisms Underlying Psychedelic-Induced Neuroplasticity. *Biochemistry* (2022) doi:10.1021/acs.biochem.1c00812.

77. Kwan, A. C., Olson, D. E., Preller, K. H. & Roth, B. L. The neural basis of psychedelic action. *Nat. Neurosci.* **25**, 1407–1419 (2022).

78. Franz X. Vollenweider, Vollenweider, F. X., Michael Kometer & Kometer, M. The neurobiology of psychedelic drugs: implications for the treatment of mood disorders. *Nat. Rev. Neurosci.* **11**, 642–651 (2010).

79. Zifan Zhen, Xueqiang Sun, Shiying Yuan, & Jiancheng Zhang. Psychoactive substances for the treatment of neuropsychiatric disorders. *Asian J. Psychiatry* (2024) doi:10.1016/j.ajp.2024.104193.

80. Maxemiliano V. Vargas *et al.* Psychedelics promote neuroplasticity through the activation of intracellular 5-HT2A receptors. *Science* **379**, 700–706 (2023).

81. Coralie Berthoux *et al.* Sustained Activation of Postsynaptic 5-HT2A Receptors Gates Plasticity at Prefrontal Cortex Synapses. *Cereb. Cortex* **29**, 1659–1669 (2019).

82. Daniel Ryskamp Rijsketic *et al.* UNRAVELing the synergistic effects of psilocybin and environment on brain-wide immediate early gene expression in mice. *Neuropsychopharmacology* **48**, 1798–1807 (2023).

83. Davoudian, P. A., Shao, L.-X. & Kwan, A. C. Shared and Distinct Brain Regions Targeted for Immediate Early Gene Expression by Ketamine and Psilocybin. *ACS Chem. Neurosci.* **14**, 468–480 (2023).

84. Ling-Xiao Shao *et al.* Psilocybin induces rapid and persistent growth of dendritic spines in frontal cortex in vivo. *bioRxiv* (2021) doi:10.1101/2021.02.17.431629.

85. Mario de la Fuente Revenga *et al.* Prolonged epigenomic and synaptic plasticity alterations following single exposure to a psychedelic in mice. *Cell Rep.* **37**, 109836 (2021).

86. de Vos, C. M. H., Mason, N. L. & Kuypers, K. P. C. Psychedelics and Neuroplasticity: A Systematic Review Unraveling the Biological Underpinnings of Psychedelics. *Front. Psychiatry* **12**, 1575 (2021).

87. Mounia Azzi *et al.* β-Arrestin-mediated activation of MAPK by inverse agonists reveals distinct active conformations for G protein-coupled receptors. *Proc. Natl. Acad. Sci. U. S. A.* **100**, 11406–11411 (2003).

88. Bruce E. Blough *et al.* Interaction of psychoactive tryptamines with biogenic amine transporters and serotonin receptor subtypes. *Psychopharmacology (Berl.)* **231**, 4135–4144 (2014).

89. Adam K. Klein *et al.* Investigation of the structure-activity relationships of psilocybin analogues. *ACS Pharmacol. Transl. Sci.* **4**, 533–542 (2020).

90. Danuta Marona-Lewicka *et al.* Distinct temporal phases in the behavioral pharmacology of LSD: dopamine D2 receptor-mediated effects in the rat and implications for psychosis. *Psychopharmacology (Berl.)* **180**, 427–435 (2005).

91. Álvaro L. Garcia-García *et al.* Erratum to: 5-HT1A receptors in mood and anxiety: recent insights into autoreceptor versus heteroreceptor function. *Psychopharmacology (Berl.)* doi:10.1007/s00213-013-3425-x.

92. Rafael Moliner *et al.* Psychedelics promote plasticity by directly binding to BDNF receptor TrkB. *Nat. Neurosci.* **26**, 1032–1041 (2023).

93. Kuglae Kim *et al.* Structure of a Hallucinogen-Activated Gq-Coupled 5-HT2A Serotonin Receptor. *Cell* **182**, (2020).

94. Daniel Wacker *et al.* Crystal Structure of an LSD-Bound Human Serotonin Receptor. *Cell* **168**, 377–389 (2017).

95. Michael Tagen *et al.* The risk of chronic psychedelic and MDMA microdosing for valvular heart disease. *J. Psychopharmacol. (Oxf.)* **37**, 876–890 (2023).

96. Robin Carhart-Harris *et al.* Neural correlates of the psychedelic state as determined by fMRI studies with psilocybin. *Proc. Natl. Acad. Sci. U. S. A.* **109**, 2138–2143 (2012).

97. Sailaja A. Goda *et al.* Serotonergic hallucinogens differentially modify gamma and high frequency oscillations in the rat nucleus accumbens. *Psychopharmacology (Berl.)* **228**, 271–282 (2013).

98. James J Gattuso *et al.* Default Mode Network Modulation by Psychedelics: A Systematic Review. *Int. J. Neuropsychopharmacol.* (2022) doi:10.1093/ijnp/pyac074.

99. Katrin H. Preller, Preller, K. H., Franz X. Vollenweider & Vollenweider, F. X. Phenomenology, Structure, and Dynamic of Psychedelic States. *Curr. Top. Behav. Neurosci.* **36**, 221–256 (2016).

100. Filip Tylš *et al.* Underlying pharmacological mechanisms of psilocin-induced broadband desynchronization and disconnection of EEG in rats. *Front. Neurosci.* **17**, (2023).

101. Franz X. Vollenweider, Vollenweider, F. X., Mark A. Geyer & Geyer, M. A. A systems model of altered consciousness: integrating natural and drug-induced psychoses. *Brain Res. Bull.* **56**, 495–507 (2001).

102. Philip R. Corlett *et al.* Hallucinations and Strong Priors. *Trends Cogn. Sci.* **23**, 114–127 (2019).

103. Manoj K Doss *et al.* Models of psychedelic drug action: modulation of cortical-subcortical circuits. *Brain* (2021) doi:10.1093/brain/awab406.

104. Clare Howarth *et al.* More than just summed neuronal activity: how multiple cell types shape the BOLD response. *Philos. Trans. R. Soc. B* **376**, 20190630–20190630 (2021).

105. Elizabeth M. C. Hillman & Hillman, E. M. C. Coupling Mechanism and Significance of the BOLD Signal: A Status Report. *Annu. Rev. Neurosci.* **37**, 161–181 (2014).

106. Paul M. Vanhoutte & Vanhoutte, P. M. Serotonin and the vascular wall. *Int. J. Cardiol.* **14**, 189–203 (1987).

107. Zvi Cohen *et al.* SEROTONIN IN THE REGULATION OF BRAIN MICROCIRCULATION. *Prog. Neurobiol.* **50**, 335–362 (1996).

108. Zhong-Ming Li *et al.* Integration of EEG/MEG with MRI and fMRI. *IEEE Eng. Med. Biol. Mag.* **25**, 46–53 (2006).

109. Padawer-Curry, J. A. *et al.* Psychedelic 5-HT2A receptor agonism: neuronal signatures and altered neurovascular coupling. *bioRxiv* 2023.09.23.559145 (2023) doi:10.1101/2023.09.23.559145.

110. Aisling Spain *et al.* Neurovascular and neuroimaging effects of the hallucinogenic serotonin receptor agonist psilocin in the rat brain. *Neuropharmacology* **99**, 210–220 (2015).

CHAPTER 4: RESCUING CEREBRAL BLOOD FLOW DEFICITS INCREASES VISUAL CORTEX ORIENTATION SELECTIVITY IN A MOUSE MODEL OF ALZHEIMER'S DISEASE

Rick T. Zirkel, Matthew Isaacson, Michael Lamont, Katharine Yang, Matthew Yi, Keri Yamaguchi, Nozomi Nishimura, Chris B. Schaffer

Meinig School of Biomedical Engineering, Cornel University, Ithaca, NY, USA

4.1 Introduction

Alzheimer's disease (AD) is a progressive neurodegenerative disorder marked by cognitive dysfunction — including memory loss, impaired reasoning, and difficulties with language and problem-solving — and is the most prevalent cause of dementia, accounting for 60–80% of cases worldwide [1]. As AD advances, affected individuals gradually lose the ability to perform daily tasks and ultimately require full-time care. At the pathological level, AD is characterized by two hallmark features: the accumulation of (1) extracellular amyloid-beta (Aβ) plaques and (2) intracellular neurofibrillary tangles composed of hyperphosphorylated tau protein [2,3,4,5]. These protein aggregates lead to widespread neuronal dysfunction, synaptic loss, and atrophy, especially in brain regions essential for memory and cognition such as the hippocampus and entorhinal cortex. Beyond these classic pathologies, AD is also associated with neuroinflammation, oxidative stress, metabolic dysregulation, and vascular impairments, which further complicate disease progression [6,7,8].

Recent research has increasingly focused on early disruptions that precede overt cognitive decline and the formation of harmful protein aggregates [9,10,11]. One key impairment is vascular dysfunction: AD patients and animal models exhibit a 25% reduction in global cerebral blood

flow (CBF), largely due to compromised small-vessel perfusion [12,13,14,15]. Capillary stalling — a process where individual capillaries become blocked by neutrophils, red blood cells, or platelet aggregates — has been shown to be significantly elevated in AD models compared to wild-type controls [16,17]. Although these stalling events affect only a small percentage of capillaries at any moment, the interdependent structure of the cerebral vasculature amplifies their impact, leading to a cascade of reduced perfusion [18]. Our lab serendipitously found that administering an antibody against the neutrophil-specific surface protein Ly6G eliminates these stalling events in APP/PS1 mice [16]. Remarkably, this intervention restores roughly two-thirds of CBF deficits within hours and significantly improves spatial memory performance. We hypothesize that restoring CBF directly rescues impaired neural activity patterns, thereby contributing to cognitive recovery.

A well-characterized example of impaired sensory processing is observed in the primary visual cortex (V1). Neurons in V1, known as simple cells, respond selectively to visual stimuli such as drifting gratings at specific orientations, as well as direction of drifting [19] (Fig. 4.1 C). Orientation selectivity refers to a neuron's preference for stimuli with a specific edge orientation, while direction selectivity means the neuron responds preferentially to motion in a particular direction. The receptive fields of these cells are defined by distinct excitatory and inhibitory regions arranged in a specific elongated pattern. This structure ensures that they respond only when a stimulus is correctly positioned and oriented — a critical process for edge detection and early feature extraction in visual processing. This hierarchical process, beginning in the retina and progressing through the lateral geniculate nucleus (LGN) to V1, is essential for accurate perception and object recognition [20]. In the APP23 x PS45 mouse model of AD, Grienberger et al. demonstrated impaired orientation tuning in layer 2/3 V1 neurons using in vivo two-photon

imaging with the calcium indicator OGB1-AM [21]. Their findings revealed that while young mice (1.5–3 months) exhibited normal tuning and visual discrimination, tuning deficits emerged as Aβ plaques accumulated, with severe impairments observed by 8–10 months. Additionally, a significant proportion of neurons became either hyperactive or hypoactive, with hyperactivity — often more prevalent near plaques — contributing most to the observed deficits. Studies such as this demonstrate a motivation to investigate AB-plaque distance as a factor of neural function.

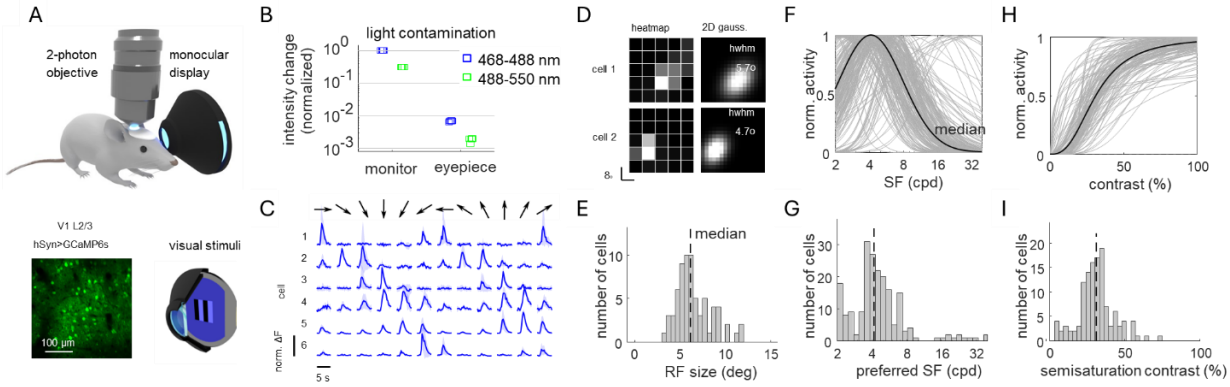

Figure 4.1 Neural recording with 13MouseGoggles Mono headset. A: Experimental setup for MouseGoggles Mono visual stimulation with two-photon imaging of V1 layer 2/3 neurons expressing GCaMP6s. **B:** Light contamination comparison between a flat LED monitor and the monocular display eyepiece. **C:** Example neuron responses to drifting grating stimuli. **D:** Receptive field (RF) maps and inferred spike rate heatmaps. **E–I:** Distributions of RF size, spatial frequency tuning, and contrast sensitivity across recorded neurons. [22] (Adapted from Isaacson 2024)

Since this orientation tuning parameter is thoroughly established, and has strong supporting evidence that it is impaired in the context of AD, in this study, we test whether impaired orientation tuning can be restored after increasing CBF in 9-11 month old APP/PS1 mice. Using two-photon excitation fluorescence microscopy (2PEF) imaging, we measure virally injected hSyn-GCaMP6s calcium activity in the same individual neurons before and after treatment (Fig 4.2 C). Simultaneously, an experimental paradigm eliciting responses of neurons to orientations of drifting gratings was conducted. Using MouseGoggles Mono VR headset (Fig. 4.1) [22], stimuli

were presented to the left eye, while calcium activity was recorded from the right hemisphere. Here we use a single eyepiece to present drifting gratings of light and dark bars with highly customized stimulation parameters, including random, repeated stimulation of 12 unique orientations of drifting gratings (Fig 4.2 A). Using Suite2P [23], a software that enables the detection and analysis of two-photon calcium imaging data, calcium transients and inferred spikes were extracted from individual neurons. Here we use it for the automatic segmentation of active cells into individual ROIs, allowing for the extraction of activity information (Fig 4.2 B). In total, calcium activity was recorded from ~1500 neurons across treatment groups (Fig 4.2 D).

Future work will extend the findings explained below by validating results in awake mice to better understand how anesthesia influences the observed effects. Additionally, we will investigate how proximity to Aβ plaques and stall-prone capillaries modulate neuronal and responses, which may provide insight into localized disruptions in neural function. Furthermore, transcriptomic analysis will be used to identify molecular signatures of different neuronal subtypes, helping to determine their specific contributions to the observed changes. Together, these approaches will refine our understanding of the mechanisms underlying neurovascular dysfunction in disease contexts.

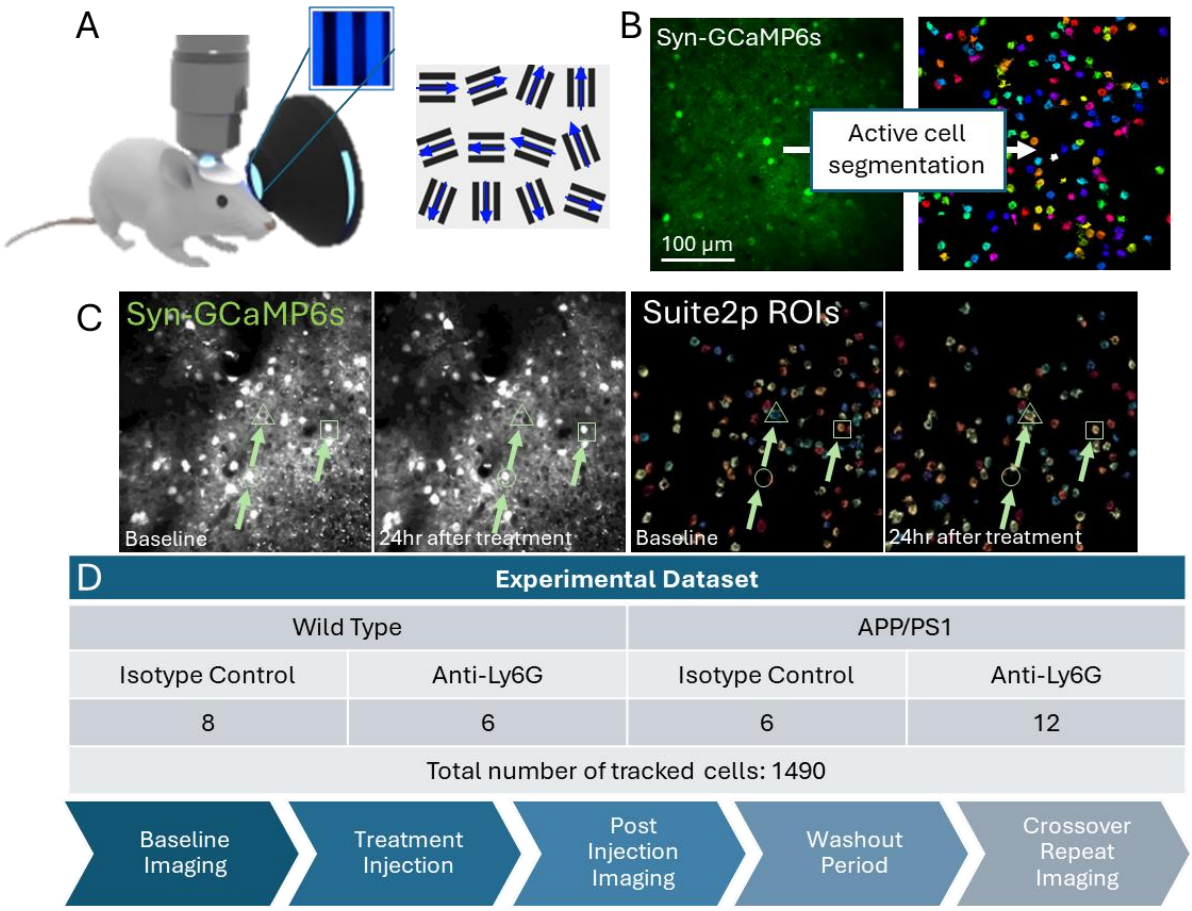

Figure 4.2 Experimental methods, dataset and protocol14. **A:** Visual stimulation using MouseGoggles Mono VR headset during two photon imaging. Orientations 0 – 270° at 22.5° interval. **B:** Automatic active cell segmentation using Suite2P. **C:** Same-cell and ROI tracking before and after treatment. **D:** Experimental dataset including treatment groups and number of mice in each group, as well as total number of neurons cross all groups. Flow chart demonstrates experimental protocol sequence for each mouse.

4.2 Results

4.2.1 Spontaneous Activity Increases after CBF Restoration in APP/PS1 Mice

We first examined the effects of anti-Ly6G administration, and the resulting increase in CBF, on spontaneous neural activity across our treatment groups. In control groups — including WT mice receiving either an isotype-control or anti-Ly6G, as well as APP/PS1 mice receiving the

isotype-control — we observed no significant differences in spontaneous activity when comparing averaged track-cell activity within the same animals. In contrast, APP/PS1 mice treated with anti-Ly6G exhibited a significant increase in fraction of active cells and spontaneous neural activity (Two-tailed Wilcoxon sign rank test; p-values = 0.031 Ly6G-fraction active cells, 0.034 for Ly6G-spontaneous activity). Notably, baseline measurements revealed that spontaneous activity in AD mice was substantially lower than in WT mice; following anti-Ly6G treatment, these AD mice showed an approximately two-thirds increase in spontaneous activity (Fig. 4.3).

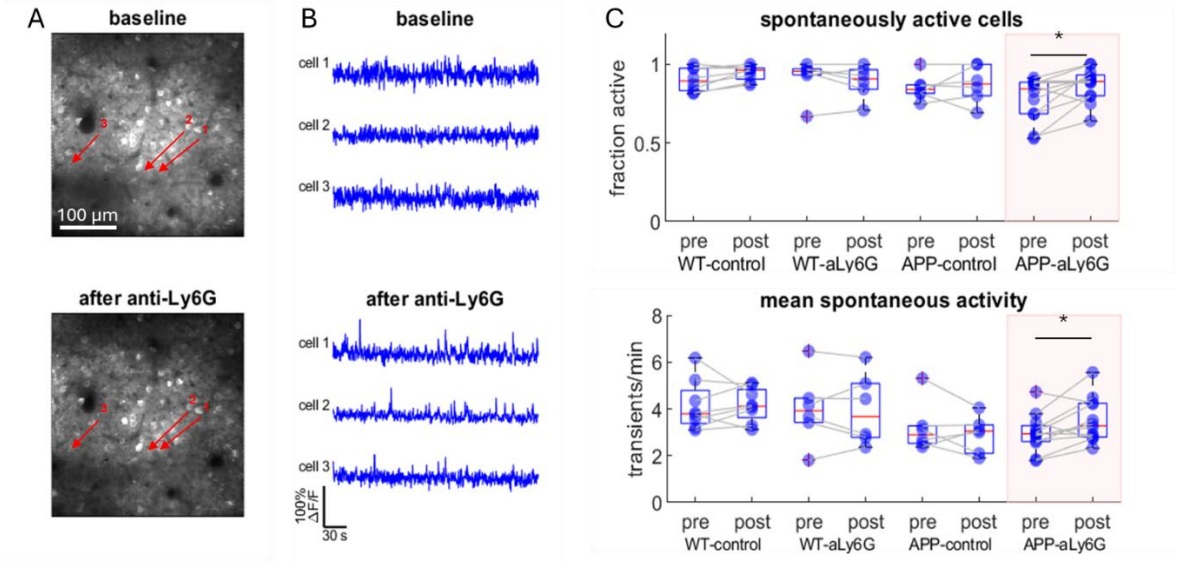

Figure 4.3 Spontaneous activity increases in APP/PS1 mice after anti-Ly6G treatment15. **A:** Three sample V1 recordings pre and post anti-Ly6G treatment. **B:** Calcium traces of neurons in A showing increased spontaneous activity after treatment. **C:** Fraction of "active" cells and mean transients/min of all cells. Each point is one mouse, lines connect same mice before and after treatment. Box plots show mean and 25th/75th percentiles, with whiskers extending to the full range of non-outlier datapoints. Two-tailed Wilcoxon sign rank test (p-values = 0.031 Ly6G-fraction active cells, 0.034 for Ly6G-spontaneous activity). WT/Iso-control (n =8); WT/anti-Ly6G (n = 6); APP/Iso-control (n = 6); APP/anti-Ly6G (n = 12); Total tracked (pre/post) neurons pooled from all conditions = 1475 cells). (* = $p < 0.05$; ** = $p < 0.01$)

4.2.2 Orientation Selectivity Increases after CBF Restoration in APP/PS1 Mice

We next investigated whether anti-Ly6G treatment and the resulting CBF restoration led to changes in neural activity patterns associated with visual processing. To quantify these changes, we measured the orientation selectivity index (OSI) and direction selectivity index (DSI) from neurons responding to drifting grating stimuli. In control groups we observed no significant differences in either OSI or DSI. However, in APP/PS1 mice that received anti-Ly6G, we found a significant increase in OSI, along with an increased proportion of neurons classified as selective for specific orientations (Two-tailed Wilcoxon sign rank test; p-values of 0.012 for Ly6G-OSI, 0.002 Ly6G-fraction selective). Notably, DSI remained unchanged across groups.

The increase in OSI indicates that the impaired neural activity patterns in AD mice are at least partially rescued by restoring cerebral blood flow. This restoration of orientation tuning suggests that improved vascular perfusion may contribute to enhanced sensory processing, which could underly the observed improvements in cognitive performance during spatial memory tasks (Fig. 4.4). These findings support the hypothesis that targeting vascular deficits in AD not only ameliorates global blood flow but also helps normalize specific neural computations critical for perception and cognition

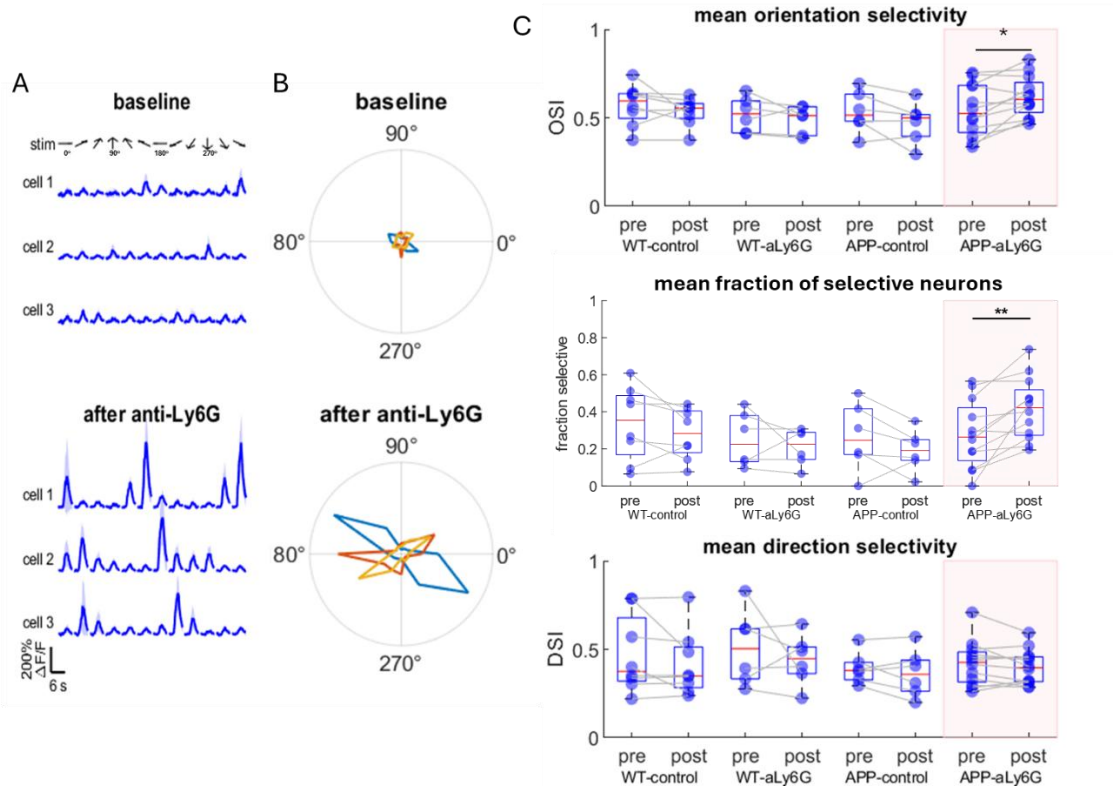

Figure 4.416 Orientation selectivity increases in APP/PS1 mice after anti-Ly6G treatment. A: Sample average calcium trace response of three cells where OSI increased after anti-Ly6G treatment. **B:** Polar plots of drifting grating response for cells in A. **C:** Mean OSI, fraction of selective neurons, and DSI for all treatment groups. Each point is one mouse, lines connect same mice before and after treatment. Box plots show mean and 25th/75th percentiles, with whiskers extending to the full range of non-outlier datapoints. Two-tailed Wilcoxon sign rank test (p-values of 0.012 for Ly6G-OSI, 0.002 Ly6G-fraction selective). These p-values are NOT corrected for multiple comparisons (5 measurement types x 4 genotype/treatment groups = 20 comparisons). After Benjamini-Hochberg correction with a false discovery rate (FDR) of 0.05, the only remaining significant result is the fraction of highly orientation-selective cells (adjusted p-value = 0.039). WT/Iso-control (n =8); WT/anti-Ly6G (n = 6); APP/Iso-control (n = 6); APP/anti-Ly6G (n = 12); Total tracked (pre/post) neurons pooled from all conditions = 1475 cells). (* = $p < 0.05$; ** = $p < 0.01$)

In addition to the statistical tests used in Figure 4.4, we employed a linear mixed-effects model to address various experimental group interactions. The model follows: Response ~ Treatment*Disease + (1|MouseID), where response is either activity, OSI, or DSI. For this modeling we used the fitlme() function in Matlab, followed by Anova() to test for treatment effects, disease effects, and Treatment-Disease interaction effects. Anova testing resulted in a

significant interaction of Treatment*Disease-OSI (p-val = 0.0002; after multiple comparison correction p-val = 0.0021). All other interactions were not statistically significant.

4.3 On going work

4.3.1 Amyloid beta plaques and Stall prone capillaries

Building on our observed improvement in orientation selectivity, we further analyzed our dataset to explore potential contributors to the observed rescue of neural function. In addition to recording calcium activity during visual stimulation, we acquired imaging stacks of fluorescently labeled Aβ plaques and cerebral vasculature (Fig. 4.5 A & B). This multimodal dataset enables us to investigate how key AD-related factors, such as plaque proximity and capillary stalling, correlate with neuronal function.

Previous studies have demonstrated that the distance between a neuron and an Aβ plaque can significantly influence neuronal activity [24]. We aim to determine whether neurons closer to plaques exhibit greater deficits in orientation selectivity, and whether these deficits are ameliorated following improved perfusion. Simultaneously, we are examining the impact of capillary stalling by measuring the distance of each neuron to the nearest stall-prone capillary. Some capillaries show recurring stalling events, and we hypothesize that neurons in close proximity to these dysfunctional vessels may have altered activity patterns. Together, these analyses will shed light on how local amyloid pathology and vascular dysfunction contribute to the impaired neural activity observed in AD and how their remediation may support cognitive improvement.

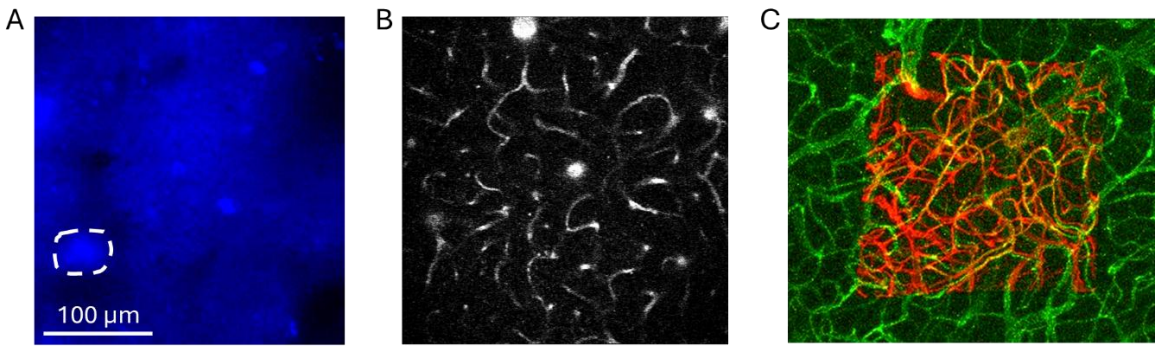

Figure 4.5 Ongoing work17. A: Amyloid-beta plaque labelling with methoxy-X04. **B:** Vasculature labeling with Texas Red 70000 MW dextran. **C:** Example matching of in vivo imaging of vasculature (red) to ex vivo brain slice of the same imaging plane (green).

4.3.2 In vivo ex vivo

We are also investigating how different neuronal subtypes contribute to impaired and improved orientation selectivity in AD by integrating in vivo and ex vivo approaches. Using two-photon calcium imaging, we record neural activity in AD mouse models, then classify neurons ex vivo with EASI-FISH spatial transcriptomics to identify excitatory and inhibitory subpopulations, including parvalbumin (PV), somatostatin (SST), and vasoactive intestinal peptide (VIP) interneurons [25,26]. This allows us to directly link neuronal activity patterns with cell type, testing whether restoring blood flow via anti-Ly6G treatment rescues cell-type specific function. A core feature of AD is an imbalance in excitation and inhibition (E/I balance), with evidence showing fast-spiking interneurons to be a critically impaired component, potentially through their high energy demands that may be restored through increased CBF [27]. We hypothesize that this restoration underlies improvements in orientation selectivity observed in APP/PS1 mice.

4.3.3 Awake imaging

After obtaining promising results with anesthetized mice, we repeated our experiments under awake conditions to verify that the improvements in orientation selectivity following CBF enhancement persist in a more natural physiological state. Anesthesia provides motion stability, which is beneficial for high-resolution imaging; however, it significantly alters cerebral blood flow, neural activity, and inflammatory responses [28]. Anesthetic agents such as isoflurane — used in the experiments described previously — and ketamine/xylazine induce vasodilation, suppress neural firing, and disrupt network dynamics — effects that vary with dosage and require constant monitoring of vital parameters. These pharmacological confounds limit the interpretability of functional studies conducted under anesthesia.

Awake imaging, although technically challenging, allows for more physiologically relevant measurements of both neural and vascular activity [29]. By eliminating the suppressive effects of anesthetics, this approach enables us to capture spontaneous and stimulus-evoked neural responses that more accurately reflect natural brain function. While beneficial for acquiring more relevant measurements, awake imaging with high-resolution imaging typically requires head fixation. This fixation can introduce stress and movement artifacts, necessitating extensive habituation protocols that vary across laboratories [30]. Despite these difficulties, awake imaging remains the preferred method for capturing dynamic, biologically relevant processes. Repeating our experiment in awake mice is thus an essential step to confirm that the improvements in orientation selectivity observed after increasing CBF are robust and applicable under natural, awake conditions.

4.4 Discussion:

Blood flow deficits in AD emerge early in disease progression, preceding hallmark symptoms such as memory loss and plaque formation. Our findings demonstrate that some neural and behavioral deficits in AD can be acutely recovered by increasing CBF. Within the short window of improved blood flow in AD mice (~3 hours), our lab previously observed enhanced cognitive performance in behavioral tasks [16], and our results indicate that this improvement is partially driven by restored neural activity patterns. This suggests that targeting cerebrovascular deficits may be a promising therapeutic avenue to delay the onset of AD symptoms. Future work should investigate the mechanisms underlying these activity improvements and determine how other impairments are affected.

Our data shows that orientation selectivity improves following CBF enhancement in APP/PS1 mice with behavioral deficits. A behavioral test for visual orientation selectivity could facilitate earlier detection of neural deficits and further elucidate how neural activity supports sensory processing. We plan to use a visual discrimination task to determine whether cortical changes result in improved perception, assessing how well mice distinguish specific angles.

4.4.1 Potential mechanisms for restored CBF improving cognition

A critical next step is understanding how restoring CBF contributes to the execution of impaired neural activity patterns. These effects likely stem from multiple interacting factors, as the relationship between neural activity and blood flow is complex. Key mechanisms may include oxygen and glucose delivery, oxidative stress, mitochondrial dysfunction, and neuroinflammation mediated by astrocytes and microglia [31,32,33,34]. Dysregulation of these processes could trigger cascading failures across multiple neurofunctional pathways, accelerating cognitive decline.

Metabolic dysfunction is a core pathological feature of AD that significantly impacts neuronal function [31,7,35]. Neurons require a constant supply of oxygen and glucose, both delivered via the vasculature. Chronic cerebral hypoperfusion in AD exacerbates metabolic deficits, limiting ATP production and disrupting ion gradients necessary for action potential firing and synaptic transmission.

Another major consequence of CBF reductions in AD is increased oxidative stress and mitochondrial dysfunction [7,36,37,38,39]. Insufficient blood flow exacerbates oxidative stress by impairing mitochondrial function, leading to excessive reactive oxygen species (ROS) production. Restoring CBF could mitigate oxidative damage to neurons and synapses, preserving normal excitability and preventing the loss of inhibitory tone caused by oxidative stress-induced synaptic dysfunction.

These metabolic deficits may particularly impact fast-spiking inhibitory interneurons, which have higher metabolic demands than other cell types due to their rapid firing activity [40,39,41,42]. A core feature of AD is an imbalance in excitation and inhibition (E/I), which disrupts network communication and contributes to cognitive decline [27,43,44]. Evidence from AD mouse models suggests that Aβ accumulation disrupts E/I balance — resulting in neuronal hyperactivity, altered slow-wave oscillations, and increased network synchrony — changes that arise early in disease progression [43]. Dysfunction in inhibitory interneurons, especially fast-spiking parvalbumin (PV)-expressing cells, plays a central role in these abnormalities. PV interneurons regulate network stability and synchrony through gamma oscillations (30–80 Hz), but their high metabolic demands make them particularly vulnerable to oxidative stress and energy deficits in AD [41,42,10].

4.4.2 Excitation/Inhibition Balance and Network Level Disruptions

To further investigate how E/I balance influences orientation selectivity, we are employing EASI-FISH spatial transcriptomics on ex vivo brain slices to classify cell subtypes, including excitatory neurons and inhibitory subpopulations such as PV, somatostatin (SST), and vasoactive intestinal peptide (VIP) interneurons. By integrating in vivo two-photon calcium imaging with ex vivo cell labeling, we can directly link neural activity with specific cell types. We hypothesize that PV interneurons are particularly affected by anti-Ly6G treatment, which restores blood flow and provides the metabolic support necessary for proper interneuron function. This restoration may re-establish E/I balance and thereby improve orientation selectivity in APP/PS1 mice.

Alzheimer's disease encompasses widespread impairments to cognitive function, including reduced orientation selectivity, many of which may similarly be influenced by reductions and restorations of CBF. One of the earliest manifestations of this dysfunction is the breakdown of the Default Mode Network (DMN), a system of interconnected brain regions that supports internally directed thought processes and memory consolidation. In AD, the DMN fails to properly deactivate during task engagement, resulting in cognitive inflexibility and memory deficits [45,46]. This disruption is associated with hippocampal hyperactivity, a feature observed in AD mouse models that correlates with impaired DMN suppression during cognitive tasks. Examining such alterations will be important next steps to expanding our understanding of how increasing CBF impacts neural activity impairments, especially in more memory relevant contexts.

Beyond large-scale network dysfunction, AD is also characterized by pathological network hypersynchrony, where aberrant neuronal synchronization disrupts normal oscillatory rhythms critical for cognition [47]. Neural oscillations, such as gamma rhythms and hippocampal Sharp

Wave Ripples (SWRs), are essential for processes like attention, working memory, and memory consolidation [48]. However, in AD, gamma power is diminished, and SWRs are weakened, contributing to cognitive impairments. Dysfunction of inhibitory interneurons, particularly PV-expressing fast-spiking cells, is a key driver of these oscillatory disruptions. These interneurons are essential for network stability, and their impairment in AD leads to excessive network excitability and a loss of precise temporal coordination. Understanding how interneurons are specifically impacted in our experimental paradigm could provide important insight into these dysfunctions and potential therapeutic targets.

4.4.3 Future Translation to Spatial Memory

Another important next step is to determine whether improved neural activity patterns following CBF restoration translate into enhanced spatial memory performance. Spatial memory relies on accurately encoding environmental cues and spatial relationships, processes mediated by the hippocampus (HPC) and medial temporal lobe. CA1 place cells fire at specific locations, creating an internal cognitive map, while entorhinal cortex grid cells generate a coordinate system for measuring distances and spatial relationships. Border cells detect environmental boundaries, and head direction cells track orientation relative to landmarks, all of which support navigation and memory retrieval [49]. In AD, degeneration of hippocampal and entorhinal circuits disrupts these encoding mechanisms, leading to spatial disorientation and memory deficits.

To build on our findings of improved orientation selectivity following CBF restoration, we plan to investigate degraded place cell mapping as a key impaired neural activity pattern in AD. Using three-photon microscopy (3PM), we will perform head-fixed imaging of HPC CA1 place cells [50]. Unlike two-photon imaging — which often requires invasive cortical removal — 3PM employs longer wavelengths to penetrate deeper into brain tissue, enabling cellular-resolution

imaging through an intact skull. This approach minimizes inflammatory artifacts and preserves the neurovascular environment. In combination with MouseGoggles for awake, head-fixed imaging, mice will navigate a virtual linear track to induce place field formation. Integrating these cutting-edge techniques will allow us to assess whether restoring CBF leads to improved spatial encoding in AD mice, ultimately linking neural improvements to cognitive recovery.

4.4.4 Broader Impact of Stall-Based Therapy

Targeting early biomarkers of Alzheimer's disease, such as cerebral blood flow (CBF) deficits, may be a more effective therapeutic strategy than focusing on later-stage hallmarks like Aβ plaques and tau tangles [51]. Blood flow impairments emerge before significant cognitive decline and neuronal loss, suggesting they play a crucial role in disease progression. Unlike amyloid and tau, which accumulate over decades and may already be irreversible by the time symptoms manifest, restoring CBF could provide immediate functional benefits by improving metabolic support to neurons, reducing oxidative stress, and preserving network function. Additionally, interventions aimed at boosting blood flow may prevent or slow the downstream cascade of neurodegeneration, making them a more viable target for early intervention and disease modification.

Further, eliminating stalled capillaries to improve blood flow could have broad therapeutic potential beyond Alzheimer's disease, benefiting a range of disorders associated with vascular impairments. Conditions such as stroke, vascular dementia, and even Parkinson's disease involve disruptions in cerebral perfusion that compromise oxygen and nutrient delivery to neurons [52,53,54,55]. In ischemic stroke, restoring microvascular flow could limit infarct size and improve recovery, while in vascular dementia, increasing CBF might help preserve cognitive function by preventing chronic hypoperfusion-induced damage. Similarly, diseases like multiple sclerosis

and diabetes-related cognitive decline involve vascular dysfunction, where interventions to reduce microvascular stalls could alleviate inflammation, oxidative stress, and metabolic deficits [56,57,58]. By enhancing cerebral perfusion, targeting vascular stalls represents a promising strategy to combat neurodegeneration across multiple disorders.

4.4.5 Limitations of Current Work

While our findings provide strong evidence that restoring cerebral blood flow (CBF) can improve neural activity in an Alzheimer's disease (AD) mouse model, several limitations should be considered. First, our study primarily focuses on short-term changes following CBF restoration, leaving open the question of whether these improvements in activity patterns persist over longer timescales, coinciding with prior evidence of sustained improvement in behavioral performance up to 15/16 months of age APP/PS1 mice [59]. AD is a progressive disease, and while acute increases in blood flow may temporarily enhance neural function, it remains unclear whether sustained interventions could provide lasting cognitive benefits or slow disease progression. Additionally, our study primarily assesses visual cortex function, which may not fully represent the broader impacts of CBF restoration on other brain regions, particularly those more directly involved in memory and executive function, such as the hippocampus and prefrontal cortex. Future studies should investigate whether similar effects are observed across different cortical and subcortical circuits to better understand the global impact of vascular dysfunction in AD.

Another limitation is that our approach does not directly distinguish between the specific mechanisms by which CBF restoration influences neural activity. While we propose that improving metabolic support and reducing oxidative stress contribute to enhanced orientation selectivity, additional factors such as changes in neuroinflammation, vascular reactivity, and glial

function could also play critical roles. Moreover, our study relies on an AD mouse model that recapitulates key aspects of the disease but does not fully capture the complexity of human AD pathology. Translating these findings to clinical applications will require validation in more physiologically relevant models, as well as studies in human patients to assess whether similar vascular interventions can effectively restore cognitive function.

4.5 Conclusion

In this study, we investigated the relationship between cerebral blood flow (CBF) deficits and neural activity impairments in an Alzheimer's disease (AD) mouse model, demonstrating that restoring CBF can acutely improve orientation selectivity in the visual cortex. By eliminating capillary stalling and increasing CBF, we observed improved spontaneous activity and orientation selectivity in V1 neurons, supporting the hypothesis that vascular deficits contribute to AD-related cortical dysfunction. Future work will focus on validating these findings in awake mice, exploring plaque proximity effects, and investigating neuronal subtype contributions using transcriptomics. These results highlight the potential of vascular-targeted therapies to mitigate early cognitive deficits in AD and underscore the importance of addressing blood flow impairments as a therapeutic strategy. By linking improvements in CBF to enhanced neural activity and cognitive processing, our work provides a foundation for future studies exploring how cerebrovascular interventions can preserve brain function and slow neurodegeneration.

4.6 Methods

4.6.1 Animals

All animal procedures complied with relevant ethical regulations and were performed after approval by the Instituational Animal Care and Use Committee of Cornell University (protocol number 2015-0029). All mice were housed in a climate-controlled facility kept at 22° C and 40-50% humidity, under a 12 h light-dark cycle with ad libitum access to food and water. All mice were ~9-11 month old APP/PS1 mice[16].

4.6.2 Surgery

Mice were anesthetized with isoflurane (3% for induction, 1% for maintenance) and placed on a feedback-controlled heating pad. Surgeries were performed on a stereotaxic apparatus where the heads of mice were fixed with two ear bars. Ointment (Puralube, Dechra) was applied to both eyes for protection. Glycopyrrolate (0.002g/100g) was given intramuscular to prevent fluid build up in the lungs. Bupivacaine (0.125% ~0.1mL) was administered below the scalp after being disinfected by iodine and 70% ethanol. An incision was made into the scalp to fully expose the skull. A 3 mm craniotomy was made above V1 (A-P 3mm, M-L 2.5 mm from Bregma, centerline) on the right hemisphere. A 50 nL bolus of AAV9-Syn-GCaMP6s (Addgene) diluted to 10^{12} vg ml^{-1} was injected to the target V1 layer 2/3 (D-V -0.2 mm from the brain surface). A 3 mm glass window then replaced the hole in the skull, and a titanium head plate was secured to the skull with Metabond. Postoperative ketoprofen (0.5 mg/100g) and dexamethasone (0.2 mg/kg) were administered subcutaneously, and the mouse was allowed to fully recover in a cage on a heating pad. Four weeks were allowed for viral expression before imaging.

4.6.3 Two-photon Imaging

Two-photon fluorescence imaging was performed using a Ti:Sapphire laser (Coherent Vision S Chameleon; 80 MHz repetition rate, 75 fs pulse duration) at 920 nm focused by a Zeiss 20x water immersion objective (working distance = 2.3 mm, NA = 1) onto the sample to excite Texas Red-conjugated 70000 MW Dextran and GCaMP6s calcium indicator, with ~35 mW power at the sample. Excitation at 780 nm was performed to excite Methoxy-X04 to acquire signal of Aβ plaque expression. Imaging signals were acquired using ScanImage software (SI2022) into separate Blue (CH1), Green (CH2) and Red (CH4) colored channels (separated by 488 (CH1/CH2), 520 (CH1&2/CH3&4) and 562 (CH3/CH4) nm long-pass dichroics; Blue channel using a 494/41 (center wavelength/bandwidth, both in nanometers) bandpass filter, Green channel using 525/70 and Red channel using 645/65). A TTL signal from the monocular display was acquired as an external trigger for image acquisition. Galvo frame scanning was acquired at 256x256 at 3.41 Hz. Stacks were acquired at 512x512 resolution at 1.06 Hz.

For anesthetized imaging, during baseline recording, mice were anesthetized with isoflurane, injected retro-orbitally with Texas Red Dextran, and were head-fixed on a 37° C heating pad. A piezo was placed under the mouse to monitor breathing and heart rate and was stabilized at 2 Hz breathing rate. After waiting 30 minutes to stabilize anesthetic depth, imaging was performed. Immediately following baseline imaging, Isotype Control or anti-Ly6G treatment was injected intraperitoneally (I.P., 4 mg/kg). Post-injection recording was repeated 24 hours later.

For awake imaging, during baseline recording, mice were anesthetized with isoflurane, injected retro-orbitally with Texas Red Dextran, and were head-fixed on a home-built treadmill stereotax and allowed to recover from anesthesia. After waiting 30 minutes to get accustomed to head fixation, imaging was performed. Immediately following baseline imaging, Isotype Control

or anti-Ly6G treatment was injected I.P. with a dosage of 4 mg/kg. Post-injection recording was repeated 24 hours later.

4.6.4 Habituation

To prepare for awake imaging, mice were habituated for 1-2 weeks prior to imaging. Imaging was performed with mice head fixed and allowed to run on a stationary treadmill. Habituation followed a progressively increased time spent head fixed on the treadmill, starting at 5 minutes, and in increments of 10-15 minutes more each day working up to 1 hour of fixation.

4.6.5 Visual Stimulus

Visual stimulation experiments were performed with anesthetized and awake, head-fixed mice by positioning a MouseGoggles Mono V1.0 display [22] at the mouse's left eye for contralateral two-photon imaging in the right hemisphere. The display was oriented to 45^{o} azimuth and 0^{o} elevation respective to the long axis of the mouse. To conduct the visual stimulus protocol, both the display and microscope were controlled by a custom Matlab script which used the ScanImage Matlab API to control frame acquisition and serial commands to control the display. Before the start of the protocol, the display was set to show an intermediate brightness blue image (i.e. the background image), and the microscope was set to record an image series of 21 frames (in a duration of 6.16 seconds) upon the rising edge of an external TTL trigger signal. At the start of each trial, the display sent a TTL signal to begin acquisition. After 2 seconds of background image presentation, a maximum-contrast blue grating image was presented on the center of the display. The pattern covered a 160x160 pixel (92.8x92.8 deg) square region, with a grating spatial wavelength of 40 pixels (23.2 deg). The grating was randomly oriented and drifted in one of twelve directions (0^{o} – 270^{o}; 22.5^{o} interval) at a temporal frequency of 1.5 Hz, for a duration of 2 seconds. After the drifting grating stimulus, the background image was again

displayed until the end of the 8-second trial. Each of the twelve stimulus directions were presented to the mouse in a random order, after which the set of 12 trials was repeated 6 times (in a new randomized order each time). The order of stimulus presentation as well as all commands and parameters sent to the display throughout the experiment was saved in a Matlab struct in the same folder as the acquired images.

4.6.6 Analysis

Imaging data were analyzed using suite2p and a custom Matlab image processing pipeline. First, the raw ScanImage data files of a single imaging session were loaded into Matlab where the GCaMP channel (green channel 2) was extracted from the multichannel .tif stacks of both spontaneous activity and visually-stimulated activity datasets, and concatenated into a single image stack. This stack was then motion-corrected using the NoRMCorre[60] algorithm so that all cell bodies were registered and stable throughout the spontaneous and stimulated activity recordings. This stabilized image stack was then saved as a .tif file and loaded into suite2p for functional neuron segmentation. The set of segmented cells were then manually curated to remove ROIs drawn over what did not appear to be cell bodies. Vectors of mean brightness change within each ROI was calculated by suite2p, which also removed noise from the neuropil activity surrounding each neuron. A vector of neural activity spikes was also calculated by suite2p through deconvolution of the GCaMP6s impulse response function from the fluorescence vector. This set of ROIs, fluorescence change vectors, and spike vectors were saved to a .mat file, one for each imaging session.

To identify pairs of matching cell ROIs in both the pre- and post-injection timepoints, the mean GCaMP images and ROI sets from both imaging sessions were loaded into a custom Matlab app which displayed the images and ROIs side-by-side. The app allowed the user to

toggle through every ROI in an imaging dataset and see the nearby image and ROIs in the matching dataset. When the same cell was identified in both datasets, the user marked the ROIs from both images as being a matching pair. After all ROIs were manually inspected, the ROI numbers of all matching pairs were saved to a .mat file (one for each pair of datasets), enabling later analysis of individual cells between pre/post timepoints.

To analyze and plot neural activity measurements from all datasets, a Matlab script looped through all imaging session folders, loading the fluorescence change values from suite2p and the manually-determined pairs of matching cells from each dataset. To visualize spontaneous activity, the fluorescence change of each cell was calculated as the fluorescence at each frame divided by the cell's baseline fluorescence. Since spontaneous activity was sparse (even for relatively hyperactive neurons), the baseline fluorescence of each neuron was estimated as the median fluorescence level. To quantify the overall spontaneous activity, the transients-per-minute value for each cell during the spontaneous imaging dataset (i.e. during no visual stimulus) was calculated similarly as in Busche et al.[24] and described briefly here. Noise was quantified by calculating the standard deviation of the fluorescence signal values which dropped below the baseline, since real neural activity results in GCaMP brightness increases whereas noise varies in both positive and negative directions. Activity transients were then calculated as fluorescence increases greater than 3 times the standard deviation of the noise, and transients-per-minute is calculated as the number of unique transients (i.e. counting consecutive frames above noise as a single transient) which occurred during the spontaneous activity recording, divided by the duration of the recording (in minutes). Cells were classified as "spontaneously active" if they averaged at least 1 transient per minute.

To analyze stimulus-evoked neural activity, the fluorescence change of each neuron to each stimulus was calculated by dividing the cell's fluorescence at every imaging frame by the cell's baseline fluorescence, in which the baseline was calculated as the average fluorescence during the 2-s pre-stimulus period. To quantify the direction selectivity of each neuron to the set of visual stimuli, the direction selectivity index (DSI) was calculated by first determining the mean response of the neuron to each of the 12 orientations of drifting gratings, calculated as the average fluorescence change value during the 2-s stimulus period. The DSI was calculated as the vector sum of the 12 response values corresponding to the 12 directions of drifting gratings, divided by the total vector length. The DSI vector was calculated in the complex plane, so the final DSI value is taken as the magnitude of this complex number. Similarly, OSI was calculated as the magnitude of the normalized vector sum, but where each response angle was taken as double the actual angle of the drifting grating so that opposite directions point the vector in the same angle. The two equations for calculating DSI and OSI from the stimulus responses shown here:

$$\mathrm{DSI}_{\mathrm{complex}} = \frac{\sum_{k=1}^{n}(i*r_k*\theta_k)}{\sum_{k=1}^{n}|r_k|};\ \mathrm{DSI} = \left|\mathrm{DSI}_{\mathrm{complex}}\right|$$

$$\mathrm{OSI}_{\mathrm{complex}} = \frac{\sum_{k=1}^{n}(2*i*r_k*\theta_k)}{\sum_{k=1}^{n}|r_k|};\ \mathrm{OSI} = \left|\mathrm{OSI}_{\mathrm{complex}}\right|$$

Where k is the number of the stimulus (n=12 stimuli), r_k is the mean response of the neuron to stimulus k, and θ_k is the direction angle of stimulus k (in radians).

To compare spontaneous activity levels, OSI, and DSI between experimental conditions, the average activity, OSI, and DSI were calculated for each mouse/imaging session individually. Fraction of highly selectivity neurons for each were calculated by the number of neurons with an

OSI>0.75 divided by the total number of tracked neurons in each mouse/imaging session individually. Statistically significant differences between pre/post timepoints were determined using the Wilcoxon signed rank test (using the signrank() function in Matlab).

References

1. 2024 Alzheimer's disease facts and figures. *Alzheimers Dement. J. Alzheimers Assoc.* (2024) doi:10.1002/alz.13809.
2. J. Paul Taylor *et al.* Toxic proteins in neurodegenerative disease. *Science* **296**, 1991–1995 (2002).
3. Zeinab Breijyeh, Breijyeh, Z., Rafik Karaman & Karaman, R. Comprehensive Review on Alzheimer's Disease: Causes and Treatment. *Molecules* **25**, 5789 (2020).
4. Christopher A. Ross, Ross, C., Ross, C. A., Michelle A. Poirier & Poirier, M. A. Protein aggregation and neurodegenerative disease. *Nat. Med.* **10**, (2004).
5. G. Brent Irvine *et al.* Protein aggregation in the brain: the molecular basis for Alzheimer's and Parkinson's diseases. *Mol. Med.* **14**, 451–464 (2008).
6. Niwa, K., Kazama, K., Younkin, S. G., Carlson, G. A. & Iadecola, C. Alterations in Cerebral Blood Flow and Glucose Utilization in Mice Overexpressing the Amyloid Precursor Protein. *Neurobiol. Dis.* **9**, 61–68 (2002).
7. Rojas-Gutierrez, E. *et al.* Alzheimer's disease and metabolic syndrome: A link from oxidative stress and inflammation to neurodegeneration. *Synap. N. Y. N* **71**, (2017).
8. Blonz, E. R. Alzheimer's Disease as the Product of a Progressive Energy Deficiency Syndrome in the Central Nervous System: The Neuroenergetic Hypothesis. *J. Alzheimers Dis.* **60**, 1223 (2017).

9. Jones, E. A., Gillespie, A. K., Yoon, S. Y., Frank, L. M. & Huang, Y. Early Hippocampal Sharp-Wave Ripple Deficits Predict Later Learning and Memory Impairments in an Alzheimer's Disease Mouse Model. *Cell Rep.* **29**, 2123-2133.e4 (2019).

10. Hijazi, S. *et al.* Early restoration of parvalbumin interneuron activity prevents memory loss and network hyperexcitability in a mouse model of Alzheimer's disease. *Mol. Psychiatry 2019 2512* **25**, 3380–3398 (2019).

11. Bezzina, C. *et al.* Early Onset of Hypersynchronous Network Activity and Expression of a Marker of Chronic Seizures in the Tg2576 Mouse Model of Alzheimer's Disease. *PLOS ONE* **10**, e0119910 (2015).

12. Roher, A. E. *et al.* Cerebral blood flow in Alzheimer's disease. *Vasc. Health Risk Manag.* **8**, 599 (2012).

13. Cruz Hernández, J. C. *et al.* Neutrophil adhesion in brain capillaries reduces cortical blood flow and impairs memory function in Alzheimer's disease mouse models. *Nat. Neurosci.* **22**, 413–420 (2019).

14. Korte, N., Nortley, R. & Attwell, D. Cerebral blood flow decrease as an early pathological mechanism in Alzheimer's disease. *Acta Neuropathol. 2020 1406* **140**, 793–810 (2020).

15. Oliver Bracko *et al.* Causes and consequences of baseline cerebral blood flow reductions in Alzheimer's disease. *J. Cereb. Blood Flow Metab.* **41**, 1501–1516 (2021).

16. Jean C. Cruz Hernández *et al.* Neutrophil adhesion in brain capillaries reduces cortical blood flow and impairs memory function in Alzheimer's disease mouse models. *Nat. Neurosci.* **22**, 413–420 (2019).

17. Reece Crumpler *et al.* Capillary Stalling: A Mechanism of Decreased Cerebral Blood Flow in AD/ADRD. *J. Exp. Neurol.* **2**, (2021).

18. Axel R. Pries *et al.* Biophysical aspects of blood flow in the microvasculature. *Cardiovasc. Res.* **32**, 654–667 (1996).

19. David H. Hubel, Hubel, D. H., D. H. Hubel, Torsten N. Wiesel & Wiesel, T. N. Receptive fields of single neurones in the cat's striate cortex. *J. Physiol.* **148**, 574–591 (1959).

20. James J. DiCarlo *et al.* How Does the Brain Solve Visual Object Recognition. *Neuron* **73**, 415–434 (2012).

21. Christine Grienberger *et al.* Staged decline of neuronal function in vivo in an animal model of Alzheimer's disease. *Nat. Commun.* **3**, 774–774 (2012).

22. Matthew Isaacson *et al.* MouseGoggles: an immersive virtual reality headset for mouse neuroscience and behavior. *Nat. Methods* (2024) doi:10.1038/s41592-024-02540-y.

23. Marius Pachitariu *et al.* Suite2p: beyond 10,000 neurons with standard two-photon microscopy. *bioRxiv* 061507 (2016) doi:10.1101/061507.

24. Marc Aurel Busche *et al.* Clusters of hyperactive neurons near amyloid plaques in a mouse model of Alzheimer's disease. *Science* **321**, 1686–1689 (2008).

25. Yuhan Wang *et al.* EASI-FISH for thick tissue defines lateral hypothalamus spatio-molecular organization. *Cell* (2021) doi:10.1016/j.cell.2021.11.024.

26. Wang, Y. *et al.* Multimodal mapping of cell types and projections in the central nucleus of the amygdala. *Cold Spring Harb. Lab. - BioRxiv* (2022) doi:10.1101/2022.10.19.512845.

27. Fernando Maestú *et al.* Neuronal excitation/inhibition imbalance: core element of a translational perspective on Alzheimer pathophysiology. *Ageing Res. Rev.* **69**, 101372–101372 (2021).

28. Kazuto Masamoto, Masamoto, K., Iwao Kanno & Kanno, I. Anesthesia and the Quantitative Evaluation of Neurovascular Coupling. *J. Cereb. Blood Flow Metab.* **32**, 1233–1247 (2012).

29. Yurong Gao *et al.* Time to wake up: Studying neurovascular coupling and brain-wide circuit function in the un-anesthetized animal. *bioRxiv* 077024 (2016) doi:10.1101/077024.

30. Qingguang Zhang *et al.* Behavioral and physiological monitoring for awake neurovascular coupling experiments: a how-to guide. *Neurophotonics* **9**, (2022).

31. Costantino Iadecola & Iadecola, C. Vascular and Metabolic Factors in Alzheimer's Disease and Related Dementias: Introduction. *Cell. Mol. Neurobiol.* **36**, 151–154 (2016).

32. Maximilian Wiesmann *et al.* Hypertension, cerebrovascular impairment, and cognitive decline in aged AβPP/PS1 mice. *Theranostics* **7**, 1277–1289 (2017).

33. Chen, W. W., Zhang, X. & Huang, W. J. Role of neuroinflammation in neurodegenerative diseases (Review). *Mol. Med. Rep.* **13**, 3391–3396 (2016).

34. Heneka, M. T. *et al.* Neuroinfl ammation in Alzheimer's disease. *Lancet Neurol.* (2015) doi:10.1016/s1474-4422(15)70016-5.

35. Daulatzai, M. A. Cerebral hypoperfusion and glucose hypometabolism: Key pathophysiological modulators promote neurodegeneration, cognitive impairment, and Alzheimer's disease. *J. Neurosci. Res.* **95**, 943–972 (2017).

36. Latini, A., Pereira, P. J. S., Couture, R., Campos, M. M. & Talbot, S. Oxidative Stress: Neuropathy, Excitability, and Neurodegeneration. *Oxid. Med. Cell. Longev.* **2019**, (2019).

37. Han, X. J. *et al.* Amyloid β-42 induces neuronal apoptosis by targeting mitochondria. *Mol. Med. Rep.* **16**, 4521–4528 (2017).

38. Johri, A. & Beal, M. F. Mitochondrial dysfunction in neurodegenerative diseases. *J. Pharmacol. Exp. Ther.* **342**, 619–630 (2012).

39. Whittaker, R. G., Turnbull, D. M., Whittington, M. A. & Cunningham, M. O. Impaired mitochondrial function abolishes gamma oscillations in the hippocampus through an effect on fast-spiking interneurons. *Brain* **134**, e180–e180 (2011).

40. Sara Hijazi, August B. Smit, & Ronald E. van Kesteren. Fast-spiking parvalbumin-positive interneurons in brain physiology and Alzheimer's disease. *Mol. Psychiatry* (2023) doi:10.1038/s41380-023-02168-y.

41. Oliver Kann & Kann, O. The interneuron energy hypothesis: Implications for brain disease. *Neurobiol. Dis.* **90**, 75–85 (2016).

42. Kann, O., Papageorgiou, I. E. & Draguhn, A. Highly energized inhibitory interneurons are a central element for information processing in cortical networks. *J. Cereb. Blood Flow Metab. Off. J. Int. Soc. Cereb. Blood Flow Metab.* **34**, 1270–1282 (2014).

43. Eva Vico Varela *et al.* Excitatory-inhibitory imbalance in Alzheimer's disease and therapeutic significance. *Neurobiol. Dis.* **127**, 605–615 (2019).

44. Marc Aurel Busche, Busche, M. A., Arthur Konnerth & Konnerth, A. Impairments of neural circuit function in Alzheimer's disease. *Philos. Trans. R. Soc. B* **371**, 20150429 (2016).

45. Michael D. Greicius *et al.* Default-mode network activity distinguishes Alzheimer's disease from healthy aging: Evidence from functional MRI. *Proc. Natl. Acad. Sci. U. S. A.* **101**, 4637–4642 (2004).

46. David T. Jones *et al.* Age-related changes in the default mode network are more advanced in Alzheimer disease. *Neurology* **77**, 1524–1531 (2011).

47. Jorge J. Palop, Palop, J. J., Lennart Mucke & Mucke, L. Network abnormalities and interneuron dysfunction in Alzheimer's disease: A multiscale perspective on abnormal neuronal activity in early AD. *Alzheimers Dement.* **16**, (2016).

48. D. Chan *et al.* Induction of specific brain oscillations may restore neural circuits and be used for the treatment of Alzheimer's disease. *J. Intern. Med.* **290**, 993–1009 (2021).

49. Azul Silva & María Cecilia Martínez. Spatial memory deficits in Alzheimer's disease and their connection to cognitive maps' formation by place cells and grid cells. *Front. Behav. Neurosci.* **16**, (2023).

50. Dimitre G. Ouzounov *et al.* In vivo three-photon imaging of activity of GCaMP6-labeled neurons deep in intact mouse brain. *Nat. Methods* **14**, 388–390 (2017).

51. David A. Drachman & Drachman, D. A. The amyloid hypothesis, time to move on: Amyloid is the downstream result, not cause, of Alzheimer's disease. *Alzheimers Dement.* **10**, 372–380 (2014).

52. Xiaoming Hu *et al.* Cerebral Vascular Disease and Neurovascular Injury in Ischemic Stroke. *Circ. Res.* **120**, 449–471 (2017).

53. Wei Cai *et al.* Dysfunction of the neurovascular unit in ischemic stroke and neurodegenerative diseases: An aging effect. *Ageing Res. Rev.* **34**, 77–87 (2017).

54. Hélène Girouard *et al.* Neurovascular coupling in the normal brain and in hypertension, stroke, and Alzheimer disease. *J. Appl. Physiol.* **100**, 328–335 (2006).

55. Mordecai Y.-T. Globus *et al.* Cerebral blood flow and cognitive impairment in Parkinson's disease. *Neurology* **35**, 1135–1135 (1985).

56. Mingrui Li *et al.* Abnormal cerebral blood flow and brain function in type 2 diabetes mellitus. *Endocrine* (2023) doi:10.1007/s12020-023-03342-6.

57. Sorabh Sharma *et al.* A pathogenic role for IL-10 signalling in capillary stalling and cognitive impairment in type 1 diabetes. *bioRxiv* (2024) doi:10.1101/2024.04.01.587630.

58. Ghaydaa A. Shehata, T. Rageh, & Safaa Amira. Cerebrovascular Changes and Multiple Sclerosis. *Mult. Scler. Relat. Disord.* (2023) doi:10.1016/j.msard.2023.105168.

59. Bracko, O. *et al.* Increasing cerebral blood flow improves cognition into late stages in Alzheimer's disease mice. *J. Cereb. Blood Flow Metab.* **40**, 1441–1452 (2020).

60. Eftychios A. Pnevmatikakis, Pnevmatikakis, E. A., Andrea Giovannucci & Giovannucci, A. NoRMCorre: An online algorithm for piecewise rigid motion correction of calcium imaging data. *bioRxiv* 108514 (2017) doi:10.1101/108514.

CHAPTER 5: PSILOCYBIN INDUCES ALTERED NEUROVASCULAR COUPLING IN VISUAL CORTEX IN VIVO

Rick T. Zirkel, Clara Liao, Matthew Isaacson, Daniel Rivera, Matthew Yi, Keri Yamaguchi, Alex C. Kwan, Nozomi Nishimura, Chris B. Schaffer

Meinig School of Biomedical Engineering, Cornel University, Ithaca, NY, USA

5.1 Introduction

The therapeutic potential of psychedelics has sparked renewed interest in treatments for mental health disorders such as depression, addiction, and anxiety [1,2,3,4]. This resurgence has spurred human clinical trials to investigate the mechanisms of psychedelic drug action, mainly with the use of functional Magnetic Resonance Imaging (fMRI) to assess brain activity [5,6,7,8,9]. Many fMRI studies investigating psychedelics have reported alterations in brain activity and connectivity patterns [5,6,7,8,9]. These include increased global connectivity, reduced default mode network integrity, and heightened entropy in brain signals. Such findings have shaped current models of how psychedelics affect cognition and consciousness.

fMRI relies on neurovascular coupling (NVC), the process by which neuronal activity is tightly associated with local blood flow changes [10]. This relationship allows fMRI to use blood-oxygen-level-dependent (BOLD) signals as a proxy for neural activity [11,12,13,14]. NVC involves multiple signaling pathways and cell types, including neurons, astrocytes, vascular smooth muscle cells, pericytes, and endothelial cells [15,16,17,18,19]. From these BOLD fluctuations, patterns of brain activity, such as functional connectivity between regions, are inferred.

However, NVC is not always perfectly maintained. Various conditions, such as oxidative stress, inflammation, endothelial dysfunction, and altered neuron-astrocyte signaling, can disrupt

this relationship [20,21,22,23]. In Alzheimer's disease, elevated reactive oxygen species (ROS) damage vascular cells, impairing signaling between neurons, astrocytes, and blood vessels [21,23]. In stroke and ischemic injury, astrocyte dysfunction and gliosis compromise their ability to regulate blood flow [20,22]. In these cases, BOLD signals may no longer accurately reflect neural activity, complicating fMRI interpretation.

Psychedelic drugs may also alter this relationship between neural activity and cerebral blood flow (CBF). Psychedelics are similar in structure to serotonin (5-HT), which causes these drugs to have a high binding affinity for various serotonin receptors [24,25], the main receptor implicated in the hallucinogenic effects of psychedelics being the 5-HT_2AR [24,26]. Serotonin, however, is a vasoactive molecule, and can have both vasoconstrictive and vasodilatory implications on the vascular system in a context and region specific manner [27,28,29]. For example, activation of 5-HT_1 or $_2$ receptors can cause the release of vasodilatory substances from endothelial cells, but can also contribute to vasoconstriction in cerebral arteries. Thus, serotonin receptor interactions of these drugs may directly alter vascular responses independent of neural activity [30,31,32], potentially confounding fMRI results. Altogether, there is a need to understand if NVC is altered to during psychedelic treatment to better inform fMRI image interpretation in clinical trials involving psychedelic drugs.

Given the potential for psychedelics to disrupt NVC, it is crucial to determine whether and how this decoupling occurs. Without this understanding, fMRI-based conclusions about psychedelic effects on brain function may be misleading, particularly in clinical trials exploring their therapeutic potential. Future research should aim to disentangle vascular and neural contributions to fMRI signals to ensure accurate interpretations of psychedelic-induced brain activity.

5.2 Results

In this paper, we investigated how the NVC relationship is affected in awake mice with the administration of the psychedelic drug psilocybin. Using both multiphoton and widefield multimodal imaging, we simultaneously measure vascular and neural responses in the visual cortex (V1) to a visual stimulus, before and after psilocybin administration. Using a MouseGoggles Mono display [33], stimuli were presented to the left eye, while calcium imaging and cerebral blood flow were recorded from the right hemisphere (Fig 5.1 A). Here we use a single eyepiece to present four-direction drifting gratings of light and dark bars to elicit a large increase of neural activity in the visual cortex, and subsequent response of blood flow (Fig 5.1 B). Multiphoton imaging gives detailed measurements at the microscale, allowing for measurements of individual capillary flow speed and neuronal activity simultaneously with the use of arbitrary linescanning (Fig 5.1 C and D). Widefield, multimodal imaging provides broader, mesoscale insights into larger blood vessel diameter, and population level CBF, blood oxygenation, and neural activity (Fig 5.1 E and F).

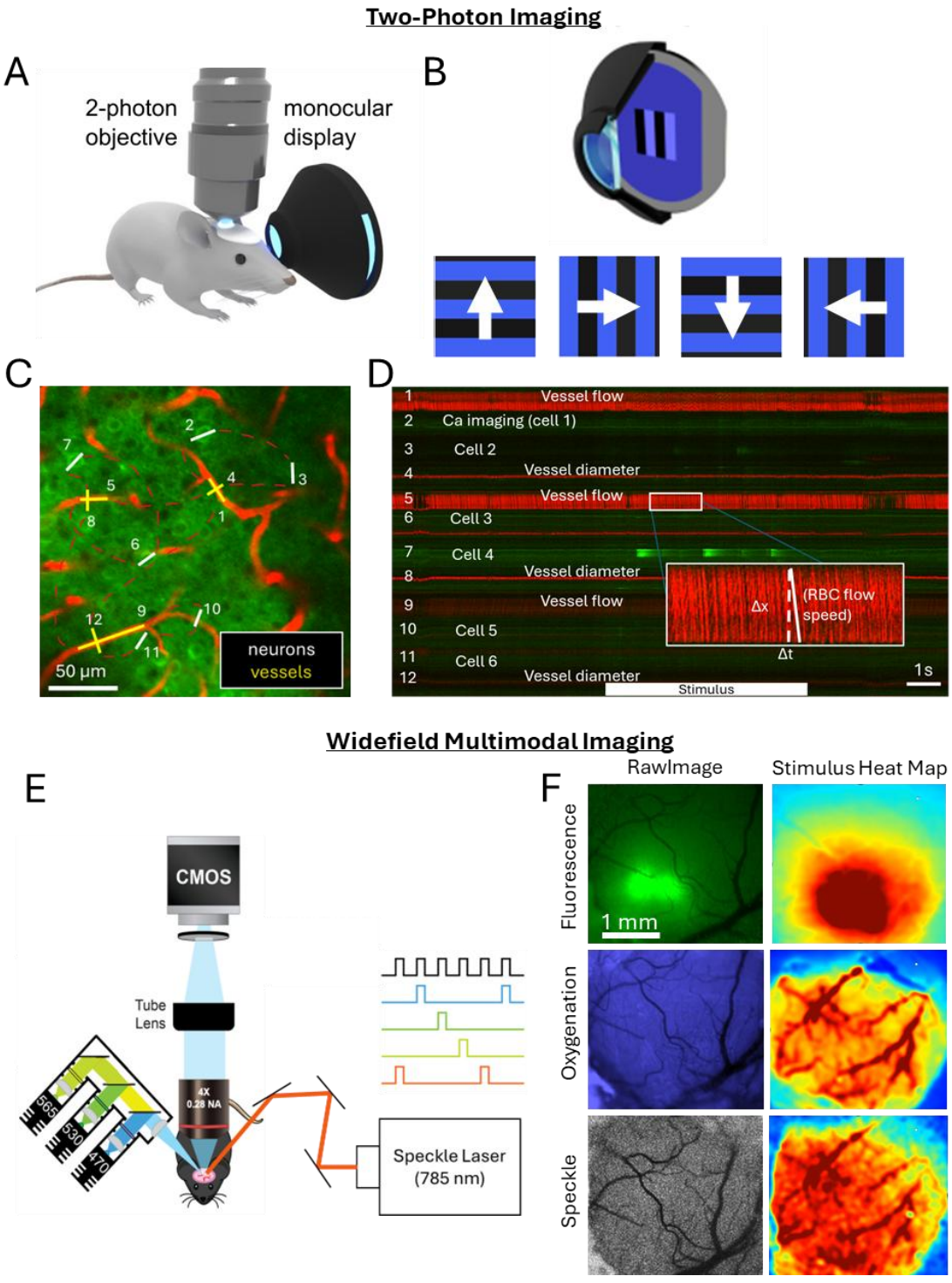

Figure 5.1 Micro- and Meso-scale imaging techniques. 18 Two-Photon Imaging **A:** MouseGoggles Monocular LED eyepiece stimulation during 2P imaging in an awake mouse. **B:** Visual stimulus paradigm of four-direction drifting gratings. **C:** Arbitrary linescan path recording calcium activity (green; white ROIs) and blood flow (red; yellow ROIs). **D:** Linearized linescan path corresponding to ROIs in C and example calculation of RBC flow speed.

Widefield Imaging **E:** Rapid succession of four excitation sources (Adapted from Rivera 2023 [34]). **F:** Raw image and stimulus heat map examples of calcium activity, intrinsic tissue oxygenation and speckle contrast CBF.

5.2.1 Psilocybin Induces Altered Neurovascular Coupling with Two-Photon Imaging

We first examined the effect of psilocybin on neuronal calcium activity and capillary blood flow and in response to a visual stimulus using multiphoton imaging. Imaging was performed 30 minutes post-psilocybin injection. This stimulus protocol consisted of 25 trials, each lasting 20s +/- 4s to ensure a return to baseline after stimulation, with visual stimulation occurring from 0-6s, as indicated by representative traces and shaded regions in panels of Figure 5.2. Our results indicate that psilocybin had no significant effect on calcium activity in response to the visual stimulus. Heat maps of individual neurons revealed no noticeable differences pre- and post-treatment (Fig. 5.2 A). This was consistent across average calcium fluorescence traces, where neurons that responded immediately following stimulation ("ON" neurons, which made up the majority of recorded neurons) showed no change post-psilocybin (Fig. 5.2 B). Quantitative analysis confirmed no significant difference comparing ctrl (post-pre) vs psilocybin (post-pre) calcium fluorescence changes during the response (p-val = 0.1297) (Fig. 5.2 C), and no shift in neuron firing type (“ON”; activated by stimulus onset, vs. “OFF”; activated by stimulus offset) was observed (Fig. 5.2 D).

After observing no significant change in calcium activity, we next compared this directly with our simultaneously recorded blood flow data to determine whether psilocybin influenced the vascular response. Characteristic blood flow changes were observed in response to visual stimulation; however, striking differences were found between pre- and post-psilocybin administration that deviated from control mice. Under control conditions, blood flow velocity increased, peaked around ~2s after stimulus onset, then reduced, showing a large velocity

undershoot after the stimulus ended. Psilocybin (1 mg/kg) administration resulted in a prolonged elevation and reduced undershoot of capillary flow speed following stimulation. Here we describe the flow response as having two phases: a "response" phase during the stimulus noted by a large increase in flow velocity, and a "recovery" phase after the stimulus has ended noted by a large undershoot of velocity before retuning to baseline. Heat maps of individual vessel fractional flow speed changes demonstrated a clear prolongation of increased flow speed post-psilocybin compared to baseline (Fig. 5.2 E). Averaging these fractional changes across all vessels, we observed a similar initial increase in flow speed across conditions; however, post-psilocybin, the elevation was prolonged, and the undershoot was reduced (Fig. 5.2 F). This resulted in a significant increase in the average flow speed change with psilocybin (post-pre) compared to control (post-pre) during the recovery phase (Fig. 5.2 H). No significant change was seen in the response phase (Fig 5.2 G). Seventeen pre/post control mice and twenty-one pre/post psilocybin mice were used for these analyses. Control (post-pre) vs psilocybin (post-pre) response/recovery p-values = 0.1437/0.0107. These p-values are not corrected for multiple comparisons (3 measurement types x 2 treatment groups = 8 comparisons). After Benjamini-Hochberg correction with a false discovery rate (FDR) of 0.05, control vs psilocybin recovery remained significant.

These findings suggest that psilocybin alters neurovascular coupling (NVC), prolonging the vascular response to stimulation without affecting neural activity.

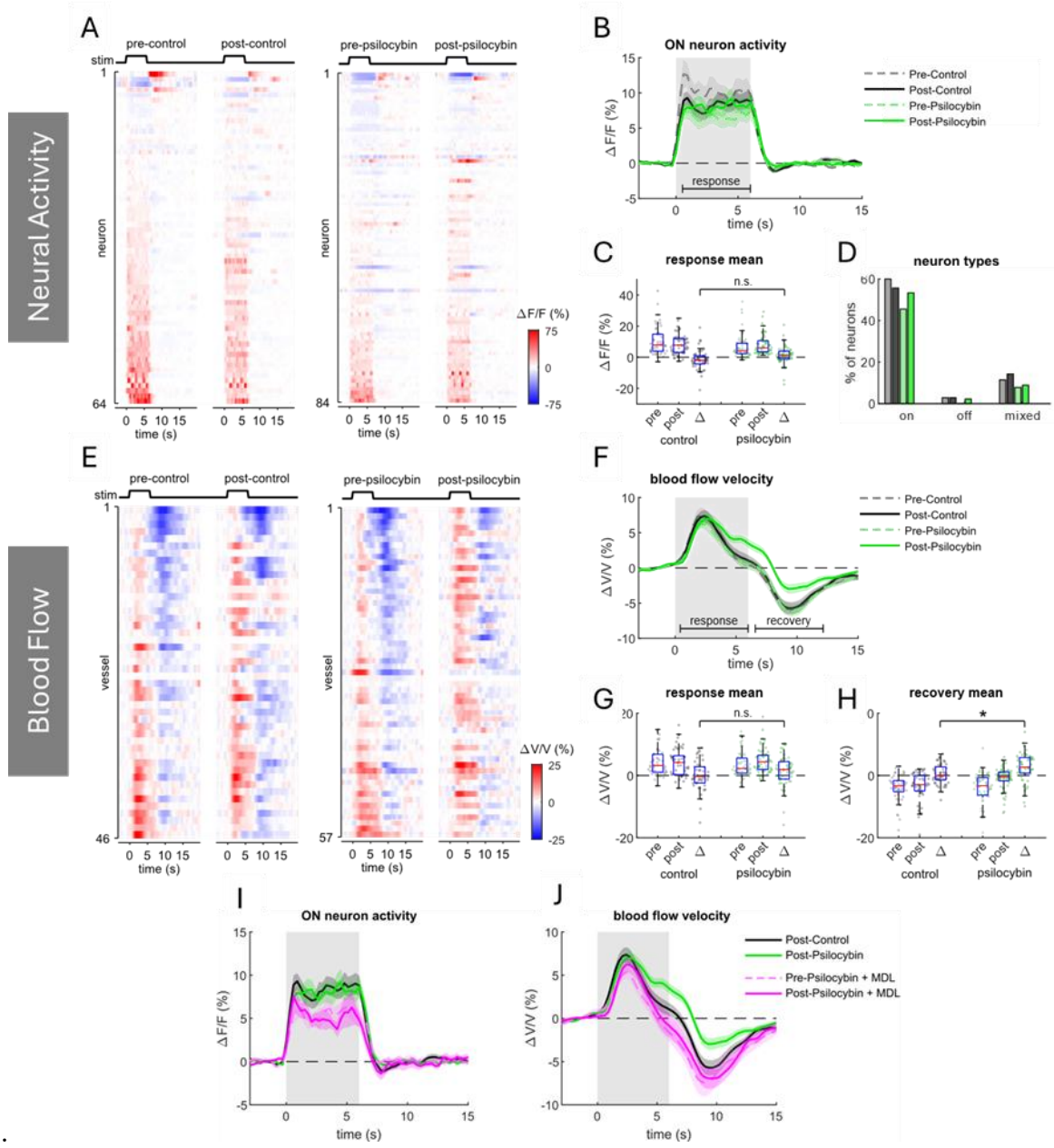

Figure 5.2 Prolonged elevation of NVC response after psilocybin administration A: Representative heat maps of change in calcium fluorescence in in individual neurons. **B:** Mean calcium fluorescence change traces for all ON neurons immediately active following the visual stimulus in each experimental group. **C:** Box plots comparing average calcium fluorescence change during response phase. Data is compared before and after treatment, as well as the change between the two timepoints. **D:** Fraction of neuronal firing type in each experimental group. **E:** Representative heat maps of fractional flow speed change in individual vessels. **F:** Mean fractional flow speed change traces for all vessels in each experimental group. **G, H:** Box plots comparing average flow during response and recovery phases. Data is compared before and after treatment, as well as the change between the two timepoints. **I:** Mean calcium fluorescence change traces for all neurons immediately active following the visual stimulus in each

experimental group. **J:** Mean fractional flow speed change traces for all vessels in each experimental group. Psilocybin data is same as shown in F, and was overlayed here as a visual comparison. Box plots show mean and $25^{th}/75^{th}$ percentiles, with whiskers extending to the full range of non-outlier datapoints. Plots of time vectors have traces as means and shaded regions as s.e.m. (standard error of measurement). Nested Anova. Neurons: 12 pre/post control mice, 15 pre/post psilocybin mice (that had at least 1 active neuron). Ctrl vs psilocybin p-val = 0.1297. Blood flow: 17 pre/post control mice, 21 pre/post psilocybin mice. Ctrl vs psilocybin response/recovery p-vals = 0.1437/0.0107. 11 pre/post psilocybin+mdl mice. These p-values are NOT corrected for multiple comparisons (4 comparisons). After Benjamini-Hochberg correction with a false discovery rate (FDR) of 0.05, recovery velocity response ctrl vs psilocybin remains significant (p = 0.0428). (* = $p < 0.05$)

To understand the mechanisms behind this decoupling between neural activity and blood flow, we examined NVC after psilocybin after administering a blocker of the 5-HT_2A receptor, MDL. Comparing our previously recorded psilocybin data with measurements taken after blocking the 5-HT_2A receptor, we observed a trend of attenuation of the prolonged blood flow increase effect seen with just psilocybin, though the result is not statistically significant since the sample size of MDL is small (Fig. 5.2 J). No evident effect on neuronal activity was observed (Fig 5.2 I).

5.2.2 Psilocybin Induces Similar Altered NVC Trend with Widefield Imaging

To assess whether these changes in NVC were evident at the population level, we conducted widefield multimodal imaging to measure cerebral blood flow (CBF), oxygenated hemoglobin (HbO), deoxygenated hemoglobin (HbR), total hemoglobin (HbT), and calcium activity simultaneously (Fig. 5.1E). Using the same visual stimulus paradigm, we analyzed NVC alterations at the mesoscale, allowing for differentiation between arterial and venous responses based on oxygenation levels. Data from 13 mice per condition, averaging over 15 trials per mouse, revealed trends consistent with our microscale findings. Laser-speckle contrast imaging trended towards a prolonged increase in fractional change in speckle contrast (K) following psilocybin (Fig. 5.3B). Speckle contrast depends on flow speed, but the relationship is complex so relative changes in speckle contrast is a useful proxy for relative changes in speed. This

prolongation was also evident in HbO and HbT changes (Fig. 5.3E, F). Notably, these effects appeared more pronounced in veins than arteries.

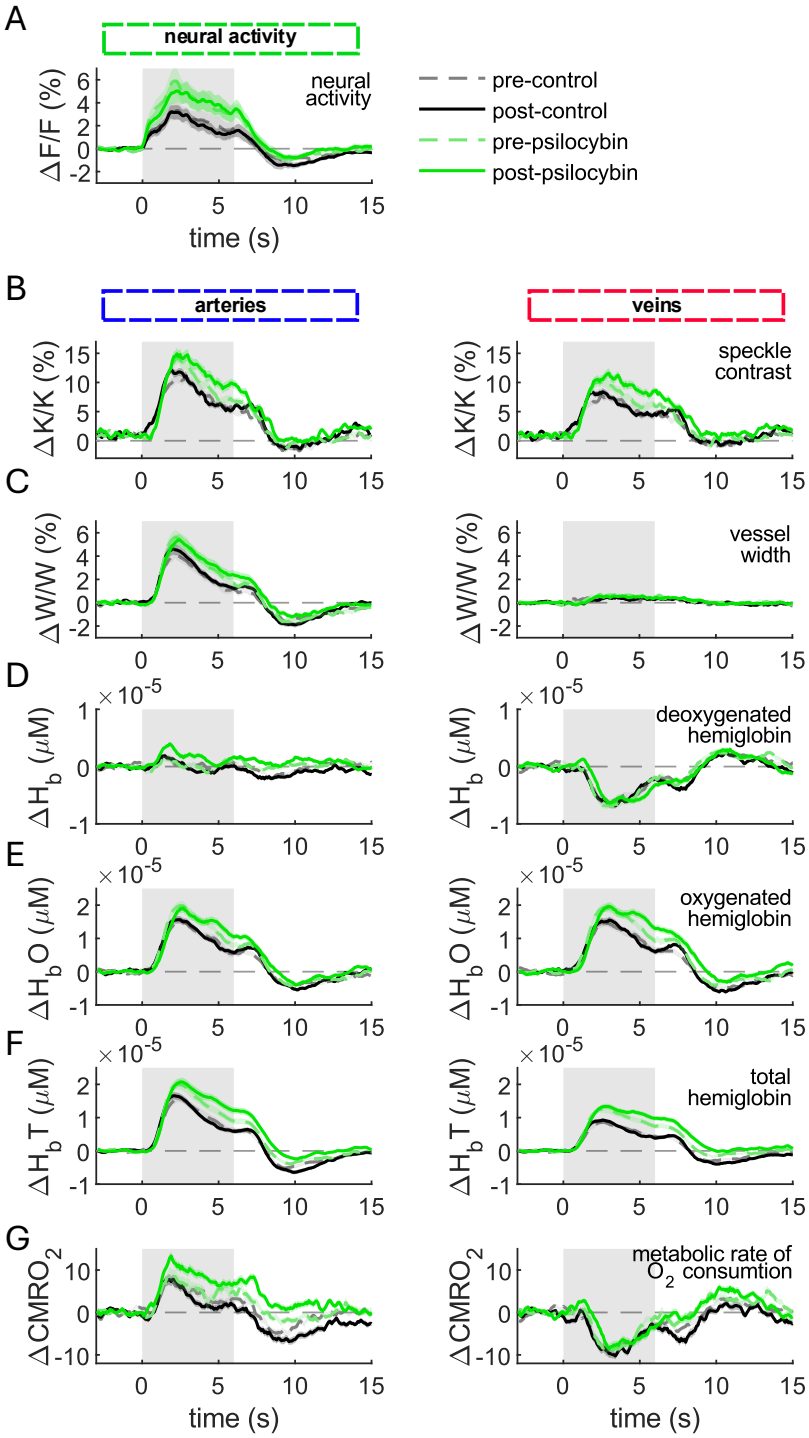

Figure 5.3 Trend of prolonged NVC response with psilocybin in widefield imaging A: 19 Mean traces of calcium fluorescence change. **B-G:** Mean traces, classified by artery or vein, of changes in fractional speckle contrast, vessel width, deoxygenated hemoglobin, oxygenated hemoglobin, total hemoglobin, and cerebral metabolic rate of oxygen consumption. All plots show mean $\pm$ s.e.m. for 13 mice/group.

We also examined simultaneously recorded fluorescence changes. Consistent with our microscale data, psilocybin did not significantly alter calcium fluorescence responses to visual stimulation (Fig. 5.3A). This multi-scale evidence further supports the conclusion that psilocybin alters NVC, prolonging blood flow responses independently of neural activity changes.

5.2.3 Psilocybin Induces Increased Baseline Blood Vessel Width

In addition to dynamic blood flow responses, we also analyzed baseline vessel widths and overall blood volume. From widefield imaging, we examined baseline vessel widths before and after treatment (Fig 5.4 A). Widefield imaging revealed a significant increase in vein width post-psilocybin when performing nested Anova. The p-value shown IS corrected for multiple comparisons: Benjamini-Hochberg correction (2 comparisons) with a false discovery rate (FDR) of 0.05; vein fractional width change due to psilocybin compared to control had an adjusted p-val = 0.001 (** = $p < 0.01$) (Fig. 5.4B&C), indicating a static vascular alteration induced by psilocybin. Further volumetric analysis using two-photon imaging stacks will allow us to assess changes in blood volume, surface vessel width, and capillary diameters, providing additional insights into baseline vascular modifications following psilocybin administration.

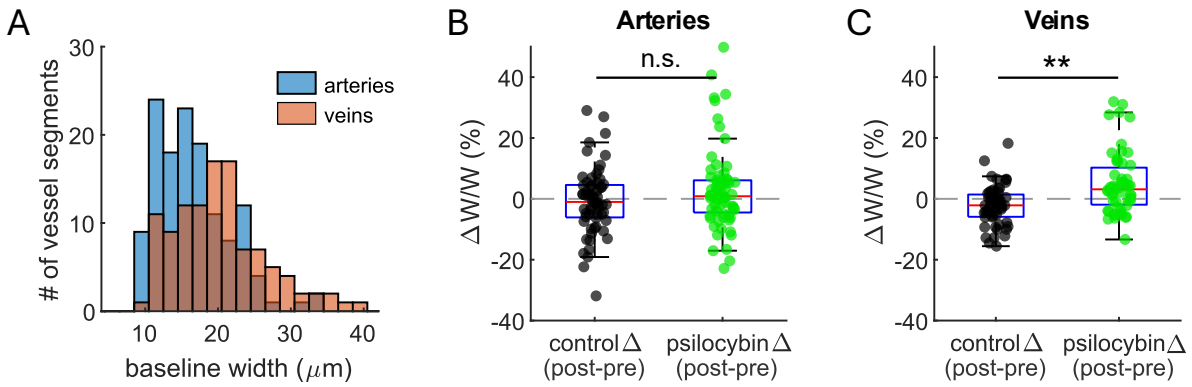

Figure 5.4 Increased baseline vessel width after psilocybin A: 20 Number of vessel segments binned by baseline vessel width for both arteries and veins (n = 13 mice/group; Control: 64 arteries, 68 veins; Psilocybin: 55 arteries, 55 veins). **B and C:** Fractional change in vessel width in the same mice before and after treatment classified by artery or vein (n = 13 mice/group). Nested Anova. The p-value shown IS corrected for multiple comparisons: Benjamini-Hochberg correction (2 comparisons) with a false discovery rate (FDR) of 0.05; adjusted p-val for arteries/veins = 0.3078/0.001. (* = $p < 0.05$; ** = $p < 0.01$)

5.3 Discussion

Our data demonstrates that psilocybin treated mice show an altered NVC response to a large visual stimulus. This altered NVC response took the form of a prolonged increase in blood flow response to visual stimulation, which was not paired with any alterations to neural activity. These resultant alterations to vascular responses that do not correspond to any changes in neural activity are confounding factors for methods such as fMRI which assume stable NVC in the context of psychedelic drugs. It is important to understand the mechanisms behind these alterations to better inform our understanding of how to most accurately interpret this relationship in psychedelic clinical studies using fMRI.

5.3.1 Potential Mechanisms of Altered NVC with Psilocybin

One potential component of the underlying cause behind altered NVC with psychedelics could be serotonin agonism. Simplifying the NVC response, following an increase in neural activity there is a dilation of blood vessels and increase in blood flow to satisfy metabolic demand. Following this response, there is a counteracting constriction of blood vessels to return the vascular system to baseline conditions. Psilocybin may differentially affect these two components of the NVC response. Based on our results that blood flow response was prolonged with psilocybin treatment during visual stimulation, while its initial onset was unchanged, it is possible that the vasoconstrictive component of the NVC response following initial dilation is being impaired, leading to a prolonged increase in blood flow. A potential mechanism for this is antagonism at serotonin receptors that are involved in vasoconstriction. Specifically, candidate receptors include the 5-HT_1A, $_1$B, and $_2$B receptors. Although psychedelics are more likely to activate these receptors to induce vasodilation or vasoconstriction, studies suggest their net effect may involve the modulation of the vascular response through a variety of interacting receptor systems rather than simple antagonism [25,11].

Beyond direct 5-HT_2 receptor antagonism, psychedelics may weaken vasoconstrictive feedback through multiple indirect serotonergic pathways. Serotonin can modulate vascular tone prejunctionally by regulating the release of noradrenaline (NA), acetylcholine (ACh), and calcitonin gene-related peptide (CGRP), depending on which 5-HT receptor subtypes are engaged [35]. Psychedelics may bias this signaling toward pathways that reduce noradrenaline-mediated vasoconstriction while enhancing CGRP-induced vasodilation, thereby extending the duration of increased blood flow. Additionally, activation of presynaptic 5-HT_1 receptors can inhibit noradrenaline release, leading to reduced sympathetic vasoconstriction, while 5-HT_7

receptor activation promotes cAMP-mediated endothelial relaxation, further countering vasoconstriction. Furthermore, the interplay between serotonin, dopamine, and acetylcholine also influences vascular dynamics. By shifting the DA-5HT balance, psychedelics could suppress noradrenergic vasoconstriction while enhancing cholinergic and CGRP-related vasodilation [25,36]. Due to the number of alternative mechanisms to alter blood flow outside direct 5-HT_2 receptor antagonism, psychedelics may be acting through a complex network of serotonergic, dopaminergic, and cholinergic interactions, ultimately weakening vasoconstrictive feedback.

5.3.2 Regional and Drug-Specific Variability in NVC Alterations

Another confounding variable is that 5HTR expression varies tremendously across different brain regions, and affinities for such receptors are inconsistent for different psychedelic metabolites [37,38]. While 5-HT_2A receptors are predominantly expressed in the cortex, others implicated in vasoactivity include 5-HT_1B — expressed in more lateral parts of the dorsal thalamus and in the striatum — and 5-HT_1A — widely expressed, particularly in the hippocampus, cortex, and amygdala. These differences indicate the possibility that such altered NVC will vary greatly in region, drug, and dose dependent contexts. Such variability presents additional challenges for precisely incorporating psychedelic-induced NVC alterations into a more informed interpretation of fMRI imaging data.

At lower doses, psychedelics may induce mild vasodilation without completely disrupting neurovascular coupling (NVC). For example, low-dose psilocybin (0.16 mg/kg) has been shown to increase CBF modestly in certain cortical areas without significantly altering neural activity [39]. However, at higher doses, 5-HTR activation may reach a threshold where direct vascular effects dominate over neural activity-driven changes, such as in the our study where we look at the effects of 1 mg/kg psilocybin doses in mice. High doses can induce excessive vasodilation,

potentially overriding normal activity-dependent control of CBF and leading to perfusion mismatches. Additionally, high doses could engage 5-HT_1A autoreceptors more strongly, leading to paradoxical vasoconstriction in some regions, further contributing to decoupling.

Different psychedelics may interact with vascular and glial systems in distinct ways, leading to potential variability in neurovascular decoupling. Classic serotonergic psychedelics like LSD and psilocybin primarily act through 5-HT_2A receptors, but they also have different affinities for 5-HT_1A, 5-HT_2C, and other receptors that modulate vascular tone [37,40]. For instance, LSD has a longer duration of action and differentially effects cortical blood flow compared to psilocybin, as well as mescaline, potentially leading to variable decoupling [41,42]. Meanwhile, compounds like mescaline, which have additional adrenergic activity, might produce more heterogeneous blood flow effects across different vascular beds [43]. Furthermore, MDMA, which releases serotonin rather than just acting as a receptor agonist, can cause prolonged vasoconstriction in some regions due to its effects on endothelial serotonin transport [44]. Our results reveal alterations specifically due to psilocybin, however such variability in drug action between different psychedelics demonstrate a need for further studies to compare drug-specific effects on NVC.

Neurovascular decoupling may be more pronounced in some brain regions than others due to differences in vascular architecture, receptor expression, and baseline NVC mechanisms [45]. The prefrontal cortex (PFC), for example, has a high density of 5-HT_2A receptors, a receptor whose activation can lead to vasodilation, and strong serotonergic modulation of its vascular system [46]. It is unlikely that 5-HT_2A receptor interactions play a dominant role in the NVC decoupling we observe, as our results suggest that psilocybin contributes to a reduction in the vasoconstrictive component of the vascular response. However, due to it's importance in the underlying mechanisms of psychedelic drug action warrants it be considered as a possible factor. Prior to

injection of psilocybin, introducing MDL as an antagonist to $5HT_2A$ receptors will provide the environment capable of determining if such altered NVC persists with or without their involvement [47]. Similar antagonism for other targets will provide an understanding of contributing receptors by process of elimination. Conversely to the PFC, subcortical regions like the striatum, where vascular control is more dependent on dopaminergic and cholinergic inputs, may exhibit different patterns of decoupling [48]. The hippocampus, with its unique pericyte-mediated microvascular control, could also be particularly susceptible to psychedelic-induced dysregulation [49,50].

The nature of a stimulus can also affect the degree of NVC decoupling under psychedelics. In tasks that involve strong sensory input, such as visual stimulation, psychedelics might enhance cortical excitability while simultaneously disrupting normal hemodynamic responses. For example, Padawer-Curry et al. showed that 2,5-Dimethoxy-4-iodoamphetamine (DOI) differentially alters calcium (enhanced) and hemodynamic (narrowed) whisker air-puff stimulus responses [31]. This suggests that psychedelics could alter stimulus-driven neurovascular dynamics by enhancing neural gain while blunting vascular reactivity. On the other hand, in tasks that require top-down cognitive control, like working memory tasks, decoupling might manifest as impaired task-related CBF responses due to excessive vasodilation in the PFC, reducing the brain's ability to direct blood flow where it is needed [51]. Our data suggests different alterations to NVC with psilocybin, which demonstrates the potential for variability in specific contexts. Differences in psychedelic drugs, brain regions, and stimulus paradigms across these studies likely contribute to the variable changes seen in NVC. Future studies should look to address these differences to elucidate what effects underly such NVC alterations with psychedelics.

5.3.3 Implications for fMRI and Neuroimaging Studies

If psychedelics cause a decoupling of blood flow responses from neural activity — and this decoupling varies across dose, drug type, brain region, and stimulus paradigm — then interpreting fMRI images in human studies becomes significantly more complicated. Since fMRI primarily relies on blood-oxygen-level-dependent (BOLD) signals as a proxy for neural activity, any direct vascular effects of psychedelics could lead to misleading conclusions about brain function.

As such, a psychedelic-induced increase in cerebral blood flow (CBF) that is independent of neural firing could lead to false positives, where areas appear hyperactive despite unchanged or even reduced neural activity. For example, if 5HT-mediated impaired vasoconstriction leads to a prolonged increase in blood flow in visual cortex but does not correspond to increased spiking activity, fMRI may overestimate psychedelic-induced visual processing changes. Conversely, if a drug disrupts normal NVC mechanisms — delaying or diminishing blood flow responses — neural activity could be underestimated. Our results show that psilocybin induced a prolongation of increased blood flow without altering neural activity, suggesting that BOLD signals from fMRI would overestimate neural activity induced by psilocybin.

Since the degree of NVC decoupling may vary across brain regions, some areas might show more reliable BOLD signals than others. For instance, highly serotonergic regions like the prefrontal cortex and visual cortex may experience stronger blood flow changes independent of neural activity, making fMRI results less trustworthy there. Meanwhile, subcortical regions with lower 5-HTR expression, like the striatum or thalamus, may have more interpretable BOLD signals.

At different psychedelic doses, the relationship between fMRI signals and neural activity might change. Low doses may induce mild vascular changes that still allow BOLD to roughly track neural firing, but at high doses, extreme vasodilation could dominate the signal, making it harder to discern neural activity from pure hemodynamic effects.

Many psychedelic studies suggest that altered brain network dynamics underlie their therapeutic effects. If these interpretations rely heavily on BOLD fMRI, the true mechanisms might be misunderstood. For example, changes attributed to increased entropy in brain activity might stem from widespread serotonin-driven vasoactivity rather than neural-level effects.

There are several ways to address this confounding variable: combining fMRI with direct neural recordings (EEG, MEG, or intracranial electrophysiology) could help disambiguate vascular from neural effects [52]. Techniques like calibrated fMRI (which accounts for baseline CBF changes) or arterial spin labeling (ASL) could improve accuracy [53,54]. Studying psychedelics with different vascular effects (e.g., psilocybin vs. ketamine) might help isolate hemodynamic confounds. Psychedelic-induced decoupling of neurovascular coupling complicates fMRI interpretation, making it crucial to consider vascular effects when analyzing results. Without accounting for direct blood flow changes, studies risk conflating hemodynamic artifacts with true neural activity alterations, potentially skewing our understanding of how these drugs affect the brain.

5.3.4 Limitations

This data shows promising evidence that psilocybin has direct implications on the vascular system that result in an alteration in NVC response, where blood flow change is no longer directly coupled to neural activity. There are several limitations to consider when interpreting our

results. Firstly, calcium imaging, while a good estimate, is not a direct measurement of neural activity. Changes in calcium response may be influencing the fluorescence changes that we observe. For this reason, further studies would benefit by recording neural activity directly through measurements such as voltage imaging or electrophysiology. Recording calcium activity is already impacted by hemoglobin absorption using widefield imaging. For this reason, we performed absorption correction, however such methods are not completely able to account for these confounds. Performing widefield imaging with a more red-shifted calcium indicator would help to eliminate these confounds more effectively.

The awake imaging performed in this project was not accompanied by any behavioral recording. Even after habituation, some level of stress may persist, necessitating behavioral monitoring to assess whether changes in imaging data correlate with animal discomfort or agitation. Parameters such as pupil size, whisking behavior, and body movement are often tracked alongside imaging data to ensure that physiological measurements are not confounded by stress-related artifacts. Future studies should implement measurement of behavior during imaging.

With widefield imaging, our current setup only allows for a FOV of 3mm in diameter. This limits our ability to determine how NVC is altered between different regions, which would allow us to determine how default mode network (DMN) activity is affected in this context, a network that is notably affected by psychedelics according to fMRI clinical studies.

Aside from imaging confounds, we also were limited in the treatment we performed. Primarily using psilocybin, and only at the single dose of 1mg/kg, limits our ability to determine how this effect may vary across different drugs and dosages. Future studies should implement these different experimental groups.

5.4 Conclusion

In this study, we investigated whether the administration of psilocybin induced an alteration in NVC, the relationship between neural activity and subsequent blood flow response. Specifically, we examined NVC in the mouse visual cortex in response to a visual stimulus using MouseGoggles with two-photon (2P) and widefield imaging. On the microscale, 2P imaging revealed a prolonged increase in blood flow response with no corresponding change in neuronal calcium activity, and widefield imaging further supported this altered NVC with similar increases in blood flow and no change in neural activity. These findings demonstrate that psilocybin induces a sustained increase in cerebral blood flow (CBF) independent of measurable changes in neural activity, highlighting a neurovascular decoupling effect. This disruption challenges the interpretation of fMRI studies, which rely on blood oxygenation-level dependent (BOLD) signals as a proxy for neural activity. The underlying mechanisms likely involve serotonergic modulation of vascular tone through 5-HT receptor subtypes and interactions with a complex array of signaling pathways. Given the regional variability in receptor expression and vascular control, psychedelic-induced NVC may vary across brain areas, drug types, and doses, further complicating fMRI interpretations. A deeper understanding of these vascular effects is essential for accurately interpreting fMRI studies with psychedelics, ensuring that changes in BOLD signals are properly attributed to neural or vascular origins.

5.5 Methods

5.5.1 Animals

All animal procedures complied with relevant ethical regulations and were performed after approval by the Institutional Animal Care and Use Committee of Cornell University (protocol number 2015-0029). All mice were housed in a climate-controlled facility kept at 22° C and 40-50% humidity, under a 12 hour light-dark cycle with ad libitum access to food and water. All mice were ~5-7 weeks old WT (htr2a +/+) mice from Htr2a-flox transgenic lines.

5.5.2 Surgery

Mice were anesthetized with isoflurane (3% for induction, 1% for maintenance) and placed on a feedback-controlled heating pad at 37º C. Surgeries were performed on a stereotaxic apparatus where the heads of mice were fixed with two ear bars. Ointment (Puralube, Dechra) was applied to both eyes for protection. Glycopyrrolate (0.002g/100g) was given intramuscular to prevent fluid build up in the lungs. Bupivacaine (0.125% ~0.1mL) was administered below the scalp after being disinfected by iodine and 70% ethanol. An incision was made into the scalp to fully expose the skull. A 3 mm craniotomy was made above V1 (A-P 3mm, M-L 2.5 mm from Bregma, centerline) on the right hemisphere. A 50 nL bolus of AAV1-CaMKII-GCaMP6f (Addgene) diluted to 10^{12} vg ml^{-1} was injected to the target V1 layer 2/3 (D-V -0.2 mm from the brain surface). A 3 mm glass window then replaced the hole in the skull, and a titanium head plate was secured to the skull with Metabond (Parkell). Postoperative ketoprofen (0.5 mg/100g) and dexamethasone (0.2 mg/kg) were administered subcutaneously, and the mouse was allowed to fully recover in a cage on a heating pad. Four weeks were allowed for viral expression before imaging.

5.5.3 Two-photon (2P) Imaging

Two-photon fluorescence imaging was performed using a Ti:Sapphire laser (Coherent Vision S Chameleon; 80 MHz repetition rate, 75 fs pulse duration) at 920 nm to excite Texas Red-conjugated 70000 MW Dextran and the CaMKII-GCaMP6f calcium indicator, with ~35 mW power at the sample. A Zeiss 20x water immersion Objective (working distance = 2.3 mm; NA = 1) was used and heated by an objective heater set at 37° C. Imaging signals were acquired using ScanImage software (SI2022) into separate Green and Red colored channels (separated by a 560 nm long-pass dichroic; Green channel using a 517/65 (center wavelength/bandwidth, both in nanometers) bandpass filter and Red channel using 645/65). A TTL signal from the monocular display was acquired into an additional unused imaging channel for synchronizing imaging with visual stimuli. Arbitrary line scanning (Cycle rate = 166.67 Hz) was used to acquire blood flow speed and diameter from vessel ROIs (n = 3 vessels/path), as well as calcium activity from neuron ROIs (n = 6 neurons/path). Frame scanning of stacks was done at 512x512 frames acquired at 1.06 Hz. During baseline recording, mice were lightly anesthetized with isoflurane to perform a retroorbital injection of Texas Red Dextran and were head fixed in an awake imaging tube rig stereotax. After 30 minutes, mice were imaged for 30 minutes. This consisted of spontaneous and stimulated (25 trials, 20s each, 0-6s visual stimulation), arbitrary linescanning, as well as acquired stacks. During post-injection recording, after injection of Texas Red dextran, saline vehicle or psilocybin was injected I.P. with a dosage of 1 mg kg^{-1}. After 30 minutes, mice were imaged for 30 minutes.

5.5.4 Calculating Red Blood Cell Velocity

To determine the velocity of red blood cells (RBCs) in vessels from linescan data, we use the Radon transform, which efficiently calculates velocity by analyzing the orientation of streaks

formed by moving RBCs in a time-space image. The streaks, visible as diagonal lines, are caused by RBC movement along the vessel. The angle of these streaks is inversely proportional to RBC velocity, with a stationary flow resulting in vertical streaks and faster flows producing horizontal streaks. The centerline velocity can be determined by measuring the slope of these streaks, which is achieved using the Radon transform to find the angle with the maximal variance in the image data [55,56].

The method involves first windowing the linescan data into short time segments, ensuring the window size is small enough to resolve high-frequency modulations such as the heart rate (~6 Hz for rats and ~10 Hz for mice). A typical window size of 40 ms is used to balance temporal resolution with adequate data for reliable velocity estimation. After normalizing the data to correct for illumination and baseline variations, the Radon transform is applied to each window. The variance of the transformed data along different angles reveals the direction of flow, and the velocity is derived from the angle corresponding to the maximal variance. This approach is robust to noise and allows for the efficient calculation of RBC velocities in real-time, even with low signal-to-noise data.

5.5.5 Widefield Imaging

Widefield, multimodal imaging was performed by acquiring images using a Basler acA0240um-NIR enhanced camera. Interleaved images of 785, 470, 530, and 565 nm illumination were acquired at 40Hz using a 785nm laser (LD785-SEV300, ThorLabs), along with three LEDs with center wavelengths of 470nm, 530nm, 565nm (ThorLabs) and corresponding the following optical bandpass filters, respectively: 469/35nm, 532/10nm, and 560/10nm (ThorLabs). A 505nm dichroic and 500nm longpass filter separated the fluorescently emitted and reflected light from the excitatory 470nm excitation for GCaMP imaging. A 4x

0.20NA objective (CFI Plan Apochromat Lambda D 4X, Nikon) was used. Imaging signals were acquired using a custom Matlab GUI. A TTL signal from the monocular display was recorded for synchronizing imaging with visual stimuli. During baseline recording, mice were lightly anesthetized with isoflurane and were head fixed in an awake imaging tube rig stereotax. After 30 minutes for anesthetic plane stabilization, mice were imaged for 30 minutes. During post-injection recording, vehicle or psilocybin was injected I.P. with a dosage of 1 mg kg-1. After 30 minutes, mice were imaged for 30 minutes.

5.5.6 Absorption Correction

Fluctuations in hemoglobin concentration, particularly during functional hyperemia, introduce an optical artifact due to the strong absorption properties of oxy- and deoxyhemoglobin. As hemoglobin absorbs both excitation and emitted fluorescence light, local changes in blood volume and oxygenation can alter the detected fluorescence intensity independent of actual neural activity. Because of this, we performed oxy/deoxy absorption correction[55] to account for these distortions impacting our GCaMP signal.

5.5.7 Habituation

To prepare for awake imaging, mice were habituated for 1-2 weeks prior to imaging. Imaging was performed with mice head fixed and allowed to remain awake in a transparent tube stereotax. Habituation followed a progressively increased time spent head fixed on the treadmill, starting at 5 minutes, and in increments of 10-15 minutes more each day working up to 1 hour of fixation. Mice were rewarded peanut butter during and after habituation.

5.5.8 Visual Stimulus

Visual stimulation experiments were performed with awake, head-fixed mice by positioning a MouseGoggles Mono display at the mouse's left eye for contralateral two-photon or widefield imaging in the right hemisphere. (Isaacson 2024) They display was oriented to 45 degrees azimuth and 0 degrees elevation respective to the long axis of the mouse. A maximum-contrast blue grating stimulus drifting at 1.5 Hz temporal frequency was presented at four directions, cycling through the direction for 0.5 s each, with the whole sequence repeated 3 times resulting in a total stimulation time of 6 s. Each trial was 16-24 s in duration, where the inter-trial delay period was chosen at random between 10-18 s. For 2P and widefield, 25 and 15 trials were recorded respectively due to data storage limits.

5.5.9 Analysis

For analysis of two-photon arbitrary line scans in Matlab, logged data was first segmented into ROIs using the logged [x,y] positions (in degrees) of the scan mirror, a feature built into the ScanImage microscope control system. Since ScanImage logs the scan mirror positions using an auxiliary DAQ device that 1) samples data at a much slower rate than the PMT digitizer, and 2) skips four position samples at the end of each line scan to save the sampled data, the scan mirror positions were first resampled to the PMT data timestamps and had missing values filled by interpolation with an Akima spline (using the fillmissing() function in Matlab with the 'makima' method). This interpolation was manually checked for every linescan to ensure accurate upsampling. Using the logged scan positions and the saved line ROI coordinates, the PMT data was segmented so that PMT values corresponding to scan positions near the drawn line ROIs were extracted for each ROI. Position values in degrees were converted into microns (0,0 located at the center of the image) using a conversion factor determined by imaging a calibration slide.

Line scans taken with a high sample rate tend to have the scan mirror positions move faster in the middle of each line ROI and round off corners between ROIs, so samples taken across a line ROI are not linearly spaced. Since our method of calculating blood flow velocity from vessel linescans depend on linearly spaced sampling (detailed below), line scan segments were first resampled onto a linearly spaced position vector for every line ROI individually. Samples were excluded if they were acquired more than 4 microns away from the ROI (a distance selected so that all vessel line scan data were sampled inside the vessel walls), which often occurred near the ends of each line ROI where the scan mirror rounded off the corner to transition between ROIs.

To calculate blood flow velocity from linearized line scans down a vessel, linescans were formatted into 2D image frames where each row contains a linearized linescan and multiple rows represent successive linescans. Blood flow velocity can be observed in the 2D images by identifying the dark shadows caused by red blood cells travelling down the vessel, which appears as angled dark bands in the 2D image (with the slope of the dark streak relating to the flow speed). The angle of dark bands (and hence blood flow speed) was determined using a Radon transform on blocks of 50 linescans. This results in a vector of flow velocity, where each velocity measurement relates to the average speed in that block of 50 linescans. Outliers in velocity measurements were manually defined minimum and maximum threshold. Data were then smoothed/downsampled to 3.33 Hz for further analysis and plotting. All flow speed vectors acquired from a single mouse were then averaged to create a single vector of flow speed change for each mouse individually. The maximum, mean, and minimum values in the average flow speed vectors were calculated for statistical comparison between experimental conditions.

To calculate neuron fluorescence from an arbitrary line scan segment drawn across the neuron, the mean brightness of that line scan segment was calculated for every frame. Neuron

type (ON, OFF, or Mixed) was determined for each neuron individually by first calculating the mean fluorescence at baseline (during the 3 seconds before visual stimulus onset), during the 6-s stimulus (excluding the first 0.3 s transient period), and during the 6-s post-stimulus period (again excluding the first 0.3 s) for every stimulus repetition (n=25 repetitions) during the pre-injection timepoint: if a neuron had significantly greater mean fluorescence during the stimulus (Wilcoxon Sign Rank test, $p<0.05$), it was classified as an ON neuron; if a neuron had significantly greater fluorescence after the stimulus, it was classified as OFF; and if a neuron had significantly greater fluorescence both during and after the stimulus, it was classified as Mixed. To create mean brightness traces of ON neurons for each mouse (which were the majority of recorded neurons), all brightness vectors of ON neurons were first normalized to their respective baselines (F/F) and then had their baselines subtracted (ΔF/F). If a single line scan contained more than one ON neuron, their ΔF/F were first averaged together to calculate the mean ON neuron response for that mouse. The mean and standard error of measurement (S.E.M.) were then calculated across all mice which contained at least one ON neuron, for each experimental condition individually. The mean ON response of each mouse was calculated by averaging the normalized brightness change during the 6-s stimulus period.

Analysis of widefield multi-channel imaging videos was performed with custom Matlab analysis pipelines. First, all raw imaging channels were Gaussian filtered using a 13x13 pixel window with a 2D Gaussian standard deviation of 3 pixels to reduce image noise. To analyze multi-exposure speckle contrast imaging, speckle contrast values were calculated using the REMI method for fast parameter estimation from the 785 nm speckle channel [58]. Relative oxygenated and deoxygenated hemoglobin concentrations (Hb and HbO) were calculated using

the 530 nm and 560 nm reflectance channels: First, the optical densities of every pixel in the 530 nm and 560 nm channels were calculated:

$$OD = \ln(\frac{I_0}{I})$$

Where I_0 is the pixel value at baseline (calculated as the average value during the 3-s pre-stimulus period), I is the current pixel value, and OD is the optical density. Next, Hb and HbO concentrations were determined using the differential pathlengths of the 530 nm and 560 nm channels and the expected extinction coefficients for Hb and HbO at these two wavelengths using the following formula and values:

$$coeff = \begin{bmatrix} 41778 & 39735 \\ 32617 & 53817 \end{bmatrix}$$

$$dpf = \begin{bmatrix} 0.0371713 \\ 0.0392168 \end{bmatrix}$$

$$cx = coeff \odot [dpf \quad dpf]$$

$$cx_{inv} = InvM(cx)$$

$$Hb = cx_{inv(1,1)} * OD_{530} + cx_{inv(1,2)} * OD_{560}$$

$$HbO = cx_{inv(2,1)} * OD_{530} + cx_{inv(2,2)} * OD_{560}$$

Where *coeff* is the extinction coefficient matrix, *dpf* is the differential pathlength factors, *cx* is the corrected coefficient matrix, and cx_{inv} is the inverse of *cx.* HbT (total hemoglobin) was calculated as the sum of HbO and HbT concentrations.

The computed Hb and HbO values were then used to correct GCaMP fluorescence values using the following equations:

$$F_{norm} = \frac{F}{F_0}$$

$$u_{a,em} = 33767 * HbO + 16450 * Hb$$

$$u_{a,ex} = 41778 * HbO + 39735 * Hb$$

$$F_{corr} = F_{norm} e^{(0.056 * u_{a,ex} + 0.056 u_{a,em})}$$

Where F is the raw fluorescence, F_0 is the baseline fluorescence, F_{norm} is the normalized fluorescence, $u_{a,em}$ is the absorption coefficient at the emission (530 nm) wavelength, $u_{a,ex}$ is the absorption coefficient at the excitation (470 nm) wavelength, and F_{corr} is the corrected fluorescence.

The average relative change in all extracted data types (e.g. speckle contrast, Hb, HbO, HbT, and corrected GCaMP fluorescence) to the visual stimulus was calculated by averaging across the 15 repetitions of the stimulus, where the images at each timepoint in a trial were linearly resampled onto a common 10 Hz time vector relative to the onset of the stimulus. This procedure created a video of the average stimulus response of each data type.

To determine which vessels in the FOV were arteries or veins, color-coded maps were first generated from the average Hb and HbO videos which took advantage of the observation that the stimulus increases Hb faster in arteries than in veins, and that the stimulus causes a greater decrease in HbO in veins than in arteries. The map of mean change in Hb from 0.5 – 1.5 s after stimulus onset (where arteries have increased more than veins) was mapped onto the blue channel, and the mean change in HbO was inverted and mapped onto the red channel, creating a map of likely arteries (in blue) and veins (in red). This map, along with the increased branching and tortuosity of arteries, was used to manually draw rectangular ROIs around vessel segments

and classify these segments as arteries or veins, where 3-6 segments of each type (all drawn on unique vessel branches) were labelled per imaging session.

To calculate the vessel diameter of the vessel segments in a video frame within each manually-drawn rectangular vessel ROI, the center line of the vessel was calculated based on the angle of the drawn ROI and the image was rotated and collapsed along the vessel length to create a single average cross section vector. A Gaussian function was then fit to the cross section, and the vessel width was estimated as the full-width at half-maximum (FWHM) of the fitted Gaussian function.

To determine the changes in the values of speckle contrast, oxygenation, and cerebral metabolic rate of oxygen consumption in artery and vein segments, binary image masks were created for every drawn rectangular vessel segment ROI, and the mean values inside the masks were calculated for every frame. To determine changes in these values in the parenchyma, a binary image mask of the vessels was created using image binarization using an adaptive threshold (imbinarize() function in Matlab) of the 530 nm reflectance channel, where vessels appear significantly darker than the surrounding tissue. The binary mask of the vessels was grown by 7 pixels (imdilate() in Matlab) to account for the 13x13 pixel window size of the Guassian filter, which blurs values up to 6 pixels in x/y directions, to minimize large value changes in the vessels from bleeding into the relatively smaller changes in parenchyma. To determine GCaMP fluorescence changes in the virally-labelled tissue, a binary image mask was first created around the brighter region of tissue in the 470 nm fluorescence channel. The mask was combined with the parenchyma mask to restrict the region to GCaMP-labelled tissue, excluding vessels. All parenchyma and GCaMP-labelled region masks were manually inspected to ensure accuracy. Using these masks, all extracted values (Hb, HbO, CMRO, Speckle,

GCaMP) were calculated on a frame-by-frame basis using their respective masks to create vectors of average changes caused by the stimulus. Vectors of each unique vessel segment of a single vessel type (artery or vein) were averaged together within each mouse to create a single artery and vein vector. The average vector and standard error of measurement was then calculated across all mice for each condition for plotting. For statistical comparison, the mean change for all values except GCaMP fluorescence were calculated by averaging the vectors of each mouse during the 12-s period beginning with the stimulus onset; the mean change in GCaMP fluorescence was calculated over the 6-s stimulus period due to the fast kinetics of GCaMP6f. Significant differences between all mean value changes for different experimental conditions were determined using the Wilcoxon Sign Rank test with Benjamini-Hochberg correction for multiple comparisons.

Denoting statistical significance in figure panels WITHOUT correcting for multiple comparisons when the number of comparisons are large, since doing so would increase the chance of type II errors (false negatives). But because it's also important to consider type I errors (false positives), we reporting the results of multiple comparison correction as well.

References

1. Fúlvio Rieli Mendes *et al.* Classic and non-classic psychedelics for substance use disorder: a review of their historic, past and current research. *Addict. Neurosci.* 100025–100025 (2022) doi:10.1016/j.addicn.2022.100025.

2. Robin Carhart-Harris, Carhart-Harris, R. L., Guy M. Goodwin & Goodwin, G. M. The Therapeutic Potential of Psychedelic Drugs: Past, Present, and Future. *Neuropsychopharmacology* **42**, 2105–2113 (2017).

3. Charles D. Nichols, Nichols, C. D., Peter S. Hendricks & Hendricks, P. S. Classic psychedelics as therapeutics for psychiatric disorders. **31**, 959–966 (2020).

4. Sarah Naher. The Potential Therapeutic Benefits and Safety of Psychedelics in the Treatment of Mental Health Conditions: A Systematic Review. *J. Sociol. Psychol. Amp Relig. Stud.* **5**, 20–39 (2023).

5. Robin Carhart-Harris *et al.* Neural correlates of the psychedelic state as determined by fMRI studies with psilocybin. *Proc. Natl. Acad. Sci. U. S. A.* **109**, 2138–2143 (2012).

6. Richard E. Daws *et al.* Increased global integration in the brain after psilocybin therapy for depression. *Nat. Med.* (2022) doi:10.1038/s41591-022-01744-z.

7. Scott Singleton *et al.* Altered brain activity and functional connectivity after MDMA-assisted therapy for post-traumatic stress disorder. *Front. Psychiatry* **13**, (2023).

8. Katrin H. Preller *et al.* Changes in global and thalamic brain connectivity in LSD-induced altered states of consciousness are attributable to the 5-HT2A receptor. *eLife* **7**, (2018).

9. J. Siegel *et al.* Psilocybin desynchronizes the human brain. *Nature* (2024) doi:10.1038/s41586-024-07624-5.

10. Lori Whitten & Whitten, L. A. Functional magnetic resonance imaging (fMRI): An invaluable tool in translational neuroscience. (2012) doi:10.3768/rtipress.2012.op.0010.1212.

11. Clare Howarth *et al.* More than just summed neuronal activity: how multiple cell types shape the BOLD response. *Philos. Trans. R. Soc. B* **376**, 20190630–20190630 (2021).

12. Damon P. Cardenas *et al.* Functional MRI during hyperbaric oxygen: Effects of oxygen on neurovascular coupling and BOLD fMRI signals. *NeuroImage* **119**, 382–389 (2015).

13. Elizabeth M. C. Hillman & Hillman, E. M. C. Coupling Mechanism and Significance of the BOLD Signal: A Status Report. *Annu. Rev. Neurosci.* **37**, 161–181 (2014).

14. Nikos K. Logothetis & Logothetis, N. K. The underpinnings of the BOLD functional magnetic resonance imaging signal. *J. Neurosci.* **23**, 3963–3971 (2003).

15. Gabor C. Petzold, Petzold, G. C., Venkatesh N. Murthy & Murthy, V. N. Role of Astrocytes in Neurovascular Coupling. *Neuron* **71**, 782–797 (2011).

16. Guerra, G. *et al.* The Role of Endothelial Ca2+ Signaling in Neurovascular Coupling: A View from the Lumen. *Int. J. Mol. Sci.* **19**, 938 (2018).

17. Hana Uhlířová *et al.* Cell type specificity of neurovascular coupling in cerebral cortex. *eLife* **5**, (2016).

18. David Rosenegger, Rosenegger, D., Grant R. Gordon & Gordon, G. R. A slow or modulatory role of astrocytes in neurovascular coupling. *Microcirculation* **22**, 197–203 (2015).

19. Samantha Schaeffer, Schaeffer, S., Costantino Iadecola & Iadecola, C. Revisiting the neurovascular unit. *Nat. Neurosci.* **24**, 1198–1209 (2021).

20. Costantino Iadecola & Iadecola, C. The Neurovascular Unit Coming of Age: A Journey through Neurovascular Coupling in Health and Disease. *Neuron* **96**, 17–42 (2017).

21. Winston M Zhu *et al.* Neurovascular coupling mechanisms in health and neurovascular uncoupling in Alzheimer's disease. *Brain* (2022) doi:10.1093/brain/awac174.

22. Hélène Girouard *et al.* Neurovascular coupling in the normal brain and in hypertension, stroke, and Alzheimer disease. *J. Appl. Physiol.* **100**, 328–335 (2006).

23. Stefano Tarantini *et al.* Impaired neurovascular coupling in aging and Alzheimer's disease: Contribution of astrocyte dysfunction and endothelial impairment to cognitive decline. *Exp. Gerontol.* **94**, 52–58 (2017).

24. G K Aghajanian, Aghajanian, G. K., Marek Gj & Marek, G. J. Serotonin and hallucinogens. *Neuropsychopharmacology* **21**, 16–23 (1999).

25. Bruce E. Blough *et al.* Interaction of psychoactive tryptamines with biogenic amine transporters and serotonin receptor subtypes. *Psychopharmacology (Berl.)* **231**, 4135–4144 (2014).

26. Mogens Madsen *et al.* Psychedelic effects of psilocybin correlate with serotonin 2A receptor occupancy and plasma psilocin levels. *Neuropsychopharmacology* **44**, 1328–1334 (2019).

27. Paul M. Vanhoutte & Vanhoutte, P. M. Serotonin and the vascular wall. *Int. J. Cardiol.* **14**, 189–203 (1987).

28. Susan G. Griffith *et al.* Serotonin as a neurotransmitter in cerebral arteries. *Brain Res.* **247**, 388–392 (1982).

29. Zvi Cohen *et al.* SEROTONIN IN THE REGULATION OF BRAIN MICROCIRCULATION. *Prog. Neurobiol.* **50**, 335–362 (1996).

30. Myers Jh *et al.* Direct and sensitizing effects of serotonin agonists and antagonists on vascular smooth muscle. *J. Cardiovasc. Pharmacol.* **7**, 44–48 (1985).

31. Jonah A. Padawer-Curry *et al.* Psychedelic 5-HT2A receptor agonism: neuronal signatures and altered neurovascular coupling. (2023) doi:10.1101/2023.09.23.559145.

32. Aisling Spain *et al.* Neurovascular and neuroimaging effects of the hallucinogenic serotonin receptor agonist psilocin in the rat brain. *Neuropharmacology* **99**, 210–220 (2015).

33. Matthew Isaacson *et al.* MouseGoggles: an immersive virtual reality headset for mouse neuroscience and behavior. *Nat. Methods* (2024) doi:10.1038/s41592-024-02540-y.

34. Rivera, D. Application of light to observe and manipulate physiological function in mouse models of neurological and cardiovascular disease. (Cornell University, 2023).

35. Abimael González-Hernández, Bruno A. Marichal-Cancino, Antoinette MaassenVanDenBrink, & Carlos M. Villalón. Serotonergic Modulation of Neurovascular Transmission: A Focus on Prejunctional 5-HT Receptors/Mechanisms. *Biomedicines* **11**, 1864–1864 (2023).

36. Inés Armando *et al.* Dopamine and Renal Function and Blood Pressure Regulation. *Compr. Physiol.* **1**, 1075–1117 (2011).

37. Jaster, A. M. & González-Maeso, J. Mechanisms and molecular targets surrounding the potential therapeutic effects of psychedelics. *Mol. Psychiatry 2023* 1–18 (2023) doi:10.1038/s41380-023-02274-x.

38. Paul Hartig *et al.* Serotonin Receptor Subtypes. *Psychopharmacol. Ser.* **10**, 15–25 (1993).

39. Rainer Kraehenmann *et al.* Psilocybin-Induced Decrease in Amygdala Reactivity Correlates with Enhanced Positive Mood in Healthy Volunteers. *Biol. Psychiatry* **78**, 572–581 (2015).

40. Thomas S. Ray & Ray, T. S. Psychedelics and the human receptorome. *PLOS ONE* **5**, (2010).

41. Holze, F. *et al.* Direct comparison of the acute effects of lysergic acid diethylamide and psilocybin in a double-blind placebo-controlled study in healthy subjects. *Neuropsychopharmacology* (2022) doi:10.1038/s41386-022-01297-2.

42. Laura Ley *et al.* Comparative acute effects of mescaline, lysergic acid diethylamide, and psilocybin in a randomized, double-blind, placebo-controlled cross-over study in healthy participants. *Neuropsychopharmacology* **48**, 1659–1667 (2023).

43. Kolaczynska, K. E. *et al.* Receptor Interaction Profiles of 4-Alkoxy-3,5-Dimethoxy-Phenethylamines (Mescaline Derivatives) and Related Amphetamines. *Front. Pharmacol.* **12**, (2022).

44. Bronwyn M. Kivell *et al.* MDMA causes a redistribution of serotonin transporter from the cell surface to the intracellular compartment by a mechanism independent of phospho-p38-mitogen activated protein kinase activation. *Neuroscience* **168**, 82–95 (2010).

45. Pierre-Michel Bernier *et al.* The morphology of the human cerebrovascular system. *Hum. Brain Mapp.* **39**, 4962–4975 (2018).

46. David Martin, Martin, D. A., Charles D. Nichols & Nichols, C. D. Psychedelics Recruit Multiple Cellular Types and Produce Complex Transcriptional Responses Within the Brain. *EBioMedicine* **11**, 262–277 (2016).

47. Alasdair M. Barr *et al.* The Selective Serotonin-2A Receptor Antagonist M100907 Reverses Behavioral Deficits in Dopamine Transporter Knockout Mice. *Neuropsychopharmacology* **29**, 221–228 (2004).

48. Jason W. Hamner *et al.* Cholinergic control of the cerebral vasculature in humans. *J. Physiol.* **590**, (2012).

49. Nicola B. Hamilton *et al.* Pericyte-mediated regulation of capillary diameter: a component of neurovascular coupling in health and disease. *Front. Neuroenergetics* **2**, 5 (2010).

50. Kira Shaw *et al.* Neurovascular coupling and oxygenation are decreased in hippocampus compared to neocortex because of microvascular differences. *Nat. Commun.* **12**, 3190–3190 (2021).

51. F.X. Vollenweider *et al.* Positron Emission Tomography and Fluorodeoxyglucose Studies of Metabolic Hyperfrontality and Psychopathology in the Psilocybin Model of Psychosis. *Neuropsychopharmacology* **16**, 357–372 (1997).

52. Zhong-Ming Li *et al.* Integration of EEG/MEG with MRI and fMRI. *IEEE Eng. Med. Biol. Mag.* **25**, 46–53 (2006).

53. Richard D. Hoge & Richard D. Hoge. Calibrated fMRI. *NeuroImage* doi:10.1016/j.neuroimage.2012.02.022.

54. Sasitorn Petcharunpaisan *et al.* Arterial spin labeling in neuroimaging. *World J. Radiol.* **2**, 384–398 (2010).

55. Shih, A. Y. *et al.* Two-photon microscopy as a tool to study blood flow and neurovascular coupling in the rodent brain. **32**, (2012).

56. Patrick J. Drew *et al.* Rapid determination of particle velocity from space-time images using the Radon transform. *J. Comput. Neurosci.* **29**, 5–11 (2010).

57. Ying Ma *et al.* Wide-field optical mapping of neural activity and brain haemodynamics: considerations and novel approaches. *Philos. Trans. R. Soc. B* **371**, 20150360 (2016).

58. Daniel Rivera & Chris B. Schaffer. Quasi-analytic solution for real-time multi-exposure speckle imaging of tissue perfusion. *Biomed. Opt. Express* **14**, 3950–3950 (2023).

CHAPTER 6: CONCLUSIONS AND FUTURE DIRECTIONS

6.1 Conclusions

The experiments in this thesis demonstrate how powerful in vivo imaging techniques are in furthering our understanding of cerebral blood flow (CBF) and neural activity, and their relationship in healthy and disease contexts (introduced in chapter 1). Elucidating the biological underpinnings of such physiology provides critical insights for both foundational knowledge and translational research. This is demonstrated here in the contexts of Alzheimer's disease (AD) (introduced in chapter 2) and psychedelics (introduced in chapter 3) with the use of the in vivo imaging techniques of microscale multiphoton [1] and mesoscale widefield multimodal imaging [2]. Experiments in this thesis focus on understanding how the relationship between CBF and neural activity is altered in the mouse primary visual cortex (V1), especially in response to specific visual stimuli. This stimulation is performed using a novel mouse visual stimulation method (MouseGoggles)[3], and when performed in tandem with in vivo imaging, allows us to probe the relationship between CBF and neural activity to investigate blood flow and neural activity in disease and therapeutic interventions.

First, in the context of AD (chapter 4), using two-photon excitation fluorescence microscopy (2PEF), we sought to understand how increasing CBF in 9-11 month old APP/PS1 mice may affect impaired neural activity patterns (introduced in chapter 2). In V1, orientation selectivity is impaired in AD mice [4], as neurons have broader tuning curves, firing in response to a broader range of drifting grating angles and directions. Comparing calcium activity in the same layer 2/3 V1 neurons before and after increasing CBF in APP/PS1 mice showed a significant increase in spontaneous activity and orientation tuning. The increase in orientation selectivity indicates that

the impaired neural activity patterns in AD mice are at least partially rescued by restoring cerebral blood flow. This restoration of orientation tuning suggests that improved vascular perfusion may contribute to enhanced sensory processing, which could underly the observed improvements in cognitive performance during spatial memory tasks [5]. These findings support the hypothesis that targeting vascular deficits in AD not only ameliorates global blood flow but also helps normalize specific neural computations critical for perception and cognition.

Second, we conducted a multiscale approach, using both 2PEF and multimodal widefield imaging, to evaluate neurovascular coupling alterations induced by psilocybin (chapter 5). Classical psychedelics, such as psilocybin, are very similar in structure to serotonin (5-HT) [6], which is a highly vasoactive molecule [7]. Therefore, we hypothesized that psilocybin may have direct implications on vascular response that are no longer coupled with neural activity. This decoupling would have clinical significance by affecting the interpretation of fMRI imaging in clinical trials with psychedelics, as such imaging relies on measuring blood flow, specifically blood-oxygen level dependent signal (BOLD), as a proxy for neural activity [8]. Again, we tested this by recording neural activity and blood flow responses in layer 2/3 of V1 in response to drifting grating stimuli. Comparing the neurovascular coupling (NVC) response pre and post psilocybin using 2P imaging showed a significant prolonged elevation of blood flow, while no effect on neural activity response was observed. These microscale results were corroborated by similar trends of widefield imaging data, which represented more relevant measures to compare to fMRI imaging as we were able to obtain blood oxygenation measures. These findings demonstrate that psilocybin induces a sustained increase in cerebral blood flow (CBF) independent of measurable neural activity, highlighting a neurovascular decoupling effect. This

disruption challenges the interpretation of fMRI studies involving psychedelics and presents reason for more informed analysis to accurately quantify neural activity.

6.2 Future Directions

The results of this thesis elucidate important findings about the interplay between CBF and neural activity in the contexts of both Alzheimer's disease and psychedelics. These results give rise to many open questions about such relationships, as well as where we go next for moving towards successfully combating the deficits of AD and accurately investigating the mechanisms of psychedelic drug action. In vivo imaging provides the critical ability to investigate these questions in live animal models. Capitalizing on the use of these tools, as well as others, will allow for a further understanding of what mechanisms underly the changes we see in our data.

6.2.1 Improved Neural Activity Impairment through CBF Restoration in Alzheimer's disease

Our data suggests that acutely increasing CBF can lead to an improvement in impaired cognitive function. This likely then contributes to the improved memory performance seen in the same paradigm in AD mice [5]. To understand how CBF leads to this improvement, there are several next steps we can take. As excitation/inhibition balance is thought to be critical for maintaining normal network communication [9], and evidence suggests that fast-spiking inhibitory neurons may be more effected by metabolic deficiencies [10], it is logical to investigate how an increase in CBF will impact cell type-specific firing patterns.

Investigating other firing patterns in the brain will provide further insight into the effects of CBF increase. Other alterations to normal cognitive functioning brought on by AD include: the breakdown of the default mode network (DMN) [11], who's altered functioning may result in

cognitive flexibility and memory deficits, as well as hypersynchronous activity [12], where aberrant neuronal synchronization disrupts normal oscillatory rhythms critical for cognition.

Another important next step is to evaluate such improvement in other impaired contexts, specifically in a manner more relevant to memory such as place cell mapping impairment in the hippocampus. Using 3P imaging in a VR environment displayed with MouseGoggles, we can evaluate this context in mice to provide further insight into how neural activity impairment is impacted by CBF.

Alzheimer's disease is commonly associated with pathological symptoms of harmful protein aggregates, including amyloid beta plaques and tau fibrillary tangles [13]. Limited success in targeting these pathologies to combat the cognitive decline associated with AD provides the motivation to investigate new avenues for therapeutic treatment [14]. These results, along with a growing body of research, shed light on metabolic and blood flow deficiencies as an important research direction [15]. Deficits in these areas occur much earlier in disease progression, prior to the formation of harmful protein aggregates as well as symptoms of cognitive decline [16]. Therefore, further investigations into these impairments may help to elucidate new therapeutic targets for treating AD early on, or even later in disease progression, as here we show an example of how increasing CBF can lead to an improvement of impaired neural activity patterns, which likely then contribute to associated improvements in memory performance.

6.2.2. Neurovascular Coupling Alterations Induced by Psychedelics

Our data demonstrates a case of neurovascular decoupling induced by psilocybin. Such prolonged elevation of blood flow response, and no alteration to neural activity, show that psilocybin can lead to a mismatch in the relationship which is heavily relied upon by fMRI

imaging. Understanding the mechanisms underlying such decoupling, and how these vary across different contexts, will be critical next steps to this work. As fMRI imaging studies investigating psychedelic drug action rely on blood-oxygen-level-dependent (BOLD) signal as a proxy for neural activity [8], being able to most accurately interpret such imaging data may benefit from further elucidating such decoupling.

Serotonin agonism may underlie psilocybin's effects on neurovascular coupling (NVC), where increased neural activity normally triggers vasodilation followed by vasoconstriction to restore baseline. Our results suggest psilocybin prolongs blood flow by impairing vasoconstriction, possibly through antagonism at 5-HT1A, 1B, and 2B receptors.[8,17] Beyond direct 5-HT_2 receptor effects, psychedelics may reduce noradrenaline-mediated vasoconstriction and enhance CGRP-induced vasodilation, further promoting prolonged blood flow [18]. Additionally, modulation of serotonin, dopamine, and acetylcholine systems may suppress vasoconstriction and enhance vasodilation, ultimately weakening vascular regulation through multiple interacting pathways. Future studies should investigate receptor-specific contributions using pharmacological antagonists and genetic models, as well as assess how these vascular effects relate to behavioral and therapeutic outcomes of psychedelics. Advanced imaging techniques, such as two-photon microscopy and fiber photometry, could further clarify the temporal dynamics of these changes at the cellular level.

Further work is also needed to address the region and drug-specific variability that is likely to contribute to differences in NVC alterations. Under psychedelics, these alterations likely vary across brain regions, drug types, and doses due to differences in 5-HT receptor expression and vascular regulation [19]. While 5-HT2A receptors are dominant in the cortex, others like 5-HT1B and 5-HT1A contribute to vasoactivity in subcortical regions, suggesting NVC changes may be

region-specific. Dose-dependent effects also play a role—low-dose psilocybin modestly increases cerebral blood flow (CBF), whereas high doses may override activity-dependent vascular responses, leading to perfusion mismatches [20]. Different psychedelics interact uniquely with vascular and glial systems, as seen with LSD's prolonged effects, mescaline's adrenergic activity, and MDMA's serotonin release-driven vasoconstriction [21]. Psilocybin's specific effects appear to weaken vasoconstriction rather than enhance vasodilation, highlighting the need for receptor-specific investigations using pharmacological antagonists. Additionally, stimulus type may influence psychedelic-induced decoupling, as other studies show sensory tasks enhancing excitability but blunting vascular responses [22], while cognitive tasks may suffer from dysregulated blood flow [23]. Future research should systematically compare drug-specific, region-dependent, and stimulus-related NVC changes to better understand the underlying mechanisms of psychedelic-induced vascular alterations.

Psychedelic-induced neurovascular decoupling complicates the interpretation of fMRI, which relies on blood-oxygen-level-dependent (BOLD) signals as a proxy for neural activity. If psychedelics increase cerebral blood flow (CBF) independently of neural firing, fMRI may produce false positives, overestimating activity in certain brain regions. Conversely, disrupted neurovascular coupling (NVC) mechanisms could lead to delayed or diminished blood flow responses, underestimating neural activity. Our results suggest that psilocybin prolongs blood flow increases without altering neural activity, indicating that fMRI may misrepresent psychedelic-induced changes. The extent of decoupling likely varies by brain region, with serotonergic areas like the prefrontal and visual cortex being more susceptible to hemodynamic distortions than subcortical regions. Dose-dependent effects further complicate matters, as low doses may still allow BOLD to approximate neural activity, whereas high doses may cause

excessive vasodilation, masking neural contributions. Since many psychedelic studies use fMRI to infer altered brain network dynamics, misinterpreting vascular effects as neural changes could skew conclusions about therapeutic mechanisms. To address this, future research should integrate fMRI with direct neural recordings (EEG, MEG, or electrophysiology), employ calibrated fMRI techniques to account for baseline CBF changes, or compare psychedelics with differing vascular effects [24,25,26]. Properly disentangling hemodynamic artifacts from neural activity is essential for accurately understanding psychedelic drug action.

References

1. Chris Xu, M. Nedergaard, Deborah J. Fowell, Peter Friedl, & Na Ji. Multiphoton fluorescence microscopy for in vivo imaging. *Cell* (2024) doi:10.1016/j.cell.2024.07.036.
2. Ying Ma *et al.* Wide-field optical mapping of neural activity and brain haemodynamics: considerations and novel approaches. *Philos. Trans. R. Soc. B* **371**, 20150360 (2016).
3. Matthew Isaacson *et al.* MouseGoggles: an immersive virtual reality headset for mouse neuroscience and behavior. *Nat. Methods* (2024) doi:10.1038/s41592-024-02540-y.
4. Christine Grienberger *et al.* Staged decline of neuronal function in vivo in an animal model of Alzheimer's disease. *Nat. Commun.* **3**, 774–774 (2012).
5. Cruz Hernández, J. C. *et al.* Neutrophil adhesion in brain capillaries reduces cortical blood flow and impairs memory function in Alzheimer's disease mouse models. *Nat. Neurosci.* **22**, 413–420 (2019).
6. G K Aghajanian, Aghajanian, G. K., Marek Gj & Marek, G. J. Serotonin and hallucinogens. *Neuropsychopharmacology* **21**, 16–23 (1999).

7. Paul M. Vanhoutte & Vanhoutte, P. M. Serotonin and the vascular wall. *Int. J. Cardiol.* **14**, 189–203 (1987).

8. Clare Howarth *et al.* More than just summed neuronal activity: how multiple cell types shape the BOLD response. *Philos. Trans. R. Soc. B* **376**, 20190630–20190630 (2021).

9. Fernando Maestú *et al.* Neuronal excitation/inhibition imbalance: core element of a translational perspective on Alzheimer pathophysiology. *Ageing Res. Rev.* **69**, 101372–101372 (2021).

10. Oliver Kann & Kann, O. The interneuron energy hypothesis: Implications for brain disease. *Neurobiol. Dis.* **90**, 75–85 (2016).

11. Michael D. Greicius *et al.* Default-mode network activity distinguishes Alzheimer's disease from healthy aging: Evidence from functional MRI. *Proc. Natl. Acad. Sci. U. S. A.* **101**, 4637–4642 (2004).

12. Palop, J. J. & Mucke, L. Network abnormalities and interneuron dysfunction in Alzheimer disease. *Nat. Rev. Neurosci.* **17**, 777–792 (2016).

13. Christopher A. Ross, Ross, C., Ross, C. A., Michelle A. Poirier & Poirier, M. A. Protein aggregation and neurodegenerative disease. *Nat. Med.* **10**, (2004).

14. David A. Drachman & Drachman, D. A. The amyloid hypothesis, time to move on: Amyloid is the downstream result, not cause, of Alzheimer's disease. *Alzheimers Dement.* **10**, 372–380 (2014).

15. Costantino Iadecola & Iadecola, C. Vascular and Metabolic Factors in Alzheimer's Disease and Related Dementias: Introduction. *Cell. Mol. Neurobiol.* **36**, 151–154 (2016).

16. Eva Vico Varela *et al.* Excitatory-inhibitory imbalance in Alzheimer's disease and therapeutic significance. *Neurobiol. Dis.* **127**, 605–615 (2019).

17. Bruce E. Blough *et al.* Interaction of psychoactive tryptamines with biogenic amine transporters and serotonin receptor subtypes. *Psychopharmacology (Berl.)* **231**, 4135–4144 (2014).

18. Abimael González-Hernández, Bruno A. Marichal-Cancino, Antoinette MaassenVanDenBrink, & Carlos M. Villalón. Serotonergic Modulation of Neurovascular Transmission: A Focus on Prejunctional 5-HT Receptors/Mechanisms. *Biomedicines* **11**, 1864–1864 (2023).

19. Alaina M. Jaster & Javier González-Maeso. Mechanisms and molecular targets surrounding the potential therapeutic effects of psychedelics. (2023) doi:10.1038/s41380-023-02274-x.

20. Rainer Kraehenmann *et al.* Psilocybin-Induced Decrease in Amygdala Reactivity Correlates with Enhanced Positive Mood in Healthy Volunteers. *Biol. Psychiatry* **78**, 572–581 (2015).

21. Laura Ley *et al.* Comparative acute effects of mescaline, lysergic acid diethylamide, and psilocybin in a randomized, double-blind, placebo-controlled cross-over study in healthy participants. *Neuropsychopharmacology* **48**, 1659–1667 (2023).

22. Jonah A. Padawer-Curry *et al.* Psychedelic 5-HT2A receptor agonism: neuronal signatures and altered neurovascular coupling. (2023) doi:10.1101/2023.09.23.559145.

23. F.X. Vollenweider *et al.* Positron Emission Tomography and Fluorodeoxyglucose Studies of Metabolic Hyperfrontality and Psychopathology in the Psilocybin Model of Psychosis. *Neuropsychopharmacology* **16**, 357–372 (1997).

24. Zhong-Ming Li *et al.* Integration of EEG/MEG with MRI and fMRI. *IEEE Eng. Med. Biol. Mag.* **25**, 46–53 (2006).

25. Richard D. Hoge & Richard D. Hoge. Calibrated fMRI. *NeuroImage* doi:10.1016/j.neuroimage.2012.02.022.

26. Sasitorn Petcharunpaisan *et al.* Arterial spin labeling in neuroimaging. *World J. Radiol.* **2**, 384–398 (2010).

APPENDIX A: ACRONYMS

2PFM – Two-Photon Fluorescence Microscopy

2P – Two-Photon

2PEF - Two-Photon Excitation Fluorescence Microscopy

AAV – Adeno-Associated Virus

Aβ – amyloid beta

AD – Alzheimer's Disease

ADRD – Alzheimer's Disease and Related Dementias

AMPA – alpha-amino-3-hydroxy-5-methyl-4-isoxazolepropionic acid

APOE4 – Apolipoprotein E4

APP – Amyloid Precursor Protein

ASL – Arterial Spin Labeling

ATP – Adenosine Triphosphate

AUD – alcohol use disorder

BDNF – Brain-Derived Neurotrophic Factor

BOLD – Blood-Oxygen-Level Dependent

CA1 – Cornu Ammonis 1 (region of hippocampus)

CBF – Cerebral Blood Flow

CCC – Cortico–Claustro–Cortical

CGRP – Calcitonin Gene-Related Peptide

CH1 – Channel 1

CNMF – Constrained Nonnegative Matrix Factorization

CPP – Conditioned Place Preference

CSTC – Cortico-Striato-Thalamo-Cortical

DA – Dopamine

DBS – Deep Brain Stimulation

DMN – Default Mode Network

DMT – Dimethyltryptamine

DOI – 2,5-Dimethoxy-4-iodoamphetamine

DREADD – Designer Receptors Exclusively Activated by Designer Drugs

DSI – Direction Selectivity Index

EASI-FISH – Expansion-Assisted Iterative Fluorescence In Situ Hybridization

EEG – Electroencephalography

EOFAD – Early-Onset Familial Alzheimer's Disease

ERK – Extracellular Signal-Regulated Kinase

EX-EM – excitation and emission

FDA – Food and Drug Administration

FITC – Fluorescein Isothiocyanate

FOV – Field of View

FWHM – Full Width at Half Maximum

GABA – Gamma-Aminobutyric Acid

GECI – Genetically Encoded Calcium Indicator

GPCR – G-Protein Coupled Receptor

GUI – Graphical User Interface

HPC – Hippocampus

HPPD – Hallucinogen Persisting Perception Disorder

HRF – Hemodynamic Response Function

HT – Hydroxytryptamine (Serotonin)

5-HT2AR – 5-Hydroxytryptamine Receptor 2A

LED – Light-emitting diode

LFP – Local Field Potential

LGN – Lateral Geniculate Nucleus

LSCI – Laser Speckle Contrast Imaging

LSD – Lysergic Acid Diethylamide

LTD – Long-term depression

LTP – Long-term potentiation

MAPK – mitogen-activated protein kinase

MDL – serotonin receptor antagonist

MDMA – 3,4-Methylenedioxymethamphetamine

MEG – Magnetoencephalography

MPFM – Multiphoton Fluorescence Microscopy

MW – Molecular weight

NA – Numerical aperture

NIR – Near-Infrared

NMDA – N-methyl-D-aspartate

NOS – Nitric Oxide Synthase

NVC – Neurovascular Coupling

OCD – Obsessive-compulsive disorder

OII – Optical Intrinsic Imaging

OSI – Orientation Selectivity Index

PAT – Psychedelic-Assisted Therapy

PBS – Phosphate Buffered Saline

PCA – Principal Component Analysis

PCP – Phencyclidine

PET – Positron Emission Tomography

PFC – Prefrontal Cortex

PKC – Protein Kinase C

PLC – Phospholipase C

PS1 – Presenilin-1

PSEN1 – Presenilin-1

PTSD – Post-traumatic stress disorder

PV – Parvalbumin

RBC – Red blood cell

REBUS – Relaxed Beliefs Under Psychedelics

ROI – Region of Interest

ROS – Reactive Oxygen Species

S.E.M. – Standard error mean

SD – standard deviation

SERT – Serotonin Transporter

SNR – Signal-to-noise ratio

SSRI – Serotonin-selective reuptake inhibitor

SST – Somatostatin

SWR – Sharp-Wave Ripple

tACS – Transcranial Alternating Current Stimulation

TMS – Transcranial Magnetic Stimulation

TRKB – tropomyosin receptor kinase B

TTL – Transistor–Transistor Logic

VIP – Vasoactive intestinal peptide

VR – Virtual Reality

WT – Wild-Type